## Factors affecting ice loads on wide structures

Morse, B.



**Publisher's version / Version de l'éditeur:**
https://doi.org/10.4224/12341009
*PERD/CHC Report; no. 1-056, 2000-06-12*

# ICE/STRUCTURE INTERACTION

## Factors Affecting Ice Loads on Wide Structures

An analysis of ice loads on the St. Lawrence River ice booms from 1994 to 2000

## PERD/CHC Report 10-56

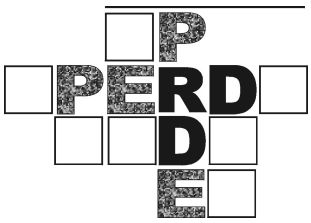


## June 12, 2000

Brian Morse
Université Laval

Table of contents

# List of Tables



# List of Figures

# 1 Acknowledgements

The report was funded by the Canadian Federal Government's Panel on Energy Research and Development (Ice/Structure Interaction programme).

On behalf of PERD, Dr. Garry Timco of the Canadian Hydraulics Centre (CHC) of the National Research Council managed the project and provided moral support.

Dr. Samir Gharbi, Université Laval, assembled the data and wrote Chapter 6 (analysis of environmental forces).

Libo Sun typed the Reference list.

Gervais Bouchard of the Canadian Coast Guard (Laurentian Region) supported CCG-RL's collaboration in the study.

Stéphane Dumont, CCG-RL retrieved and provided all the force data. He also looked after the calibration of the load cells and wrote a historical account of the booms' evolution. He also provided advice and comments (but has not yet seen this report). He is the engineer responsible for the booms and the technical group looking after the data and the boom maintenance and improvement. With the principal author and others, he helped developed the data acquisition systems.

Marc Choquette, CCG-RL helped design, improve and deploy the booms. He also provided many insights and comments. He is responsible for most photographs shown in the report. He oversees the data acquisition and boom maintenance. Marc also provided almost all the photographs and sketches contained in this report.

Marc Savard, CCG-RL also helped improve and deploy the booms. He also is responsible for the maintenance of the data acquisition systems and data retrieval. He provided access to all the environmental data and videos of the booms.

We note that a number of partners and clients participated in the boom's design and evolution. Particularly, CHC, Fleet Technology, Le Groupe Conseil LaSalle, INRS-Eau and Donald Carter.

We thank Ed Stander for his review.

We are very grateful to all who have helped (and will, no doubt, continue to help) in this project.

# 2 Disclaimer

This report was prepared to the best of our knowledge using the best information we had at hand. Nevertheless there may be some errors or omissions. In this case, the principal author takes full responsibility.

# ICE/STRUCTURE INTERACTION
# Factors Affecting Ice Loads on Wide Structures

## June 12, 2000

Brian Morse
Université Laval

## 3 Introduction

Ice booms are very wide structures intended to provoke the formation of a stable ice cover and/or retain or store ice in a certain location. They can be deployed on rivers to manage ice or at sea to contain an oil spill or to protect a fixed structure. A simple one span boom consisting of 13 cylindrical steel pontoons is shown in Figure 3.1.

Figure 3.1. Wakefield ice boom (courtesy of Fleet Technology)

More typically, as shown in the following sketch, booms are multi-span structures:

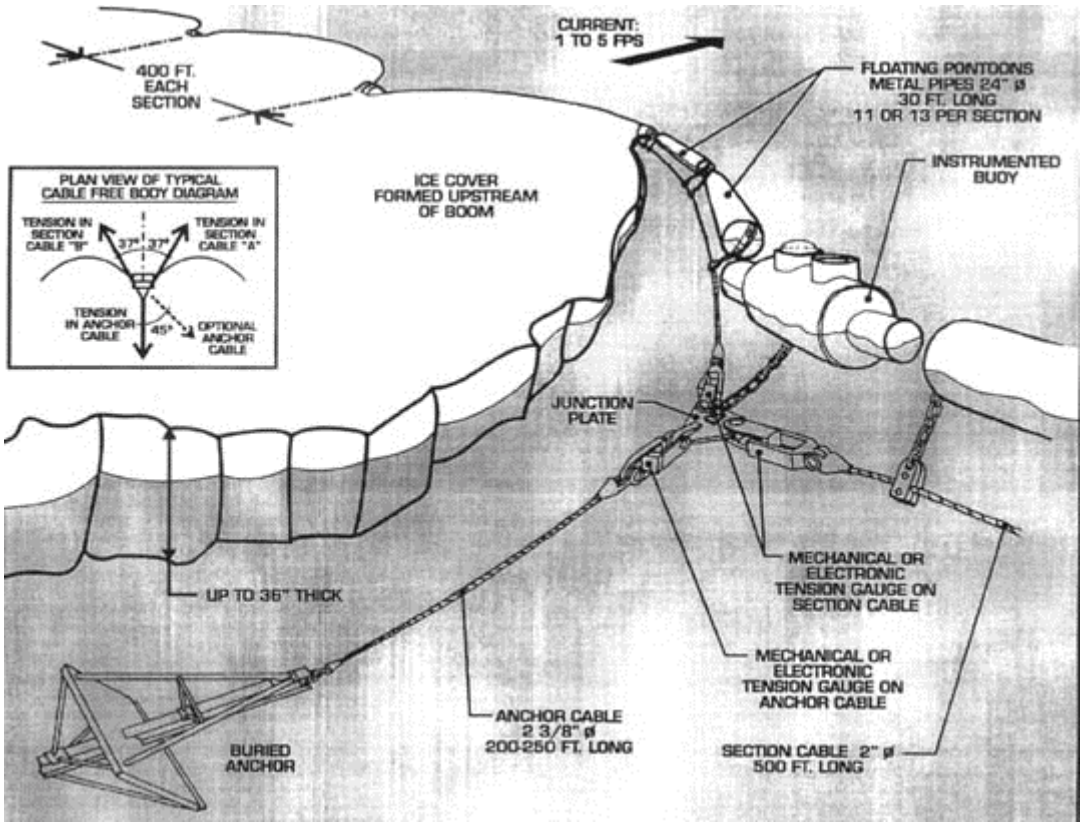


Figure 3.2. Three-dimensional view of a multi-span ice boom, Yamachiche, Québec

Historically, there were many ice booms deployed in the 1960s. They were composed primarily of rectangular 14" by 22" Douglas Fir pontoons Following a major ice jam at Lac St. Pierre on the St. Lawrence River in February, 1993, the principal author designed and deployed a new boom based on cylindrical pontoons similar to the ones shown in Figures 3.1 and 3.2.

It was essential to deploy the booms quickly to prevent another ice jam in order to restore confidence in winter navigation on the river. As such, three consultants were called upon to aid in the design. Donald Carter (1995) did some analytical work. Fleet Technology (1993 & 1996) did some analytical studies and some very rudimentary physical model studies. The Canadian Hydraulics Centre (1995) performed detailed model studies of both a typical boom section and different pontoon geometries and densities. Le Groupe Conseil LaSalle (1993) performed a physical model of Lac St. Pierre to help optimise the location of the booms. INRS-Eau (1993 and 1994) complemented the work using a 2-dimensional study.

A prototype section was installed in Lac St. Pierre in 1993. The section seemed to perform very well and as such, a new boom consisting of 18 sections and 13 pontoons

per section was designed and constructed (with some assistance from Public Works Canada) in 1994. Each section was 400 ft (122 m) wide. All pontoons were 30" (61 cm) in diameter except for sections 5, 10 and 15 (see Annexe 1) which were constructed out of 76 cm pontoons. After observing the performance of the boom during the first winter, a 19 section was added on the south side (section no. 0), all 76 cm pontoons were removed and replaced with 61 cm pontoons and all sections were reduced from 13 to 11 pontoons per section. The extra section was added to promote the ice cover interaction with the artificial islands. The 76 cm booms were replaced because it was noted that these sections carried too much of the load for no good reason. Two pontoons per section were removed to avoid the pontoons hitting in to each other under wave action (during the no-ice period). (Removing 2 pontoons per section did not noticeably reduce the boom's efficiency in subsequent years).

As can be seen in Figure 3.2, the booms were deployed with load cells to measure forces in the cables. After a couple of years of deployment, a statistical analysis of the measured loads was performed primarily by the Canadian Hydraulics Centre (Cornett et al, 1997 and 1998). In addition, these booms were monitored in real time using an Integrated Ice Information System (Morse & Crookshank, 1998).

Due to the success of these booms and the enthusiasm of Fleet Technology, a number of similar booms have recently been deployed elsewhere. Locations include the Rideau River, the Ottawa River, the Pickering nuclear power station and Lake Erie. Ice booms are also proposed for the Chaudière River, to prevent jams at the Missouri / Mississippi Rivers (Tuthill and Gooch, 1998) and to control ice on the St. Maurice River (Carter, 2000).

Regarding estimated loads, Cornett et al. (1997 & 1998) demonstrated that maximum recorded loads on ice booms follow a Gumbel distribution. Timco and Cornett (1994) measured model forces required to free a boom which is frozen into an ice sheet. They also measured forces generated by ice pieces accumulating in front of booms of various sizes and shapes. Foltyn and Tuthill (1996) presented loads measured on booms deployed across North America.

Abdelnour et al (1994) and Cornett and Timco (1995) demonstrate that measured loads depend on boom geometry (size, shape and relative density) and the nature of the links between the pontoons and the cable. For Douglas Fir pontoons, Le Groupe Conseil LaSalle showed that applied forces were very dependent on the nature of the ice sheet geometry at the ice/structure interface. In the physical model studies, Cornett and Timco confirmed this finding.

Michel (1966), among others, demonstrated that loading is a function of the driving forces such as water currents and wind. In fact, he suggested that the most critical conditions could be those generated by wind.

Both the laboratory work and the statistical analysis work on prototype data done at the Canadian Hydraulics Centre (CHC) showed that applied loads are a stochastic process.

# 4 The issues

There are principally two issues regarding these booms. First, despite all the research conducted to date, there is still no definitive document that clearly describes and quantifies the ice/structure interaction for these booms. Second, there is no document that describes the performance of the booms in view of their design.

# 5 Scope of work

In this report, we would like to address these two issues.

First, we estimate ice/structure loading based on three theoretical approaches:

1. We describe different formulas to calculate the environmental forces that the ice cover can apply on the structure. This section is based on very traditional formula and has been applied to calculate potentially extreme loading conditions. It does not take into account an alternative expression developed by Carter (2000) because at the time of writing, we have not yet received his permission to do so. It does not use Shen's (2000) new material aggregate ice model for ice accumulations. It does not use historically recorded wind speed and flow rate data to calculate historical estimates of the ice loading. This data was received to late from the Canadian Coast Guard to include it in this report.

2. The second component of our analysis is an attempt to estimate the maximum applied force that an ice sheet can deliver under bucking and flexural modes of failure. We note that Timco and Cornett's study indicates that for booms similar to the ones examined here (61 cm pontoons), the mode of failure is flexural.

3. The third component of the theoretical analysis is a little more detailed. Using a simple perpendicular-faced ice sheet, based on an analysis of the boom geometry, we develop equations describing the boom's capability to retain the ice.

Second, we present the measured data over the last five winters at three ice booms on the St. Lawrence River. The locations are, from upstream to downstream, Lavaltrie (10 sections), Lanoraie (11 sections) and Yamachiche (20 sections) (see Figure 5.1).

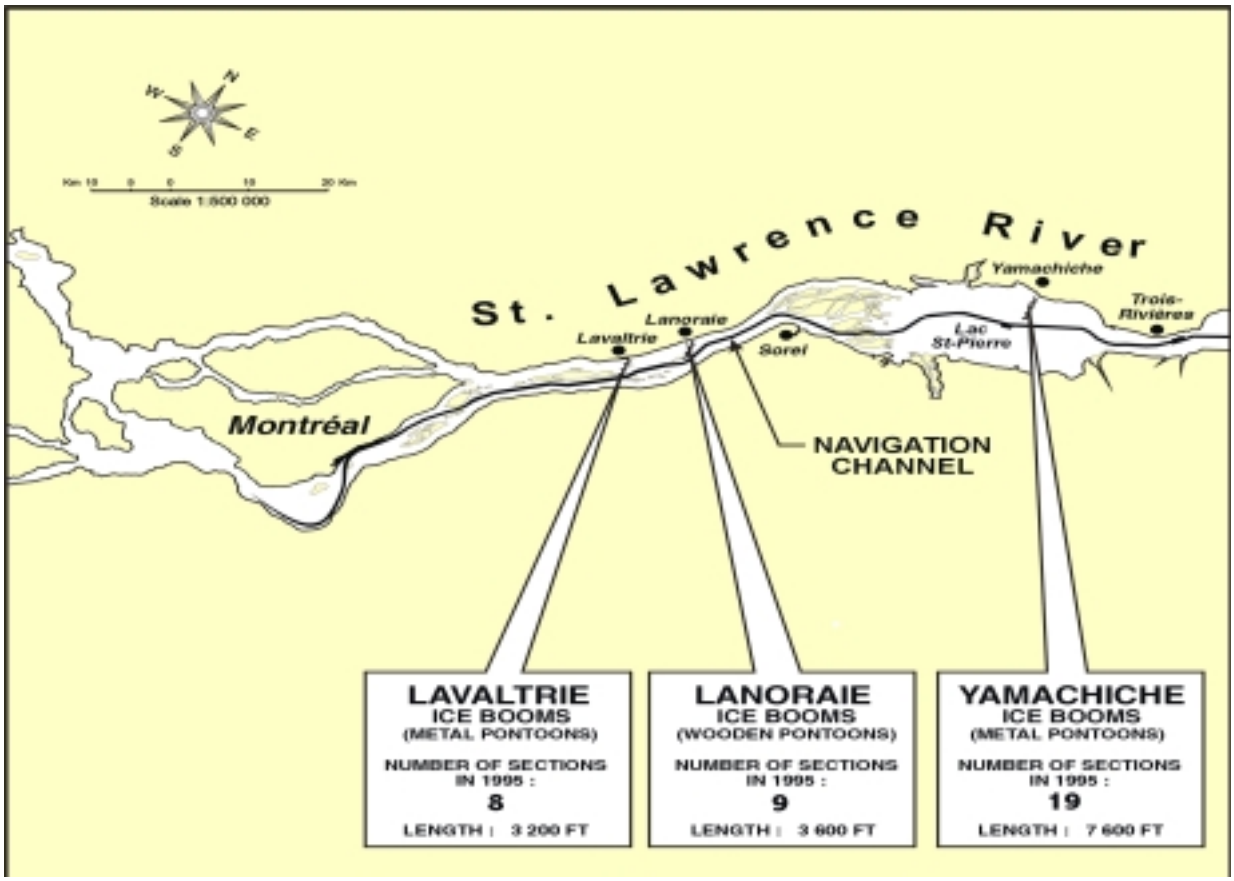


Figure 5.1. Location of St. Lawrence River Ice booms
(Note no. of sections in 1999 is 10, 10 and 20 respectively)

We analyse the force balance equation between the forces in the section cables and the anchor cable. This is followed by an analysis of the force interplay between the tension in one section cable and its neighbour. We analyse spatial distribution of the line loads applied on the anchor cables. Using a spectral analysis we analyse the forcing frequencies and periods. We perform a statistical analysis of the maximum annual measured loads.

During the whole report, we will provide information regarding the performance of the boom, the expected loading and the associated design criteria. We hope to make a more formal summary of these findings at a latter time.

We are proud of some elements of this report. We feel that it does significantly contribute to the advancement of our understanding of the interaction between ice and wide flexible structures form a theoretical point of view, from a temporal-spatial point of view and from a statistical point of view. We also believe that its makes some inroads to explain the large variability in measured loads.

# 6 Environmental Forces

## 6.1 Theoretical background

Many authors have studied loads generated by ice accumulations against ice booms. The most important forces result from water shear on the underside of the ice cover, the wind stress on the ice cover surface and the down slope component of the gravity forces on ice accumulation. Additional forces include ice impact forces, hydrodynamic forces on the frontal edge of the ice accumulation and forces resulting from vessel passing close to the boom (Foltyn and Tuthill, 1996).

The total force on an ice boom ca be expressed as the sum of the following forces:

$$P = F_w \pm F_a + W_i + P_i + P_w + F_v \qquad (6.1)$$

Where:

$F_w$ : water shear on the underside of the ice accumulation

$F_a$ : wind drag force on the ice cover

$W_i$ : down-slope component of the gravity force on the ice accumulation

$P_i$ : force resulting from ice impact

$P_w$ : hydrodynamic force on the frontal edge of the ice accumulation

$F_v$ : force resulting from vessel passage

Latyshenkoff (1946) showed experimentally that as the length of the ice accumulation behind the boom increased, the load exerted by the ice did not build up indefinitely but reached some maximum value. One of the most common problems of the determination of the forces exerted by an ice field is estimating the length or area of the ice cover that contributes to the ice load on the boom. In the literature, there are essentially two approaches to determine the contributing area pushing against an ice boom. The first, normally referred to as Caquot's theory uses the grain in a silo analogy. Ice is considered to be a granular material confined within two parallel side walls. The second approach is used where confinement is unlimited. In this case, the ice accumulation takes on the form of a triangle. The area behind the boom is dependent on the boom width and the apex angle of the triangle.

## 6.2 Environmental ice loads under laterally confined conditions

In 1959, Beccat and Michel (1959) applied Janseen's grain elevator theory. They concluded :
- a part of the ice load is applied to the river banks through the arching of inter ice floes
- the maximum force on ice booms is achieved when the reaction of the banks is equal to any additional incremental load added upstream on the ice accumulation.

- parabolic arches corresponding to the principle directions of the internal inter ice floe stresses make up the final equilibrium load system.

The stress distribution in an ice accumulation is similar to the one of the two-dimensional grain elevator with a top load. The total stress is made up of tangential force ($\tau$) and force exerted at the frontal edge ($p_0$) (see Figure 6.1)

The total force exerted on an arch at a distance x from the edge is given by

$$F = p_0 B \exp\left(-\xi \frac{x}{B}\right) + \frac{\tau B^2}{\xi}\left(1 - \exp\left(-\xi \frac{x}{B}\right)\right) \qquad (6.2)$$

Where:

B: channel width

$\xi$ : coefficient of lateral confinement which depends on angle friction of the ice on the shore (Michel, 1978).

By taking a value $\xi = 0.3$, Michel (1978) obtained the final formulas:

$$F = F_\infty\left(1 - \alpha \exp\left(-0.3\frac{x}{B}\right)\right)$$
$$F_\infty = 3.3\tau B^2 \qquad (6.3)$$
$$\alpha = 1 - \frac{p_0}{3.3\tau B}$$

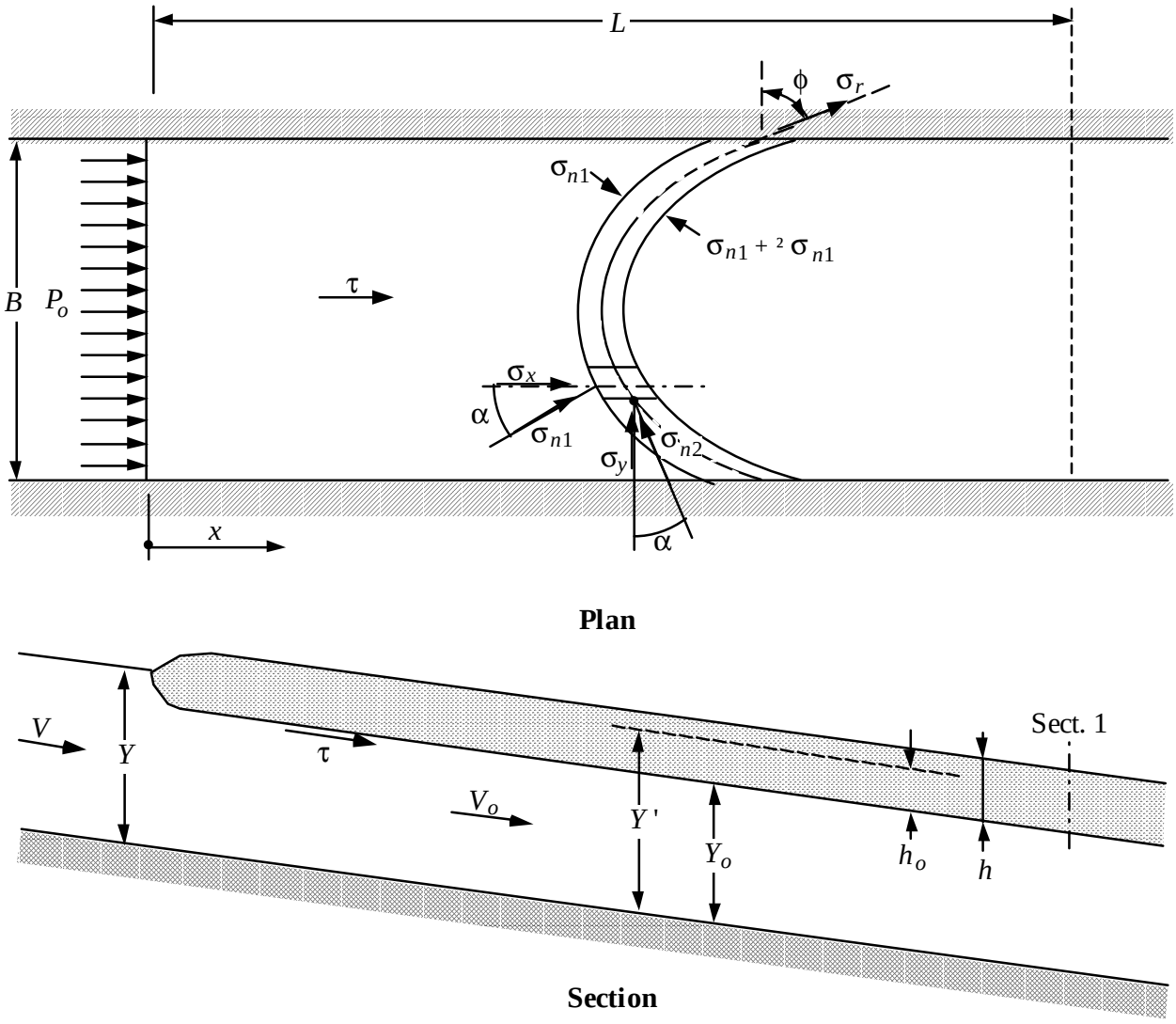


Figure 6.1 : General stress distribution in an ice cover (Michel, 1978)

The tangential force is calculated as follows:

$$\tau = \tau_w + \tau_a + \eta \qquad (6.4)$$

Where

$\tau_w$ : water tangential stress

$\tau_a$ : wind tangential stress

η: longitudinal component of the weight of the ice accumulation

$$\tau_w = \rho C_D V^2 \qquad (6.5)$$

where $V$ is the water velocity (m/s), $\rho$ is the mass density of water (1000 kg/m3) and $C_D$ is the drag coefficient of water.

Suggested values of $C_D$ are presented in the following table.

Table 6.1: Measured water drag coefficients (based on Carter, 1995)*-

| Author | $C_D$ (1m) X 10-3 |
|---|---|
| Johannessen (1970) very rough | 26.6 |
| rough | 12.8 |
| smooth | 13.4 |
| Untersteiner & Badgley (1965) | 10.5 |
| McPhee (1975) | 3.4 |
| Campbell (1965) | 12.0 |
| Hunkins(1966) | 7.8 |
| Michel (1978) | 3.9 |
| Carter (1995) | 41.3 |

$$\tau_a = \rho_{air} C_{Dair} U^2 \qquad (6.6)$$

where $U$ is the wind velocity (m/s), $\rho_{air}$ is the mass density of air (1.293 kg/m3 at 0oC) and $C_{Dair}$ is the drag coefficient of flowing air over the ice cover.

The range of values of $C_{Dair}$ reported by Michel (1978) is 1.3x10-3 to 4.4x10-3. Foltyn and Tuthill (1996) gave a range 1.7x10-3 – 2.2x10-3.

The gravity stress is given by :

$$\eta = (1-e)\gamma_{ice} hS \qquad (6.7)$$

where $\gamma_{ice}$ is the specific weight of ice and *e* is the porosity (0.3), it is found

$$\eta = 4410hS \qquad (6.8)$$

The hydrodynamic force on the frontal edge ($p_0$) is given by the momentum theory. This force is generally neglected in the computation of forces exerted by ice on structures.

Michel (1978) estimated the maximum hydraulic thrust and thrust caused by wind by using the following assumptions:

the porosity of the ice accumulation = 0.3

the internal angle of friction = $30^o$

the wind speed = 33 m/s at standard 10 m above the ground

Michel (1966, 1978) proposed the following formula to determine the ultimate push of an ice accumulation against a boom :

Maximum hydraulic-induced load ($P_w$):

$$P_w = 0.016\ h^2\ B\ (kN) \qquad (6.9)$$

where *h* is the ice thickness (m) and *B* is the width (m).

Maximum wind-induced load ($P_a$):

$$P_a = 0.0176\ B^2\ \ (kN) \qquad (6.10)$$

However, since the ice accumulation cannot thicken by an amount greater than the river depth (H), (the river bottom would then take a great part of the load), there is a limitation given by

$$P_a \leq 1.0h^2\ B \qquad (6.11)$$

Michel (1978) stated that the maximum possible thrust on a structure could readily be obtained from equations 6.9 to 6.11.

For a grounded ice field in a depth of water H (m), Carter (1994) deduced from Michel's analysis that the maximum ice line load (w in kN/m) can be written as follows:

$$w = 1.0\ H^2 \qquad (6.12)$$

Carter (1994) used this equation to compare loads calculated by this limiting value with those measured experimentally on the Yamachiche ice booms on Lac St. Pierre. He characterised the correlation as very good given the dynamics of the loads in question.

## 6.3 Environmental ice loads under laterally unconfined conditions

The ice force depends on the size of the ice accumulation in front of the boom. The problem of the determination of the extent of the upstream ice accumulation has been studied since 1935 by many investigators. Latshynekoff (1946) found experimentally that the length of the ice cover attained a constant value after a length of three to four times the width of the field. The U.S. Army Corps of Engineers (1999) recommends to derive ice loads acting on the boom from an area that extends upstream an amount corresponding to five river widths. Abdelnour and al. (1993, 1996) estimated this area by evaluating the apex angle (see Figure 6.2). They state (1996) « The area covered by ice pieces retained by the boom will probably increase steadily during an event, starting with the areas in front of the individual spans (e.g. the areas labelled A1 to A8 in Figure 6.2). When two or more adjacent spans are completely filled with ice, ice pieces will then collect over a large area (e.g. areas B, C, D and E in Figure 1.2 ). The ice area will increase until it covers the total width of the boom. This will produce the highest ice forces on the boom as the ice area has reached its maximum. »

An ice cover length of three to four times longer than the width of the boom is equivalent to an apex angle ranging from 15° to 20° (Abdelnour and al. 1993). Abdelnour and al. (1991) found that an apex angle of 60° correlated well the drag force required to drive the ice cover past two different types of bridge piers at Laviolette Bridge on the St-Lawrence River. Consequently they used an apex angle of 60° in the study of Lavaltrie ice boom.

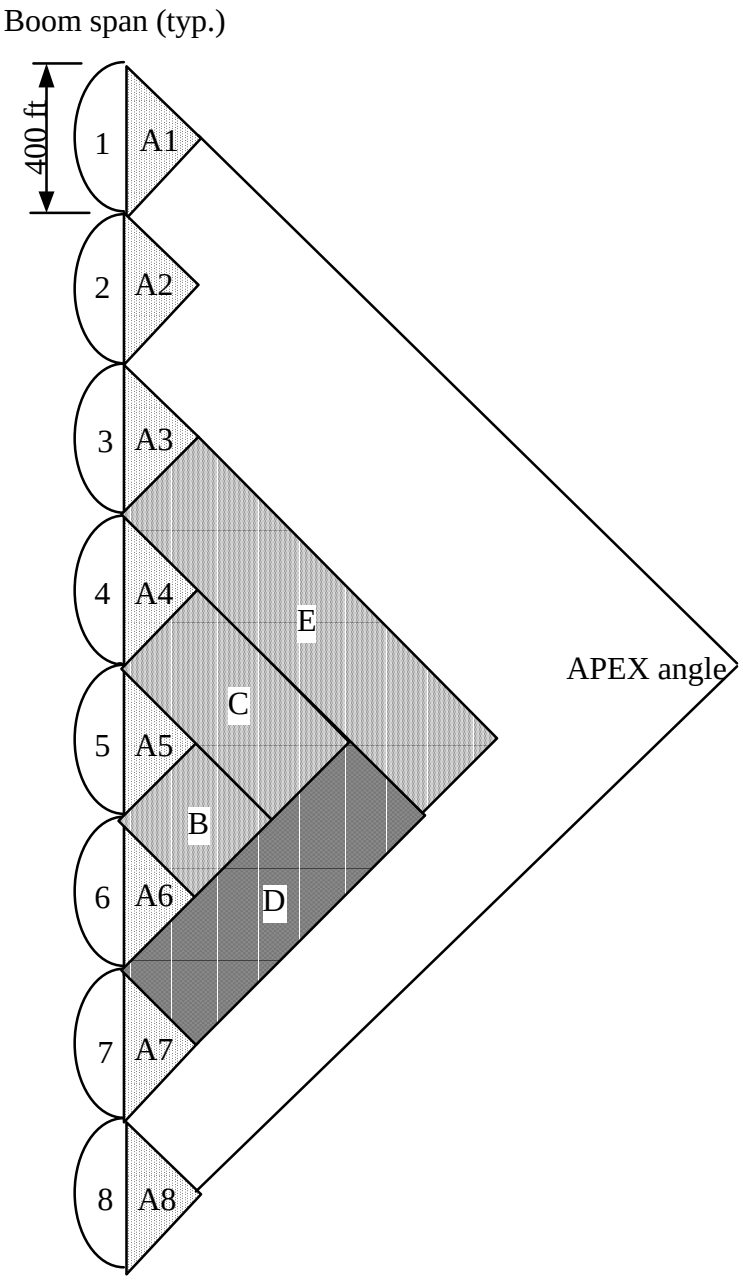


Figure 6.2: Ice accumulation in front of the boom (Abdelnour et al. (1993))

Abdelnour et al. (1995) assume that the ice accumulation in front of the boom is acted upon by wind and current forces. With their approach the currents and winds are assumed to be uniform over the area of ice cover. The wind and current forces were predicted as follows :

$$F_{current} = \rho C_D V^2 A_c \tag{1.13}$$

$$F_{windt} = \rho C_{Dair} U^2 A_w \tag{1.14}$$

Where $F_{current}$ and $F_{wind}$ are the current and wind drag forces respectively and $A_c$ and $A_w$ are the surface areas of the ice cover acted upon the current and the wind respectively given by

$$A_c = A_w = \frac{B^2}{4\tan(\alpha/2)} \tag{1.15}$$

where $\alpha$ is the apex angle of the triangular ice area upstream the boom.

It should be noted that the U.S. Army corps of Engineers determines the ice forces by using

$$A_c = A_w = 5B^2 \tag{1.16}$$

For estimating the value of drag coefficient current, Abdelnour et al. (1995), expected a rafted ice cover. A value for $C_D$ = 0.015 was selected in the analysis of forces acting on Lac St-Pierre ice booms and $C_{Dair}$ was taken as 0.0033. These values were found to be within the range of the loads measured by Cowper et al. (1994). It should be mentioned that these values are not constant during the winter. The ice is rough during the ice formation stage and becomes smoother when the ice consolidated (Abdelnour et al., 1995)

The line load is given by:

$$W = \frac{B}{4\tan(\alpha/2)}\left[1000 C_D V^2 + 1.293 C_{Dair} U^2\right] \tag{1.17}$$

With the values of the drag coefficients and the apex angle assumed by Abdelnour et al. (1995), equation (1.17) becomes:

$$w = 0.433B\left[15V^2 + 0.0043U^2\right] \tag{1.18}$$

## 6.4 **Environmental loads for St. Lawrence River booms**

The wind velocity, the water currents and the ice thickness are prerequisite to the determination of loads on ice booms.

### 6.4.1 Water currents

For the Yamachiche boom, experimental observations were made on the northern part of Lac St-Pierre during the month of January 1995 and are reported by Carter (1995).

Current profiles were made at ten locations under the ice covers. The average value of all current velocity is calculated by Carter (1995). The maximum velocity of all average values is 0,27 m/s and the mean velocity is approximately 0.16 m/s. The average current velocity in Lac S-Pierre was also obtained by Abdelnour et al. (1994) from a 2D hydrodynamic model run. The average current velocity reported is 0.35 m/s for open water current conditions.

For Lavaltrie and Lanoraie boom, an ice survey was made by the St Lawrence Ship Channel group (Department of Transport) in January, February and March 1973. The values obtained are summarised in Table 6.2.

Table 6.2 Average and maximal currents at Lanoraie and Lavaltrie

| Location | maximal current (m/s) | average currents (m/s) | discharge at Sorel (m3/s) |
|---|---|---|---|
| Lanoraie | 0.66 | 0.32 | 11540 |
| Lavaltrie | 0.55 | 0.38 | 11334 |

It should be noted that these measurements were made a few metres downstream of booms. The estimated discharge in the St. Lawrence river at Sorel at that time show that the currents were measured under very in high winter discharge conditions.

Beauchemin and Pellegrin, 1969, measured the surface currents at Lavaltrie boom location. The average values are summarised in table 6.3

Table 6.3. Average surface currents at Lavaltrie boom location

| Survey time and date | Mean surface current across full width of boom (m/s) | Mean surface current across boom spans 2, 3 and 4 (m/s) |
|---|---|---|
| 13h00 June 2, 1969 | 0.70 | 0.68 |
| 15h00 June 2, 1969 | 0.67 | 0.64 |

Since the Lavaltrie ice boom is located in channels parallel to the navigation channel, for the same discharge in the river, the current near the boom is expected to be lower in winter than it is in summer. Once an ice cover forms upstream of the boom, because of the increased resistance on that side of the island, relatively more of the flow will follow the main (navigation) channel.

Finally, Abdelnour et al. assumed a "design current" of 0.76 m/s for the study of Lavaltrie ice boom. The current used for the Lanoraie ice boom is slightly less than 0.70 m/s (Abdelnour et al., 1995).

## 6.5 Wind conditions

The wind speeds were recorded at Sorel weather station for winter 1994/1995. The wind speeds normal to the ice boom for Lavaltrie, Yamachiche and Lanoraie are shown in Figure 6.3 (Abdelnour et al., 1995). This figure indicates that the normal wind speeds are almost identical for all three booms. So, it can be assumed that all three booms are at a $45^{o}$ angle with the north direction (Abdelnour et al., 1995). This angle corresponds to Lavaltrie's one. In a previous study, Abdelnour et al. (1993) suggested a design wind of 11.2 m/s acted perpendicularly on the boom.

Using the data of wind speed and direction recorded in January 20-21, 1995, Carter (1995) reported an estimated value of 20.6 m/s for wind speed in the northern part of Lac St-Pierre.

## 6.6 Ice thickness

There are many meteorological and hydrodynamic factors which affect ice formation and growth. The ice conditions in Lac St-Pierre have been described by earlier work (Carter, 1980, Abdelnour et al 1989). Border ice thickness during December is less than 10 cm and increases during the months of January and a full ice cover in February. An approximate value of 90 cm can be reached in March (Abdelnour, 1995).

Measured ice thickness in Lac St-Pierre for the years 1983 to 1986 has been presented in Abdelnour et al. (1989) (Figure 6.4). Ice thickness differs from one location to another and from one year to year. The maximal value recorded is about 70 cm.

Experimental observations are also made on the northern part of Lac St-Pierre during the month of February 1996 (Carter, 1995). The data obtained give an average value of approximately 38 cm for the ice thickness.

From the statistical study of the freezing index, Carter (1994) provided a predication of the average and maximum ice thickness along the St Lawrence waterways (see Figure 6.5). The values has been obtained by the use of this equation:

$$z = \alpha\sqrt{s} \tag{6.18}$$

Where z is the thickness of the ice cover (inches), s is the freezing degree-day accumulation (°F-days) and $\alpha$ is a shelter coefficient having a value ranged from 0.4 to 1.

Table 6.4 gives the mean values for the 20-year period and the probable ice thickness for three various intervals of recurrence 5, 10 and 50 years.

Table 6.4. Maximum and average ice thickness (cm) for Lac St-Pierre (Carter, 1995)

| | Mean value | Periods of recurrence | | |
|---|---|---|---|---|
| | | 5 years | 10 years | 50 years |
| Maximum thickness | 111 | 118 | 121 | 127 |
| Average thickness | 78 | 83 | 85 | 89 |

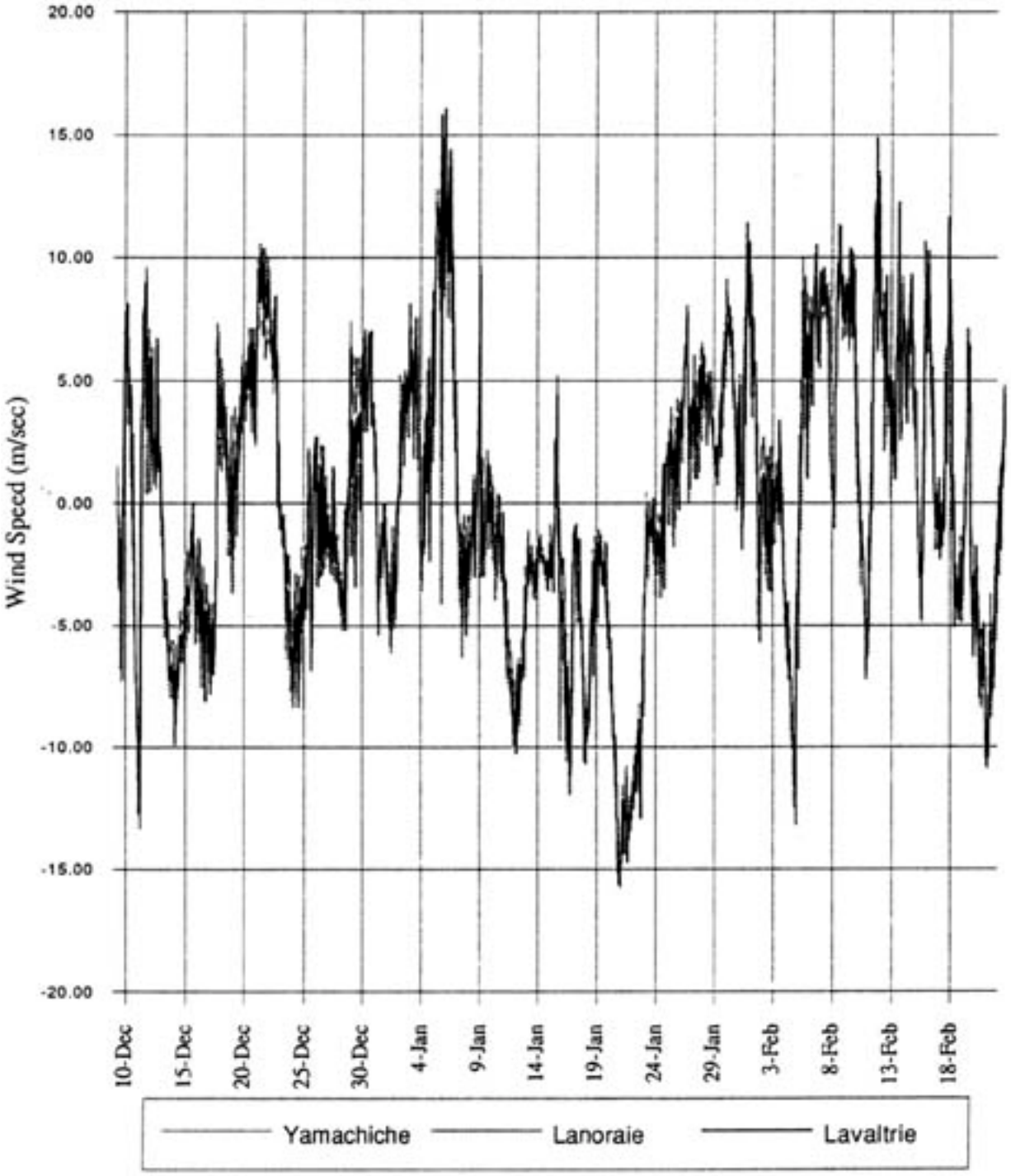


Figure 6.3: Wind speed normal to the ice booms – Winter 1994/1995 (Data from Sorel weather station in Lac-St Pierre (Abdelnour et al., 1995).

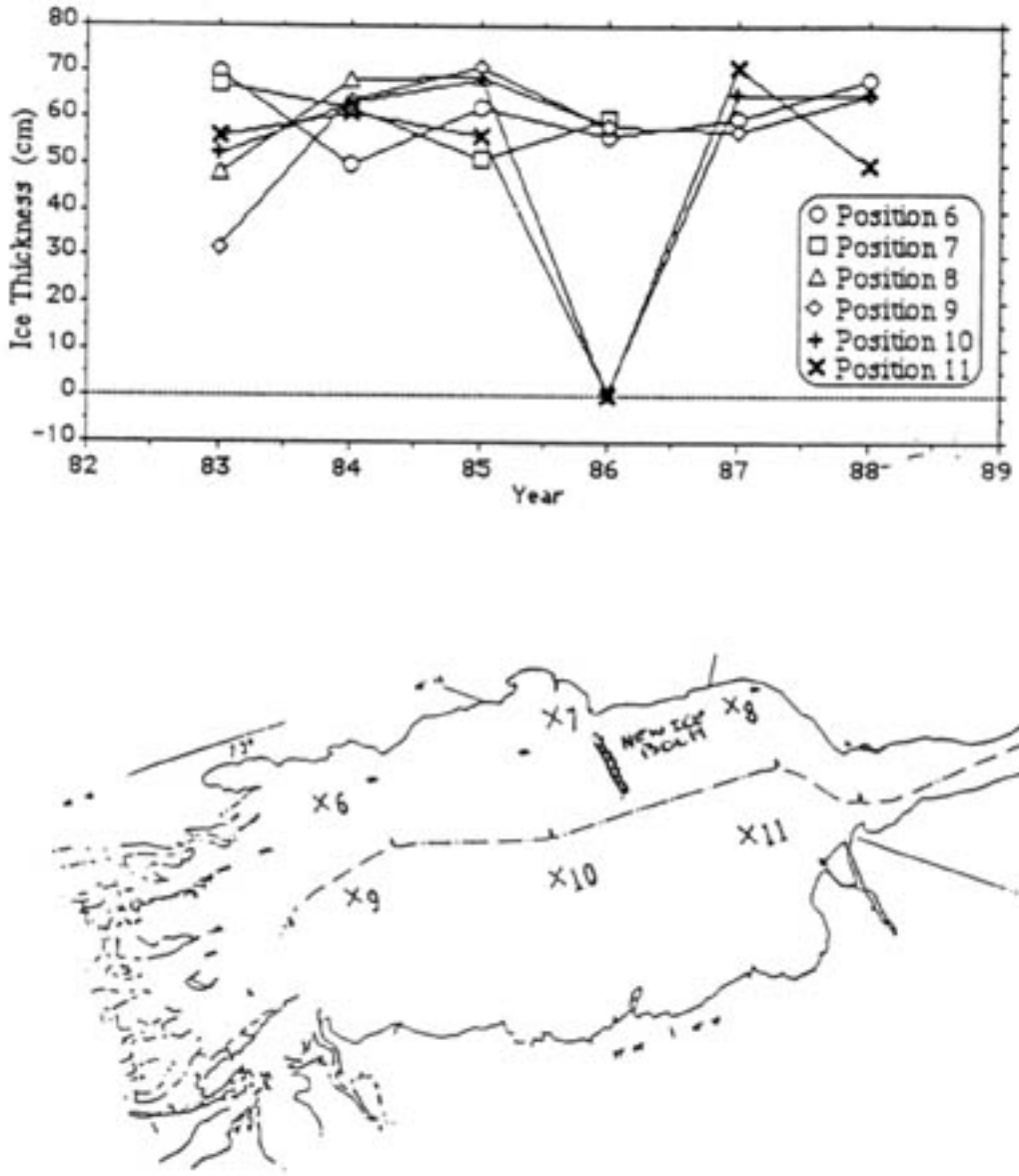


Figure 6.4: Measured ice thickness and its location on Lac St-Pierre (Abdelnour et al. 1994).

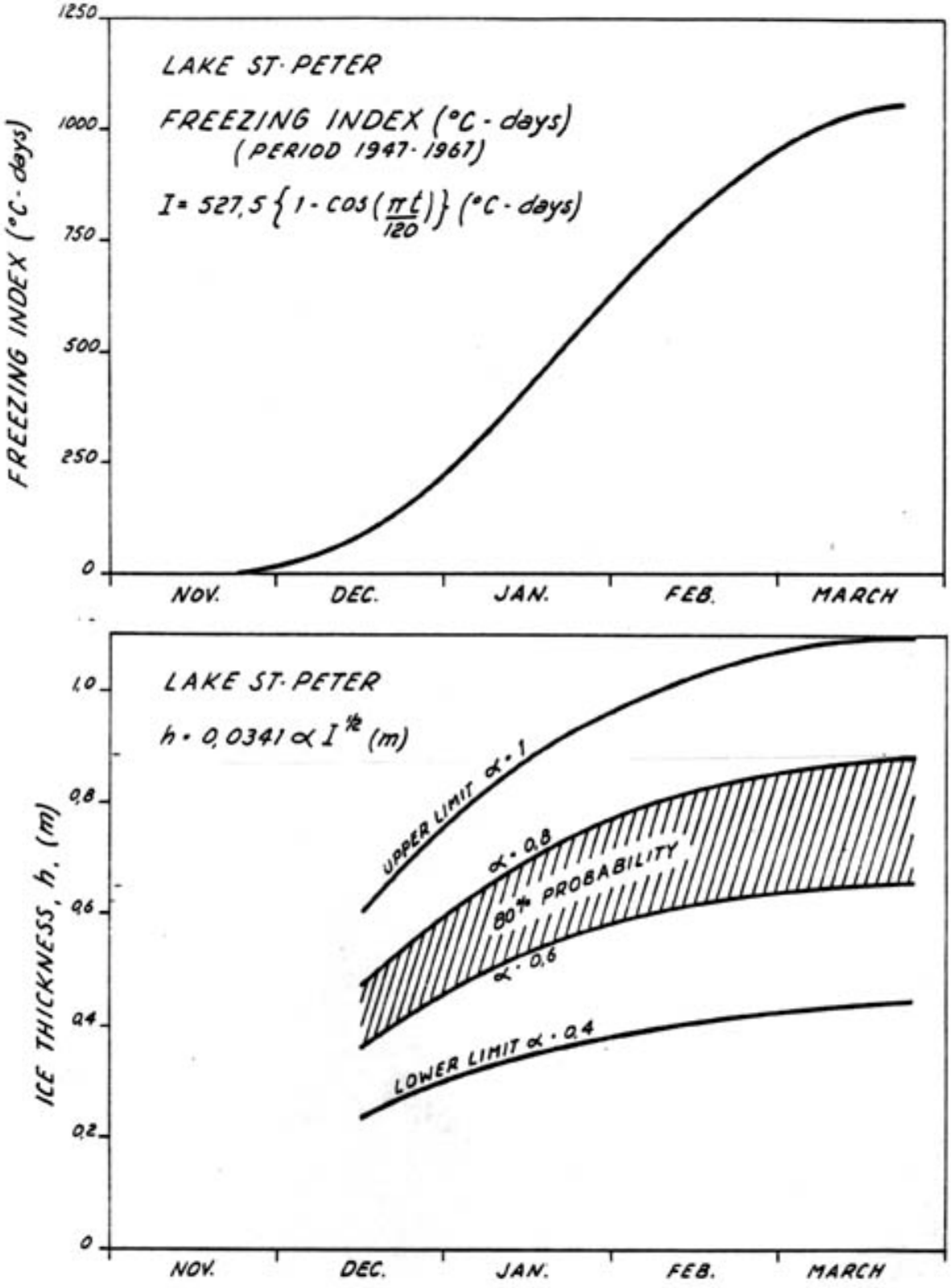


Figure 6.5: Predicted ice thickness on Lac St-Pierre (Carter, 1995)

## 6.7 Force calculation

The ice forces acting on the ice boom were calculated using equations suggested by Michel (1966, 1978) and Carter (1995, 1999) and the approach developed by Abdelnour et al. (1993, 1995). For the drag coefficients, we use the values suggested by Carter 1995 because these values were deduced from experimental observations of wind and currents made in Lac St-Pierre in 1995. The drag coefficients adopted are

For water $C_D$ at 1 m = 41.1 x$10^{-3}$

For wind $C_D$ at 10 m = 3.4 x$10^{-3}$

### 6.7.1 Michel's equation

In order to use Michel's equation, the water level is required. The daily water levels in Lac St-Pierre for a number of winters are shown in Figure 1.6. The water level fluctuates from 3.7 m to 6.3 m. The average value of water is approximately 4.5 m. So the force per unit width is calculated as follows:

$$w = 1.0\ H^2\ (\text{kN/m}) = 20.2\ (\text{kN/m}) \qquad (6.20)$$

The value given by the above equation is the maximal trust that can be exerted on a boom (under the influence of the wind force). It should be noted that equation 6.20 should not be applied for Lavaltrie and Lanoraie since the current there is relatively high and therefore the ice accumulation doesn't ground.

The equation given by Abdelnour et al. is expressed as follows:

$$w = \frac{B}{4\tan(\alpha/2)}\left[1000 C_D V^2 + 1.293 C_{Dair} U^2\right] \qquad (6.21)$$

With the value of drag coefficient estimated by Carter (1995), it may be written as:

$$w = \frac{B}{4\tan(\alpha/2)}\left[41.1 V^2 + 0.0044 U^2\right] \qquad (6.22)$$

A $60^o$ apex angle and a 20.6 m wind speed are assumed in this study. So equation (1.22) becomes:

$$w = 0.433 B \left[41.1 V^2 + 1.87\right] \qquad (6.23)$$

The forces obtained for the three ice boom are shown in Table 6.5.

Table 6.5. Average forces estimated by Abdelnour et al. equation (kN/m)

| Boom location | With average velocity | With maximal velocity |
|---|---|---|
| Yamachiche | 3.1 | 5.1 |
| Lanoraie | 3.2 | 10.4 |
| Lavaltrie | 8.2 | 15.1 |

### 6.7.2 Comparison of estimated forces

The comparison of maximal values of line load estimated by different methods is shown in Table 6.6. The values obtained by Michel's equations are higher than those estimated by equations suggested by Abdelnour et al. It should be mentioned that Abdelnour et al. assumed a triangular area of ice accumulation which does not always correspond to in-situ observations. The ice field can be fully or partially confined. Alternatively, the triangular of ice accumulation sometimes extends to the shore. The area should be multiplied approximately by two to get more realistic values of forces. On the other hand, because the fields are not always fully confined, one cannot use the Caquot approach in all cases.

Table 6.6. Maximal forces estimated by different equations (kN/m)

| Boom location | Michel's equations | Abdelnour et al.'s equations |
|---|---|---|
| Yamachiche | 20.2 | 5.1 |
| Lanoraie | 21.6 | 10.4 |
| Lavaltrie | 21.5 | 15.1 |

# 7 Analysis of Ice/Structure interaction

## 7.1 Analysis of load retaining capacity

Previously, we have estimated the magnitude of the ice push on the boom. We saw that it was a function of the effective area of the ice sheet and the environmental driving forces. In this chapter, we will examine the boom's ability to counteract a push. We will see that it is primarily a function of the size of the boom and the thickness of the ice sheet.

To our knowledge, previous analyses of a boom's ice retention capacity have been one- or two-dimensional. However, in reality, booms behave in a fully three-dimensional fashion. While the following analyses remain primarily two-dimensional, we will at least try to incorporate some of the three dimensional aspects of a booms behaviour.

### 7.1.1 Anchor cables

Anchor cables have a catenary shape. Under small loading conditions, the anchor cables rest on the river bed. As soon as important loads are applied, the cable becomes taut from anchor to junction plate. Consider the boom at Yamachiche. Typically, the junction plates are about 2 m above the bottom. The anchor cables are 38 m in length. Applying the equations for a catenary, at the water surface, under small loads, the cable forms a 5° angle with the horizon. At larger loads, the angle approaches 3° (= arcsine(2/38)). In the previous analysis, we assumed that the barrels attached to the junction plates (see Figure 3.3) have sufficient buoyancy to keep the junction plates afloat. However, strictly speaking, the junction plates' depth below the surface depends on total water depth (2 to 6 m), the cable's length (normally 38 m depending on how precisely the anchors were installed), on the barrel dimensions, on the ice conditions around the barrel and on the applied load. We also note that at Lavaltrie and Lanoraie, the water depths are greater (typically 5,5 m) but the cable are longer (typically 76 m) and therefore the calculated angles of 3° to 5° presented above are still approximately correct for all St. Lawrence River boom locations.

### 7.1.2 Section cables

The section cables start at the junction plates. Although we have just seen that their depth below the surface (at the junction plate) is variable, in normal conditions, we can assume it to be equal to that distance from the junction plate to the centre of floatation of the junction barrel. In the case of the Yamachiche booms, this value is about 1,5 m.

As we move along the section cable away from the junction plate, pontoons are attached and keep the cable afloat near the water surface. As the ice applies a load on the pontoons, they pull the section cable up nearer the surface. Therefore, the depth of the cable near the pontoon will depend on the diameter of the pontoon (0,61 m in our case),

the length of chain connecting the pontoon to the cable and the angle that the chains make with the horizon. For the sake of argument, let's say that the chain is about 1,2 m long and the angle of the chain is 10 degrees. The cable will then be about 0,8 m below the surface.

So at the junction plate, the section cable is about 1,5 m below the surface whereas in the middle of the cable, under the stretching of the cable by the applied force on the pontoons, the cable will be about 0.8 m below the surface. If we assume that this climb is linear between the plate and the middle portion of the cable, we can calculate its horizontal rise = about 0.3°. The calculation is based on a linear distance between the plate and the middle of the cable equal to the sag = 137 m (0.3° = arcsine((1,5-0,8)/137).

### 7.1.3 Connecting chains

Let's now consider the chains. At one end of the chain, the net applied force on the pontoon is horizontal. Any vertical forces are counterbalanced by the buoyancy of the pontoons. At the other end of the chain, it is being pulled down by the cable at an angle of 0,3°. The chain must also support its own net weight and that of the cable's under water. The chain's weight is negligible and given that the cable weight is relatively small (6.4 pounds per foot), under high loading conditions, since the forces at each end of the chain are near horizontal, the chain itself will tend to form a very small angle with the horizon. Its actual value is presented in Figure 7.3.

The above reasoning about the anchor cable, section cable and the chains will govern our analysis of the force required to fully submerge the pontoons.

In an ideal analysis all pontoons attached to the section cable should be individually examined. In a complete analysis, there are important lateral forces that must be considered. It is only the centre pontoon that is perpendicular to the flow. All other pontoons have loads applied at an angle to the current (due to the aggregate characteristics of the ice). Starting with the pontoons near the junction plate, the booms form an angle of about 56° with respect to the flow. This angle promotes the concentration of ice towards the centre of the section cables. Therefore, the loads applied at centre pontoons are much larger than those applied on the pontoons near the junction plates. In addition, due to the projected buoyancy of the pontoons per unit width, the resisting force per unit width is larger near the junction plates than it is at mid-span. Finally, in the centre, there is greater lateral confinement of the accumulation. These three facts explain why we will often see an ice run only over the central 5 pontoons.

Notwithstanding the latter, we will analyse the retaining capacity of the centre pontoon only. After multiplying by the number of pontoons per section cable (11), we will calculate approximate the retaining capacity of the section cable. Given the fact that we are not doing a force balance on each pontoon, we realise that the analysis is simplistic.

Really, a complete analysis of the three dimensional structure of the boom and of the applied ice loads is required but is beyond the scope of this effort.

### 7.1.4 Pontoons

Referring to Figure 3.1, assuming that acceleration is zero, we can write the static force equilibrium for different components.

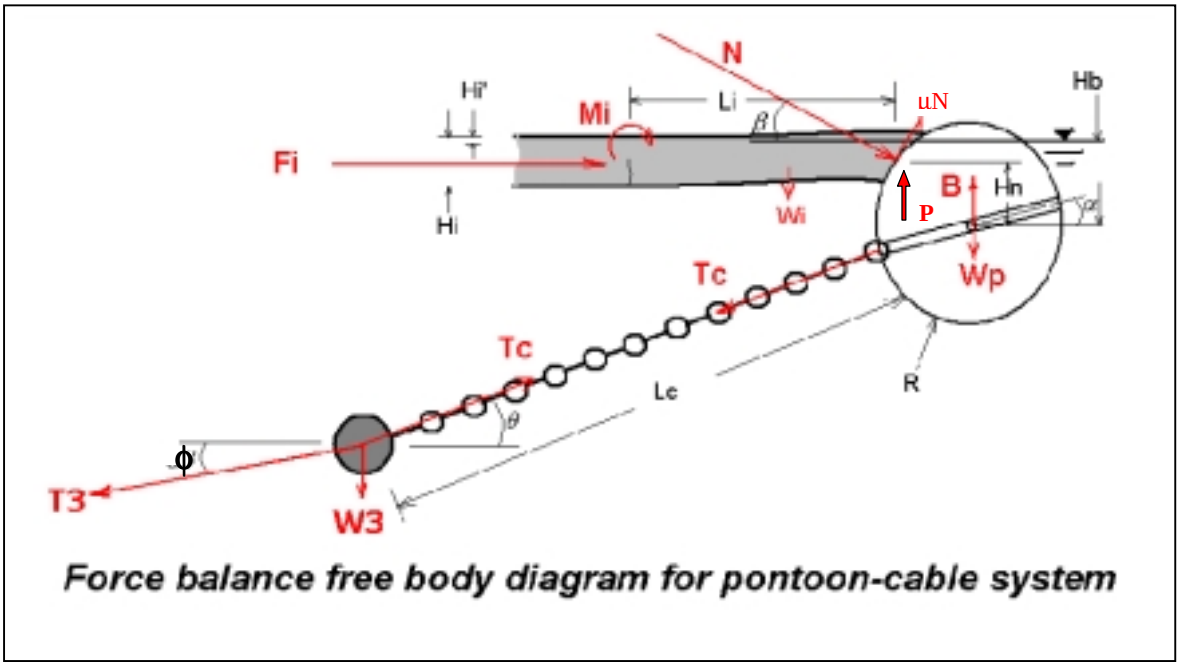


*Force balance free body diagram for pontoon-cable system*

Figure 7.1 Definition sketch for pontoon force balance equations

### 7.1.5 For pontoon equilibrium:

$$7.1..Moment:.....(Tc\cos(\theta))(R\sin(\alpha))-(Tc\sin(\theta))(R\cos(\alpha))+\mu NR=0$$

$$7.2..Horizontal:...N\cos(\beta)-Tc\cos(\theta)+\mu N\sin(\beta)=0$$

$$7.3..Vertical:.....N\sin(\beta)+Wp-B+Tc\sin(\theta)-\mu N\cos(\beta)=0$$

### 7.1.6 For section cable equilibrium:

$$7.4..Horizontal:...T_3\cos(\alpha_3)-Tc\cos(\theta)=0$$

$$7.5..Vertical:.....T_3\sin(\alpha_3)-Tc\sin(\theta)+W_3'=0$$

### 7.1.7 From geometric relationships:

$$7.6..Buoyancy...B = \gamma Lp(R^2(\cos(\delta)\sin(\delta) + \pi - \delta/\pi)$$

$$.....where.....\delta = \arccos(Hb/R)$$

$$7.7..Load.at....\beta = \arcsin[(Hb - 0{,}5Hi - Hi')/R]$$

### 7.1.8 For the ice sheet:

$$7.8a..Horizontal....Fi = N\cos(\beta) + \mu N\sin(\beta)$$

$$7.8b..Vertical.....P = N\sin(\beta) - \mu N\cos(\beta)$$

### 7.1.9 For the whole thing:

$$7.9..Horizontal....T_3\cos(\phi) - N\cos(\beta) + \mu N\sin(\beta) = 0$$

where the angles are defined in Figure 7.1 and:

$T_c$ is the tension in the chain (kN)
R is the pontoon radius (m)
$\mu$ is the coefficient of ice/steel kinetic friction (-)
N is the normal load applied by the ice sheet (kN)
$W_p$ is the weight of the boom (kN)
B is the buoyancy for of the boom (kN)
$T_3$ is the tension in the cable caused by the pontoon (kN)
$W_3$' is the net weight of the cable and chains in water (kN)
$\gamma$ is the density of water (kN/m$^3$)
$L_p$ is the length of the pontoon (m)
$H_b$ is the submergence of the pontoon (m)
$H_i$ is the ice thickness (m)
$F_i$ is the horizontal thrust of the ice sheet (kN)
$\alpha$ is the angle of rotation of the pontoon
$\beta$ is the angle of contact between the ice sheet and the pontoon
$\delta$ is an angle proportional to the degree of submergence of the pontoon
$\phi$ is the angle at which the section cable is being pulled with respect to the horizon
$\theta$ is the angle of the chain with respect to the horizon

Note that the analysis is made for a whole pontoon. Therefore (11 times $F_i$) is the load in the anchor cable (kN) and (0.5 times Tc) is the actual load in each chain (kN).

For the solution of these non-linear equations, we assumed that the pontoon was fully submerged ($H_b$ = R). We then solved the equations by trial and error using an Excel spreadsheet. Note that $\phi$ changes very little nor are the equations overly sensitive to the value of $\alpha$.

The results of the analysis are given in the following Figures.

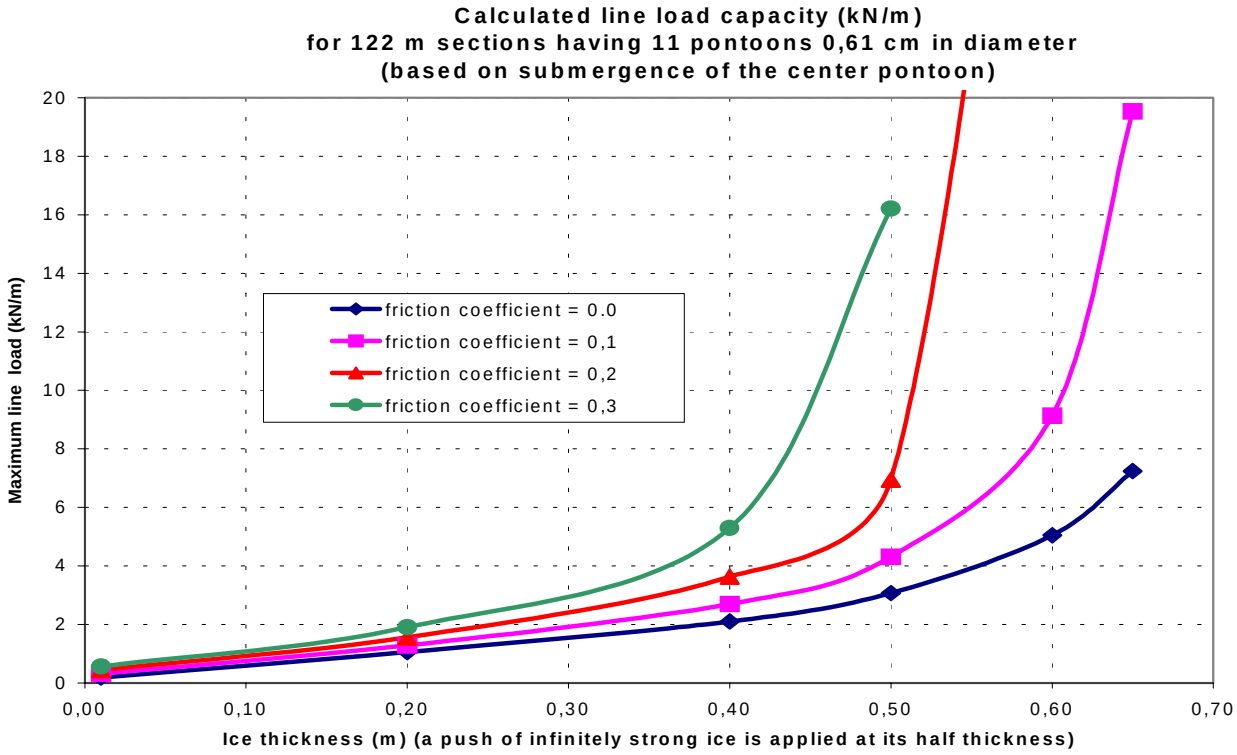


Figure 7.2 Calculated line load capacity (kN/m)

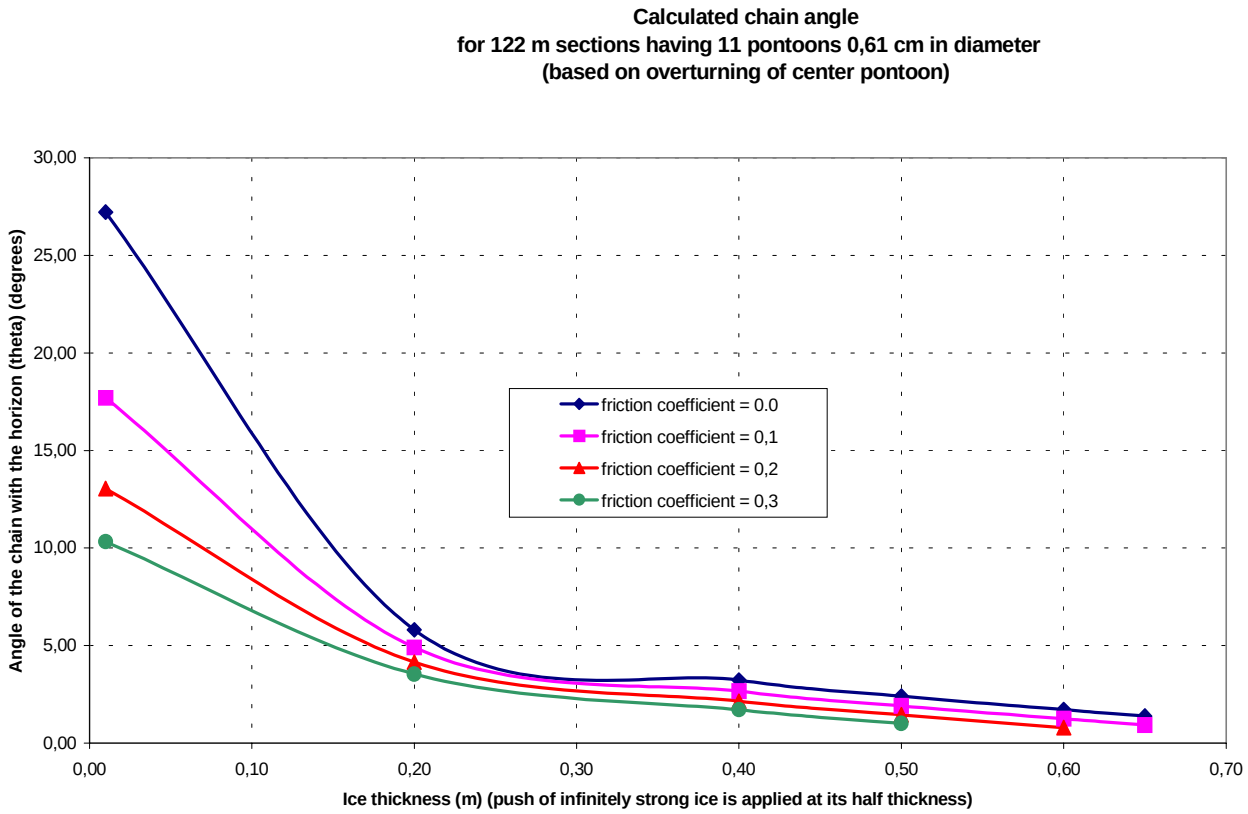


Figure 7.3 Calculated chain angle

Figure 7.2 demonstrates that the calculated boom capacity corresponds very well to observed values. We note that retention capacity increases more or less linearly until such time as a critical ice thickness is reach. The resistance capacity then skyrockets. The critical thickness is a function of the friction coefficient $\mu$. For $\mu = 0$, the critical thickness is about 70 cm. For $\mu = 0.1$, the critical thickness is about 60 cm. For $\mu = 0.2$, the critical thickness is about 50 cm. For $\mu = 0.3$, the critical thickness is about 45 cm.

The angle that the chain makes with the horizon is presented in Figure 7.3. As soon as there is any applied force at all, the angle becomes less than 5 degrees.

Figure 4 shows that at small loads, the rotation of the pontoon is very sensitive to the coefficient of friction. This means that the booms are rotating a good deal at the beginning of the season. As soon as significant forces are applied, the pontoons stop rotating. They take on a stable angle to counter the rotation produced by the friction between the ice and the pontoon.

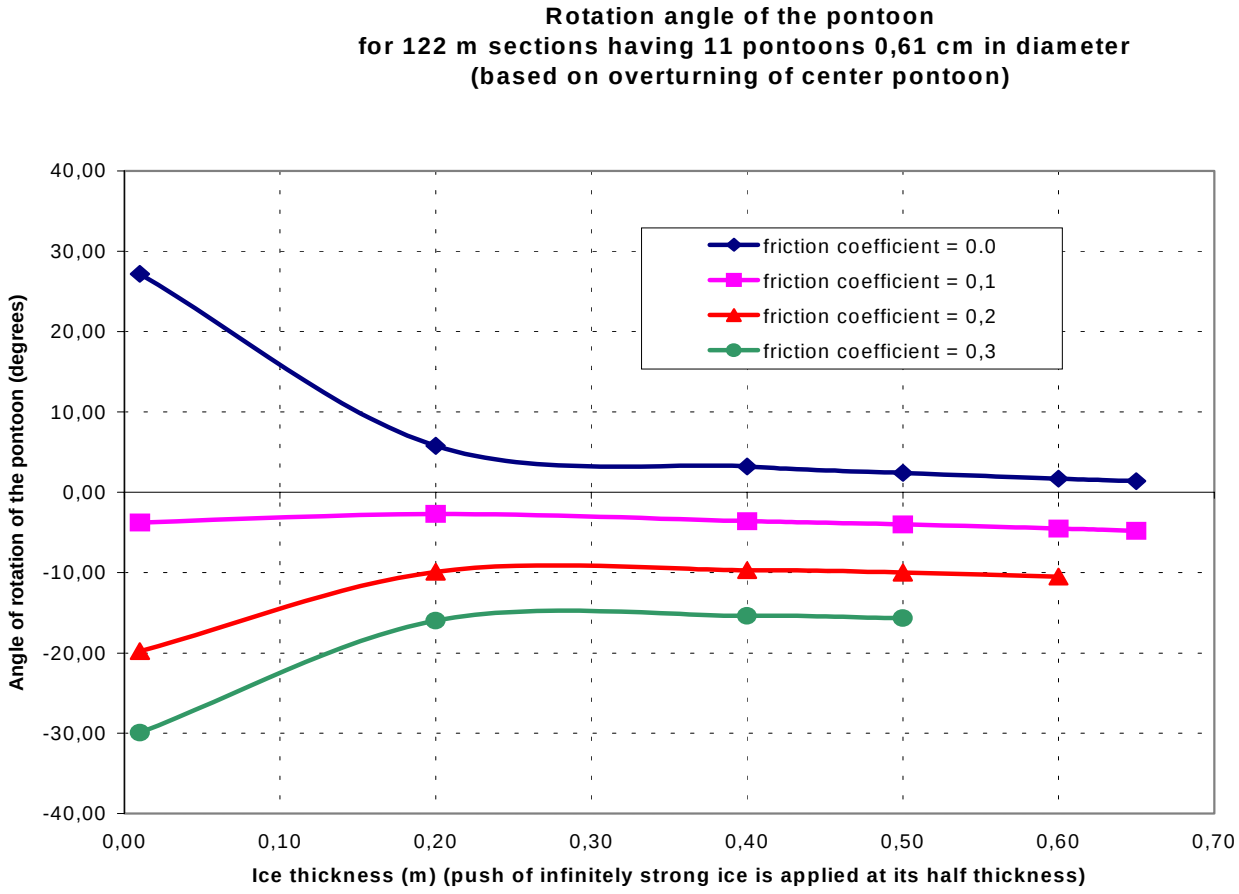


Figure 7.4 Rotation angle of the pontoon

Figure 7.5 presents the tension in the chains. We note that as soon as the forces become interesting, the working load limit of the chains (75 kN) is exceeded. We also know that, occasionally chains break. (The ultimate load of the chains is evaluated at about 450 kN). To achieve this load, the ice must be somehow wedged in or frozen into the boom.

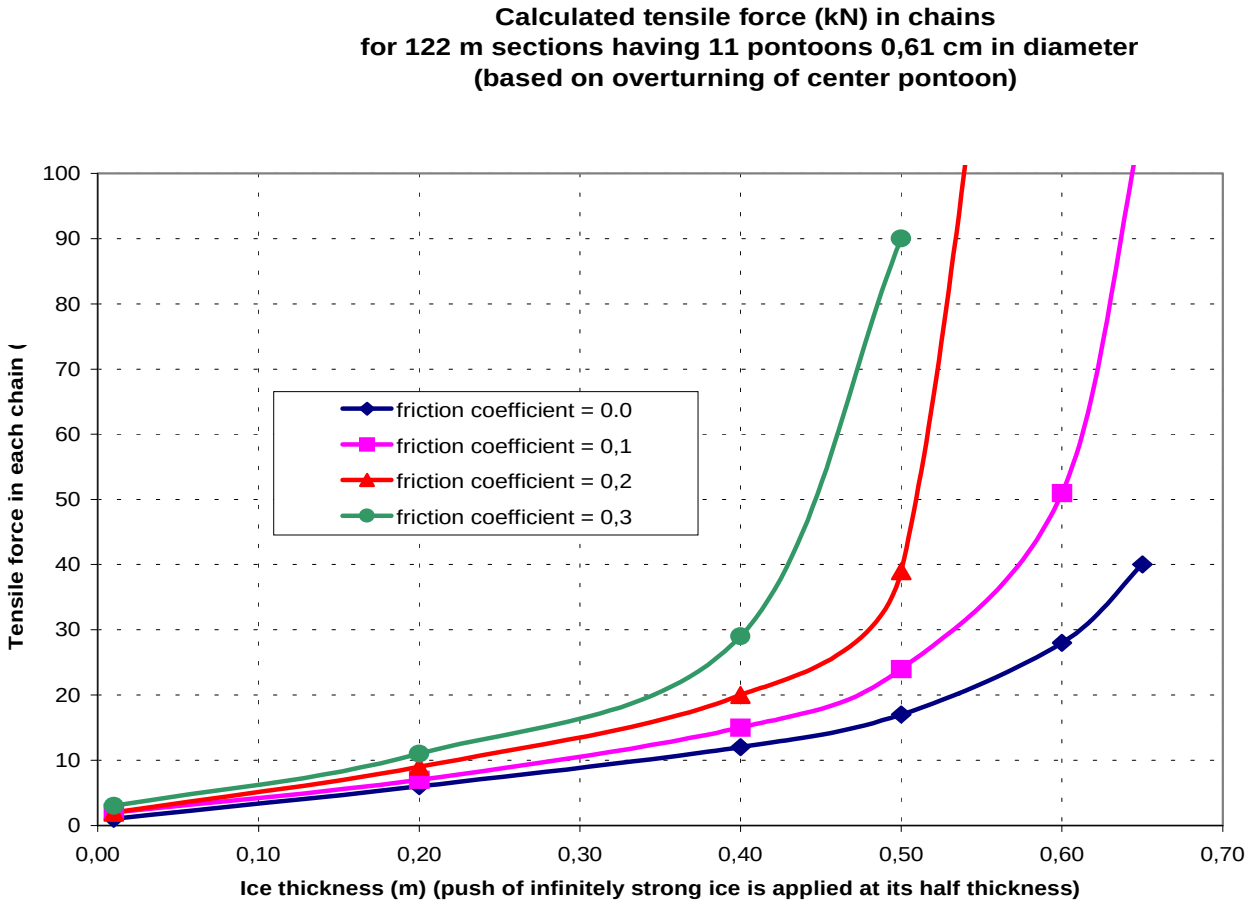


Figure 7.5 Calculated tensile force (kN) in chains

### 7.1.10 Summary

The above analysis provides very realistic values of both forces and angles. The analysis for the 65 cm cover is the limiting applied force and is essentially valid for any cover greater than 65 cm. The actual ice boom's retention capacity is very sensitive to the ice/pontoon interface geometry and adhesion. Of course, the calculated values assume that the ice sheet is infinitely strong and can therefore generate these pushes. On the sketch 7.1, we can see that the horizontal push $F_i$ must be transformed (by $M_i$ and $W_i$) into a normal push N without the ice sheet cracking. Thinner ice sheets will not be able to support this transformation. They will break in flexure before they are able to

push with sufficient force to fully submerge the pontoon. This limitation is discussed more fully in section 7.2 of this report.

### 7.1.11 Limitations regarding the ice/structure interface

In the foregoing analysis, we assumed that the ice formed a perpendicular face at the pontoon interface. In reality many different boundary conditions may exist. In one known case where there was structural failure near the north shore at Lavaltrie in1999, the ice interface was semi-circular. In other words, it surrounded the boom like a glove. At the time, the ice was thick and strong. There was no way the pontoons could submerge and avoid the applied load. Given the imposing environmental forces that can be generated by the border ice sheet near the bank, the only choice was for the structure to break. The ice face may take on a semi-circular form is when the cover forms during a substantial snow fall. The ice congeals in the shape of the pontoons. On the St. Lawrence River, this usually happens when the wind is contrary to the current. Should the cover have sufficient chance to freeze and the wind dramatically change directions and speeds, it is possible that high loads could subsequently be generated.

More typical loading conditions are those described in the CHC by Timco & Cornett, 1994, Figures 5.10 and 5.30). During failure of the ice cover, rubble accumulates upstream of the boom. At the lake Erie boom, ice accumulations are also reported. In fact for boom studies, it is virtually always assumed that there is an accumulation of ice pieces occurs upstream of the structure. Based on my observations over the last 6 years of the St. Lawrence ice booms and those of Marc Choquette's over the last 25 years, I am not convinced that ice rubble accumulates to any great extent in front of the those booms. I think that during the ice cover formation, there is some pushing and shoving. However, given the weak Froude numbers associated with ice booms, I believe that the thickening is very limited before the cover backs up. Within the next few days, these pieces have frozen together into a solid sheet. Then, when environmental driving forces become great, there can be four possible scenarios:

1. If the ice/structure interface is semi-circular (as witnessed at Lavaltrie in 1999), the section cables of the boom break.
2. If the ice/structure interface is more or less as describe in the sketch above, then equations 7.1 to 7.9 apply: The forces increase until which time the pontoons submerge and the ice cover overtops the pontoons. Once this begins to happen, it does not stop until such time as the full ice cover is gone.
3. Finally, during melt conditions, the ice may become weak. At this time, the cover stops adhering to the bank and the cover breaks as the pieces form an ice run over the pontoon and are gone. This possibility corresponds to the ice breaking in flexure.
4. The final possibility is of an ice cover frozen into the booms. This situation is discussed in the CHC laboratory study (Timco and Cornett, 1994, Figure 5.12, page 55). If the ice is thin and was formed at such a time when there was virtually no force applied to the boom, as the force increases, the boom can rotate and break the cover. However, if the ice is thick or if it was frozen in under high loading conditions,

the above analysis shows that break-out will be very difficult. Fortunately, this type of event is not a frequent one in ice booms deployed to date.

## 7.2 Analysis of flexural resistance

In an analysis of ice overthrusting during the breakup of intact river-ice covers, Demuth and Prouse (1990) provide the following equation to describe the vertical force P of the boom on the ice sheet (see Figure 7.1 above) required to break an ice sheet in bending:

$$7.10 \ldots P = \left[\frac{S e^{\frac{\pi}{4}}}{6 \sin\left(\frac{\pi}{4}\right)}\right]\left[\frac{3KH_i^{\,5}}{E(1-\nu^2)^3}\right]^{1/4}$$

where S is the tensile strength of the ice (it can vary widely depending primarily on temperature - say 400 kPa), e is the natural number 2.718, K is the foundation stiffness of water (= gρ = 10 kN/m$^3$), E is the effective strain modulus (normally 3 GPa), υ is the Poisson ratio (normally = 0.3) and as before $H_i$ is the ice thickness (m).

This equation is based on the work of Mellor (1986). He show (Figure 6) that it is a valid simplification of a more general equation as long as the ratio of the axial force ($F_i$) to the vertical force P is less than 20.

An analysis of Figure 7.1 and equations 7.8a and 7.8b shows that this ratio can be expressed as follows:

$$7.11 \ldots . F_i / P = \frac{[\cos\beta + \mu \sin\beta]}{[\sin\beta - \mu \cos\beta]}$$

In our application, for all but the thickest ice sheets ($H_i$ > 0,5) and the highest values of friction (μ > 0.2), the assumption is valid: Therefore, the calculated value of P given by 7.10 is valid (within 3% of the exact solution).

In Demuth and Prouse's application, they considered the force $F_t$ required to push a sheet of ice on top of another just after overthrusting occurred. For this scenario they assumed that $\beta = 0$. Substituting into equation 7.11 gives follows:

$$7.12....F_i = \mu_k P$$

where $\mu_k$ is the ice to ice friction coefficient (= 0.3). For example, for an ice sheet 60 cm thick having a flexural resistance of 400 kPa the maximum horizontal load prior to breaking in flexure is $F_i$ = 2 kN/m.

In our case, when the ice sheet breaks in bending near the boom, given the geometry at the ice/boom interface, the axial load $F_i$ may be greater than that calculated using equation 7.12. In addition, whereas Mellor showed that the axial force does not cause additional significant moments (since $F_i/P < 20$), the axial force does tend to reduce the tensile stress in the ice sheet prior to failure by an amount equal to $F_i/H_i$. Incorporating these two concepts leads to the following adaptation of equations 7.10 and 7.11:

$$7.13....F_i = \left[ \frac{\left( S + \frac{F_i}{H_i} \right) e^{\frac{\pi}{4}}}{6 \sin\left(\frac{\pi}{4}\right)} \right] \left[ \frac{3KH_i^{\,5}}{E(1-\nu^2)^3} \right]^{1/4} \frac{[\cos\beta + \mu \sin\beta]}{[\sin\beta - \mu\cos\beta]}$$

This equation was evaluated for critical conditions at the ice/boom interface. Once again, we assumed the 61 cm boom was just submerged. For a chosen value of ice strength S and thickness $H_i$, we calculated $\beta$ from equation 7.7 and using equation 7.13, by trial and error in an Excel spreadsheet, we determined $F_i$. It was found that the value of friction $\mu$ at the ice/boom interface had virtually no effect on calculated results for ice sheets less than 50 cm. The dependency on the ice strength S was linear.

The following are the results:

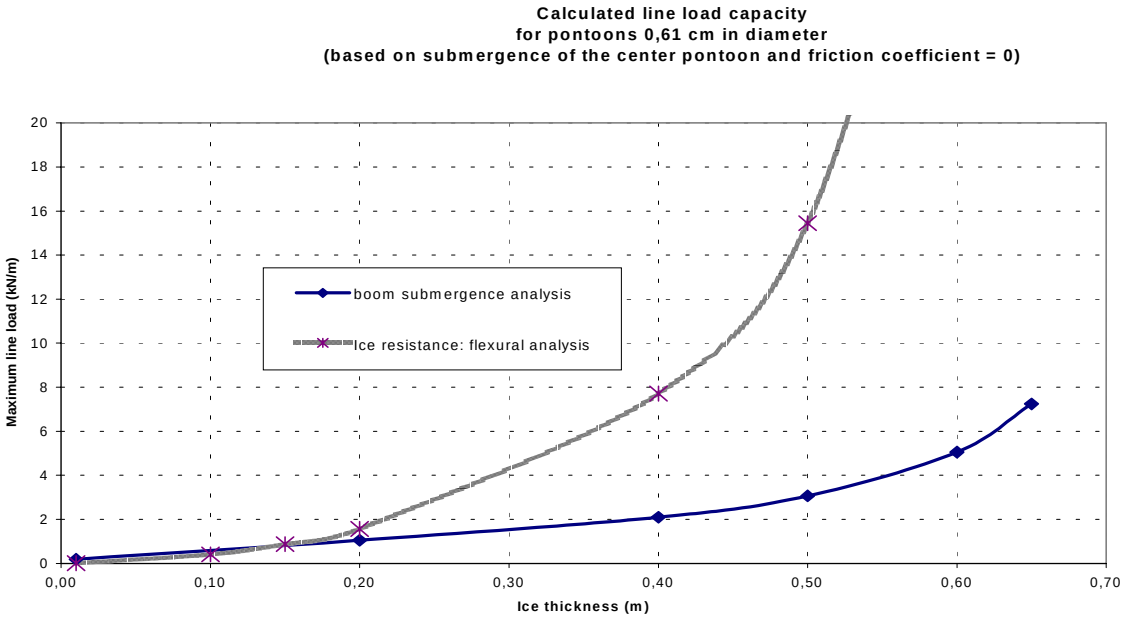


Figure 7.6 Comparison of line loads based on boom retention capacity and internal strength of ice against breaking in flexure

The ratio of calculated stresses from bending and boom stayed virtually constant for all values of $\mu$ tested except the very high combined values of both $\mu$ and $H_i$.

The following figure shows the ratio of values:

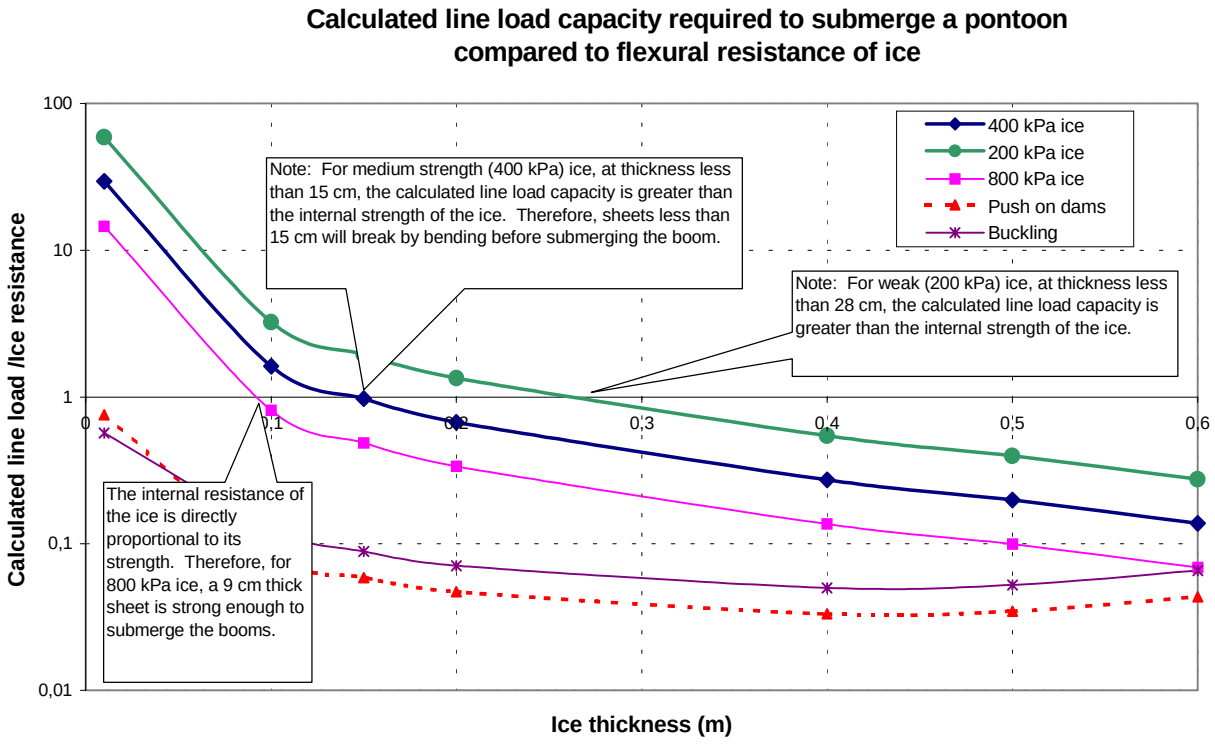


Figure 7.7 Ratio of ice boom line load capacity to internal resistance of the ice accumulation under flexural failure and buckling.

We note that as soon as the ice is at all thick, its flexural strength is greater than the boom's capacity to hold it back. Depending on the ice strength, the critical thickness is 9, 15 and 28 cm for ice 800, 400 and 200 kPa. So thin and weak ice sheets will fail in bending while thicker and stronger ice sheets submerge the booms rather than break.

Also included in the figure is the boom's capacity to retain ice as compared with ice's internal resistance to failure by buckling. Two curves are provided. The first is based on the work done by Sodhi and Nevel (1980) as reported by Timco (1986, Figure 4):

$$7.13....F_i = CK\left(\frac{EH_i^{\,3}}{12K(1-\nu^2)}\right)^{0.5}$$

where C is a dimensionless factor which depends on the structure's width and on the friction coefficient. For wide structures, we chose C between 1 to 2 depending on the value of $\mu$. The figure demonstrates that for standard values of Young's modulus, for

ice thickness greater than 10 cm, the retaining force of the boom is 10 times less than the internal strength of the ice in buckling. Therefore when forces are large and the sheet is greater than 10 cm, the boom will submerge – the ice will not buckle.

Also shown in Figure 7.7 is the ratio of the boom's retention capacity as compared with extreme forces generated on dams in reservoirs as derived by Carter (1999):

$$7.14....F_i = 250H_i^{1.25}$$

Clearly, equation 7.14 is derived for completely different conditions and from different principles. It is only included for sake of comparison of loads that are generated on wide flexible structures (booms) to those generated on wide fixed structures (dams). Depending on ice thickness, the load on booms is 0.05 to 0.1 times that on a fixed structure.

In interpreting Figure 7.7, one must also recall that the analysis was made for a 61 cm boom only. For larger booms, the retention capacity is approximately proportional to the buoyancy force at submergence. For a given pontoon density, the buoyancy force is proportional to the square of the pontoon's diameter.

# 8 Estimating ultimate applied loads: Methodology

## 8.1 From elements that occasionally break

### 8.1.1 Anchor cables

Applied forces are estimated using one of three methods. When a structural component breaks, we can assume that applied force is equal to the ultimate breaking strength of the component. Sometimes, this can be inferred with a fair degree of confidence. For example, the standard 2 inch diameter "6/19 bridge rope" (traditionally used for section cables and also previously used for anchor cables) has a specified breaking strength of 169 tons (1503 kN). Depending on production conditions, the actual breaking strength is probably 2% higher (1530 kN).

However, one must also factor in the condition of the element at the time of breakage. For example, in 1994-1995, a number of anchor cables broke at Lanoraie. They were about 8 years old. From experience, we know that these cables were weakened through fatigue some 2 m below the junction plate. So the strength of the cable at the time of the break is a guess. One could assume any value between 25% and 90% of the original value. In this case, Using an estimated value 75%, the applied load during 1994-95 was therefore in the order of 1530 x 75% = 1200 kN. This corresponds to a line load of 1200/122 m = 10,3 kN/m.

One can also infer applied loads when the cables don't break. Knowing the ultimate cable strengths, if the cables don't break, the applied loads were less than that value. For example, at Lavaltrie and Lanoraie, from their initial deployment in the late 1960's up to 1995, when the booms were made out of Douglas fir (14" x 22" x 30'), when the anchor cables were new, there were no breaks during many years of deployment. This leads to the conclusion that the applied line loads did not exceed 1530/122 = 12,3 kN/m.

### 8.1.2 Section cables

One must also take into account the way that the load is applied. The specified ultimate strengths are for cables loaded in tension only. Often, other loads are applied to the cables, particularly the section cables that hold the booms. The pontoons apply a load perpendicular to the axis of the cable and thereby add to the axial loads. The cable clamps wear the cable at the contact points reducing its strength by some value (2% to 10%?). Depending on the age of the cable, this reduction must be applied when a section cable breaks.

Figure 8.1 Cable clamp twisting a section cable

Other structural elements that have broken are the "fuses" installed on the section cables. The fuses are "weak links" installed between the junction plates and the section cables. They ensure that if the applied load is too large, the fuse blows before the anchor cable breaks. The inclusion of fuses was necessary at Lavaltrie and Lanoraie because the initial design of the boom was faulty. Under the original design, the same cable was used for anchor cables as was used for section cables. Without the fuses, given the fact that the load in the anchor cable is about 63% higher than in the section cables, it is obvious that the anchor cable will break before the section cables do.

This is highly undesirable because once an anchor cable breaks, its entire load is immediately transferred to the neighbouring anchor cable causing it to break too. The ensuing domino effect causes all anchor cables to fail in sequence causing a massive failure of the structure. This is what happened at Lavaltrie in 1994-1995. Since it is very difficult and expensive to replace the anchor cables with ones that have greater strength, we opted to insert fuses in the section cables so that they would break before the anchor cables would. The fuses have the appearance of a tension link. They were built and tested by a local contractor. Given that a fairly good quality control was used, the breaking load of the fuses is estimated at between 75 and 85 tons (670 to 760 kN). In both 1999 and 2000, fuses broke on the northern most section of the Lavaltrie boom. This corresponds to a line load of at least 6 kN/m.

(It should also be noted that we tried to increase the strength of the anchor cables by changing the cable from a "rope" to a "bridge strand" but we were limited by the size of the connection at the anchor itself. On the newly constructed Yamachiche boom, no fuses are required because the anchor cables are properly dimensioned to support at least 1.8 times the section cable strength).

### 8.1.3 Chains

There are also some 3 to 8 chains that break annually. Estimating the corresponding force is more difficult in this case for two reasons. First, two types of 7/8 inch chains are used. The most common is a grade 30 chain that has a working load limit (WLL) of 12,800 lbs (57 kN). However, there is also some grade 80 mixed in and it has a WLL of 34,200 lbs (152 kN). The specified breaking strength of chain is four (4) times the WLL. However, the actual breaking strength is not provided by the manufacturer. We will assume it is 2% higher. When a old chain breaks, we will assume it to be 3% lower. In this case, assuming a break in a grade 30 chain, the applied force in about 4x57x97% = 220 kN. This corresponds to a local line load of 220 kN per chain x 22 chains per section cable / (122 m per section cable) = 40 kN/m.

## 8.2 From mechanical means

The second way to estimate the ultimate applied load on the boom cables is through mechanical means. Since it is difficult to measure tensile forces, they are converted to compression forces through the use of a cage developed for that purpose. One end of

the cage fits into the junction plate while the other end is attached to the cable (see Figure 3.1). The cage is made in two parts such that it is possible to fit a ball bearing sandwich in the cage that will be compressed as the tension in the cable augments. Figure 8.2 and 8.3 show a small cage used to measure tensile forces on chains.

The sandwich is composed of two 2 cm thick pieces of aluminium about 7 cm by 7 cm square which hold three hard steel ball bearings in place forming an equilateral triangle. The bearings are about 1 cm in diameter and are prevented from moving around by the use of a foam keeping them in position. The more the sandwich is compressed the more the bearings are driven into the aluminium plates. Similar to the Brinell hardness test, the degree of penetration indicates the applied load. (Also in the cage is a load cell sampling the load twice a second that is connected to a data acquisition unit).

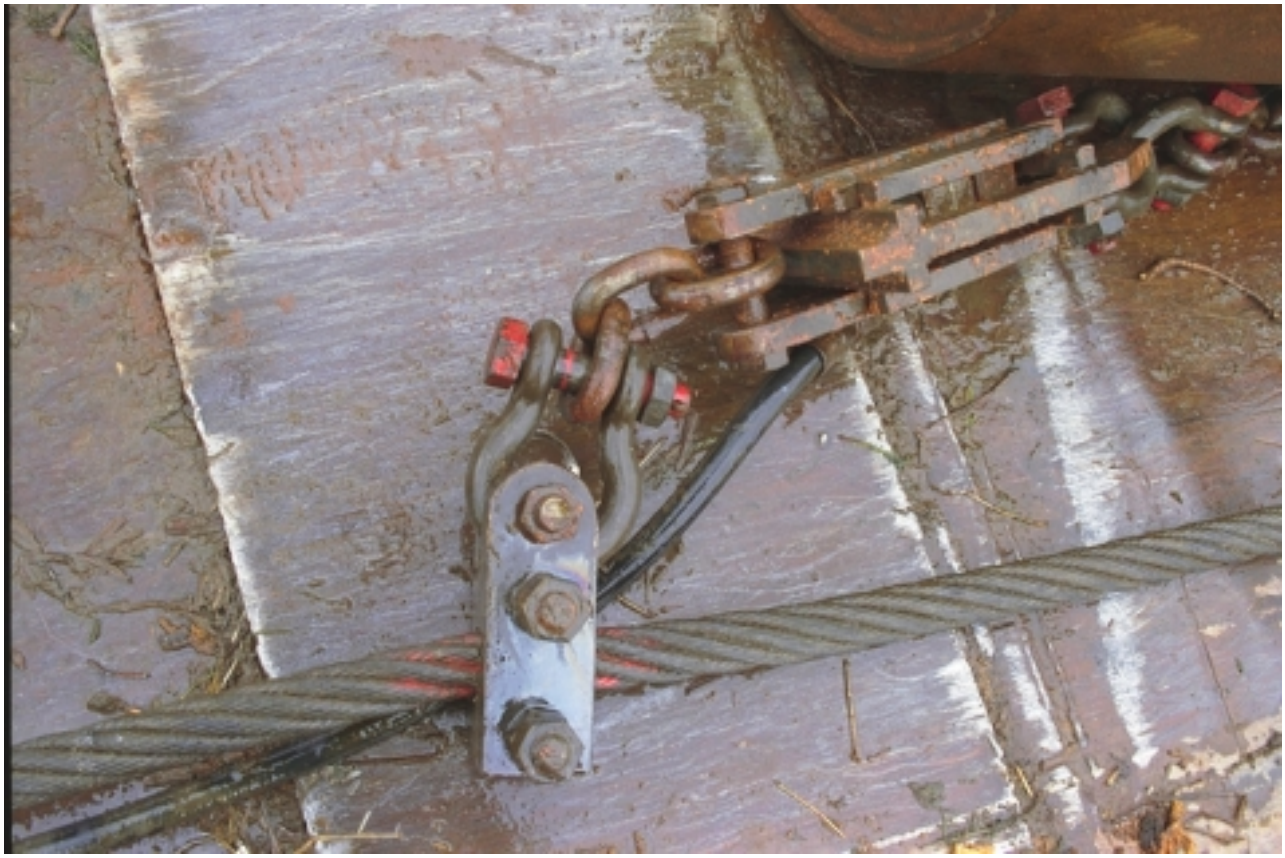

Figure 8.2 Very small cage deployed on chain between pontoon and section cable

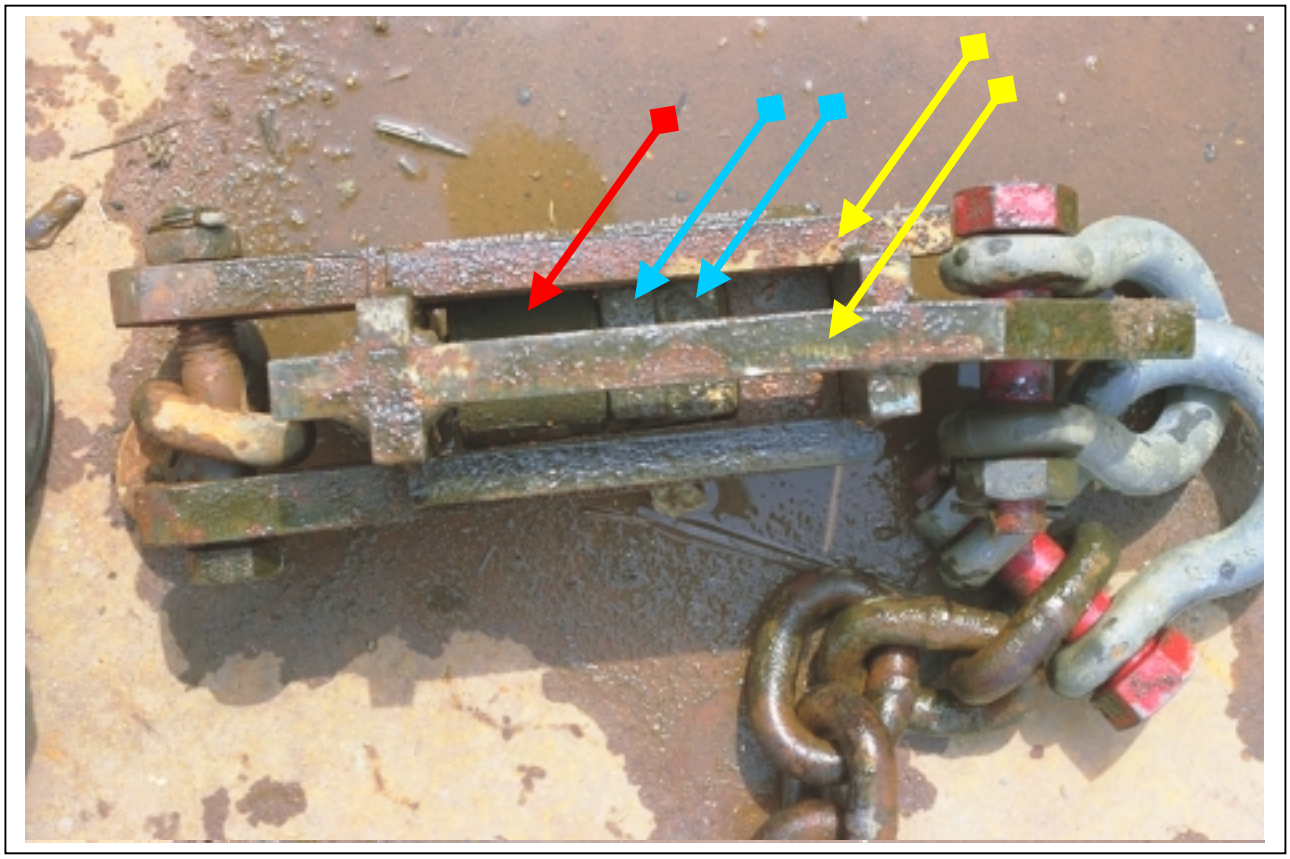

Figure 8.3 Load cell and ball bearing sandwich (for chains)

*It shows the principle of converting tensile force acting on the chain into a compressive force within the cage. The two yellow (plain) arrows point to the two distinct parts of the cage. The blue arrows (with balls at the tail) point to the aluminium plates which form the sandwich. In between the plates are three ball bearings (not visible) which are compressed into the sandwich as the tensile forces in the chain increase. The red arrow (diamond at the tail) points to the load cell which is in series with the sandwich and is also compressed at the same time as the ball bearings. This particular instrument was set up on the prototype boom deployed during the winter of 1993-94. Very early in the season, the data communication cable between the load cell and the data acquisition CR10 unit broke and so no load cell data was retrieved. This particular instrument for forces on chains has not been deployed since.*

Figure 8.4 Typical load cell deployment at Yamachiche boom

*(Note large cage for anchor cable (bottom) and smaller cages for section cables (top). Teflon-coated yellow armoured cables link load cells in cages to data acquisition unit in barrel (top out of view). Note pontoons in the background which will be deployed under the supervision of the foreman Georges Gouin (far right))*

Figure 8.5 Load cells ready for deployment

*(This is another view of the previous photo. Note the huge barrel which houses the CR10 data acquisition system and data transmission system. The domes on top of the barrel serve as antennas for real-time data transmission to a local booster station).*

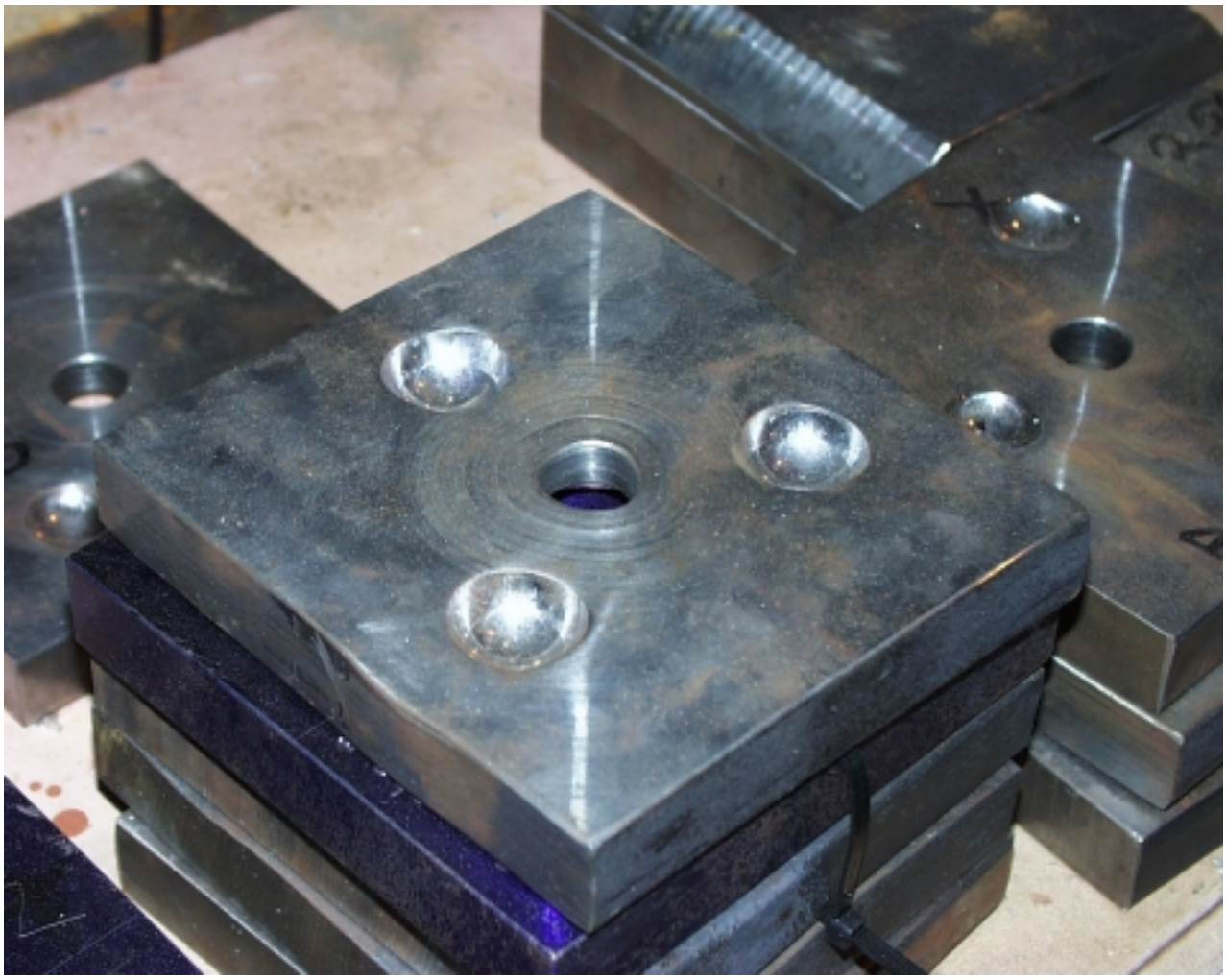

Figure 8.6 Extreme penetration of ball bearings into aluminium plates for the most extreme event on record at Yamachiche on anchor cable no. 17 in February-March 1999. Estimated load: 1820 to 1970 kN

*(We believe that the load was generated because the pontoons were frozen into the border ice near the bank. After a rise in water level, the ice sheet broke away from the bank and tore the boom in that location)*

Load-penetration relationships are developed in a workshop. The sandwich is put in a press and loaded in steps. The resulting penetration measured. Normally, the load is applied three times to account for the effects of possible dynamic loading in the field. The press was calibrated using a load cell.

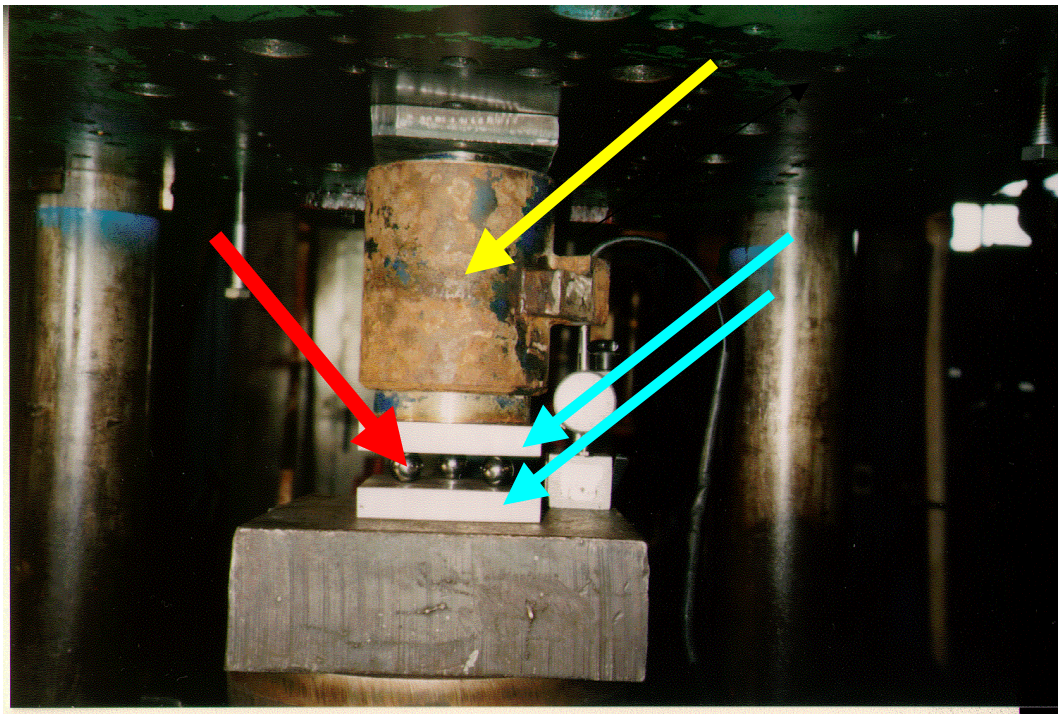

Figure 8.7 Press used in workshop to calibrate mechanical measurements of loads

*(Note the ball bearing sandwich consisting of two plates (blue arrows) holding three ball bearings (one of which is shown by the red arrow) which is in series with an off-the shelf load cell (yellow arrow) that is used to validate the recorded loads of the press).*

For the Yamachiche boom, the Canadian Coast Guard (CCG) installed a ball bearing sandwich at about every second section cable. Some anchor cables were also equipped in a similar manner and one anchor cable was also monitored at both Lavaltrie and Lanoraie.

Since the effect of sustained high level loading on the penetration of the bearings into the aluminium plates was unknown, we made a comparison values estimated by mechanical means and those maximum loads registered by the load cells. We know that they were measuring the same phenomenon since the load cells were placed in series with the sandwich in the same metal cages (e.g., Figure 8.2).

The following Table 8.1 and associated Figure 8.8 is a comparison of estimated maximum loads measured in the field using ball bearing sandwiches as compared with the maximum recorded values using the load cells. (For the location of junction plates, please refer to Annex 1. Basically, for Yamachiche, there are 20 junction plates numbered 0 through 19 from the south to the north shore respectively):

| | Mechanical measurements ultimate load (kN) | Load cell maximum load (kN) | Difference: (1) - (2) (kN) |
|---|---|---|---|
| Lavaltrie 95-96 | 641 | 673 | -32 |
| Lavaltrie 96-97 | 1139 | 1023 | 116 |
| Lavaltrie 97-98 | 855 | 675 | 180 |
| Lavaltrie 98-99 | 732 | 404 | 328 |
| Lanoraie 95-96 | 645 | 667 | -22 |
| Lanoraie 97-98 | 723 | 637 | 86 |
| Yamachiche no. 4 96-97 | 746 | 762 | -16 |
| Yamachiche no. 4 97-98 | 437 | 426 | 11 |
| Yamachiche no. 9 96-97 | 1142 | 1084 | 58 |
| Yamachiche no. 9 97-98 | 495 | 447 | 48 |
| Yamachiche no. 14 96-97 | 1142 | 932 | 210 |
| Yamachiche no. 14 97-98 | 447 | 403 | 44 |
| Yamachiche no.11S 95-96 | 1260 | 1225 | 35 |

Table 8.1 Comparison of ultimate annual loads from mechanical means and load cells.

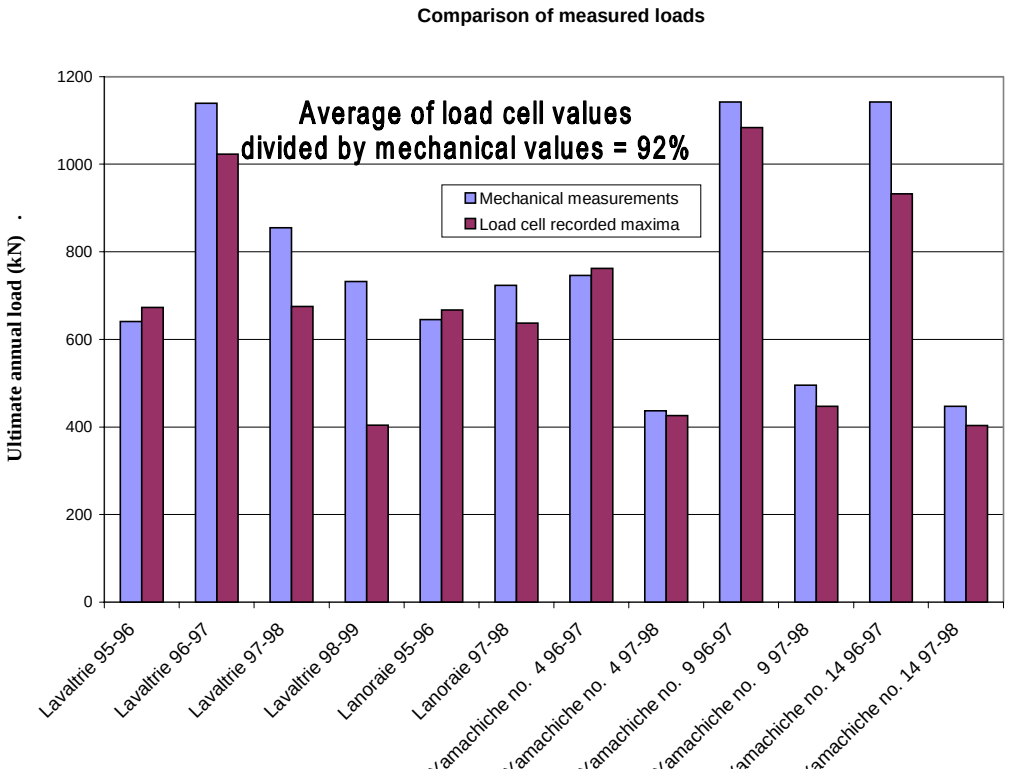


Figure 8.8 Comparison of measured loads from ball bearing sandwich and load cells.

Excluded from the comparison are values from the 1994-1995 winter. For that winter, we are unsure of the exact location of the gauges. Except for Lavaltrie 98-99, the comparison of estimated ultimate loads is excellent. (We believe that the exception was caused by a malfunction of the load cell.) With very little scatter, we can see that the extreme loads estimated mechanical means are about 8% higher than those recorded using the load cells. Whenever two measurements aren't the same, it is always uncertain as to which one is right. However the load cells are laboratory calibrated. We explain the 8% difference by the fact that the calibration curve is based on the load being applied only three times whereas in reality, the sandwich is being compressed all winter. As such, in all our analyses, we subtracted 8% from the calibration curve when we worked with ball-bearing estimates.

## 8.3 From load cells

As already mentioned above, the final method of estimating applied loads is by examining load cell data. Whereas Fleet Technology uses calibrated custom made tension links to measure loads on the New York Power booms, CCG opted to use "off the shelf" load cells. The advantage is cost and ease of calibration. The disadvantage is that one must build special cages to house the cells. (However, as shown above, this also provides the opportunity to include a ball bearing sandwich as a backup).

The load cells are connected to Campbell Scientific CR10 data loggers via cables that have a double sheath. The first is a double armoured rubber tube which is in turn shielded by a Teflon hose (to minimise friction). The CR10 is powered by three independent battery packs. Under normal conditions all three packs drain equally. However, should one pack become faulty, a diode prevents it from draining the other two. In this way, power is assured for the whole winter period.

The CR10 is programmed to sample twice a second. Every two minutes, it saves the maximum and the instantaneous recorded load. In our analysis, the maximum two minute values were always used. During a previous in-house analysis, we showed that, on average instantaneous forces were about 2% to 5% lower than maximum recorded values over a two minute period. This gives some idea about the relative non-importance of high frequency loading. Because the ice booms are flexible, most of the high frequency energy is absorbed by the structure.

The CR10 also records temperature and battery voltage. Temperature data has not been analysed in this study.

Three times a day, the CR10 wakes up a radio-modem for data transfer. In the office in Québec City, some 100 km away, an automated phone dial up is initiated to a nearby tower that serves as a boosting station. When the barrel containing the CR10 is not frozen under the ice cover, the call goes through and the near real-time data is downloaded.

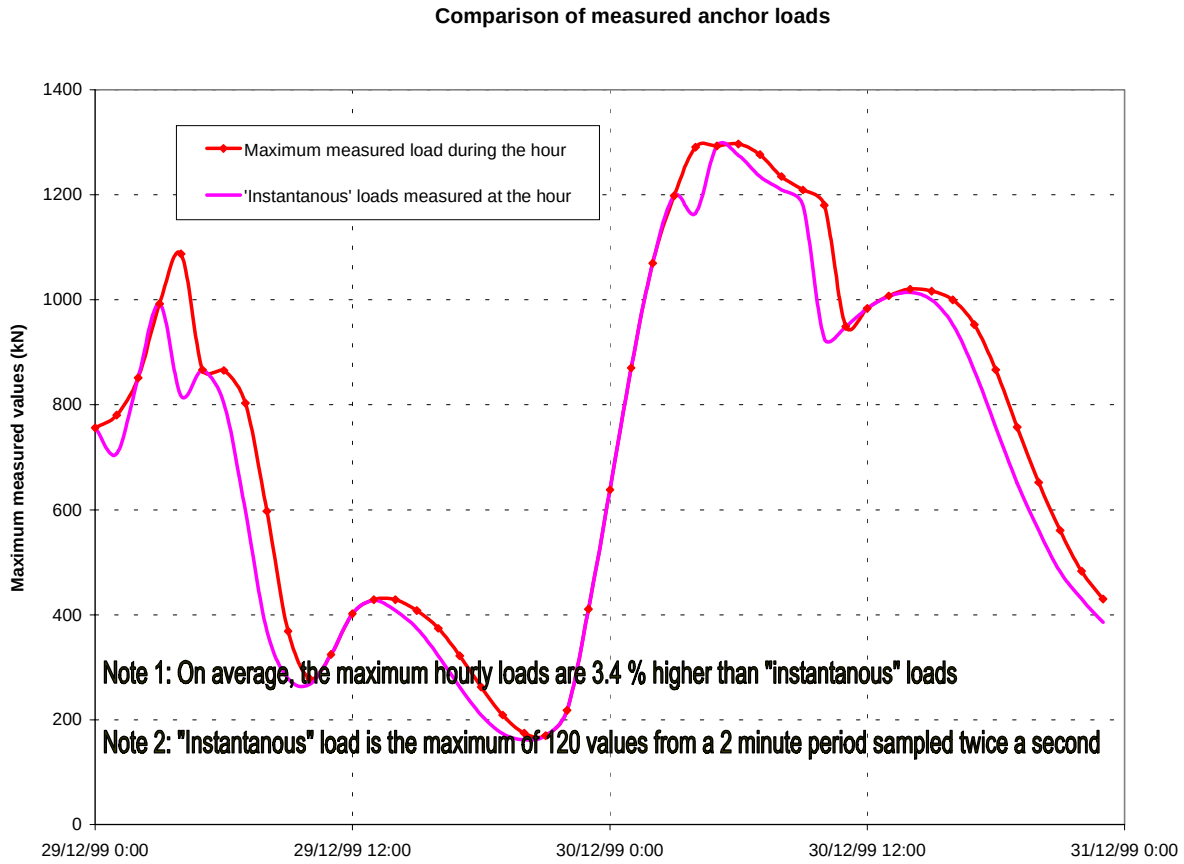


Figure 8.9 Comparison of measured anchor loads: maximum hourly load compared to the two minute instantaneous value

Once the data is received, a system devised by Stéphane Dumont, ing. at CCG is used to automatically look up the most recent calibration coefficients for the individual load cells and the conversion to pounds, tons or kN is made according to the user's choice. Usually, CCG works in tons. However, we use kN in this report. We occasionally convert the anchor loads into a line load (kN/m) by dividing by the section width (122 m).

Once collected, the hourly loads are plotted using QUATTRO PRO. Two types of hourly loads are recorded using the macros devised by Dumont. First, the two-minute maximum values are recorded on the hour. In a second column, the hourly maximum value is saved. For operational purposes, only the hourly maximum values are posted. For this study, depending on the nature of the analysis one or the other value was used. Figure 8.9 shows a typical recording of both values. During the whole year of 1999-2000 at Yamachiche junction plate no. 4, the maximum hourly value was greater than the average of the maximum two minute values by 3.4%. Combining the two finds, the maximum hourly value is about 5 to 8% higher than the average of values sampled at 2 Hz.

At some locations, both section cables and anchor cables were equipped with load cells. This is the only such deployment known to the authors. In addition to providing redundancy, both section cables and anchor cables were monitored to investigate the dynamic behaviour of the flexible structure. During the analysis of the break of the boom cables at Lavaltrie, some suggested that the sum of forces in the cables at the junction plate could be very different from zero. We wanted to refute this hypothesis. Also, we

wanted to establish the interdependencies between the loads in one cable and those in a neighbour in order to investigate eccentric loading. Finally, some section cables are monitored for operational reasons which will be explained in another section of this report.

Data at various locations over a 5 year period indicates that there is a small zeroing error in the load cells. Typically instead of reading zero during no-load conditions, the load cells will read anywhere from +/- 20 kN. This may be due to drifting in the load cells, to the extra resistance in the cabling system between the load cell and the data recorder or to the variation in water temperature. In any case, normally the error is in the +/- 10 kN range and the offset seems to be very consistent during the whole season. To account for this slight discrepancy, after the calibration curve is applied, we made a small additional adjustment to zero the data vector.

In the following example, we examine the loads in the cables joined at junction plate no. 4 at Yamachiche during 1999-2000 winter. The anchor cable read 18 to 20 kN during a no load condition. This is believed to be more or less accurate because there is some drag on the cable due to water forces prior to the ice season. The section no.3 cable read about –19 kN prior to the ice season. We therefore added 19kN to the calibration in order to get a reading of zero. (Admittedly, we could have added an additional 10 kN to account for water drag but we chose not too). The section cable no. 4 read – 3 kN prior to the ice season. We therefore added 3 kN to the calibrated values.

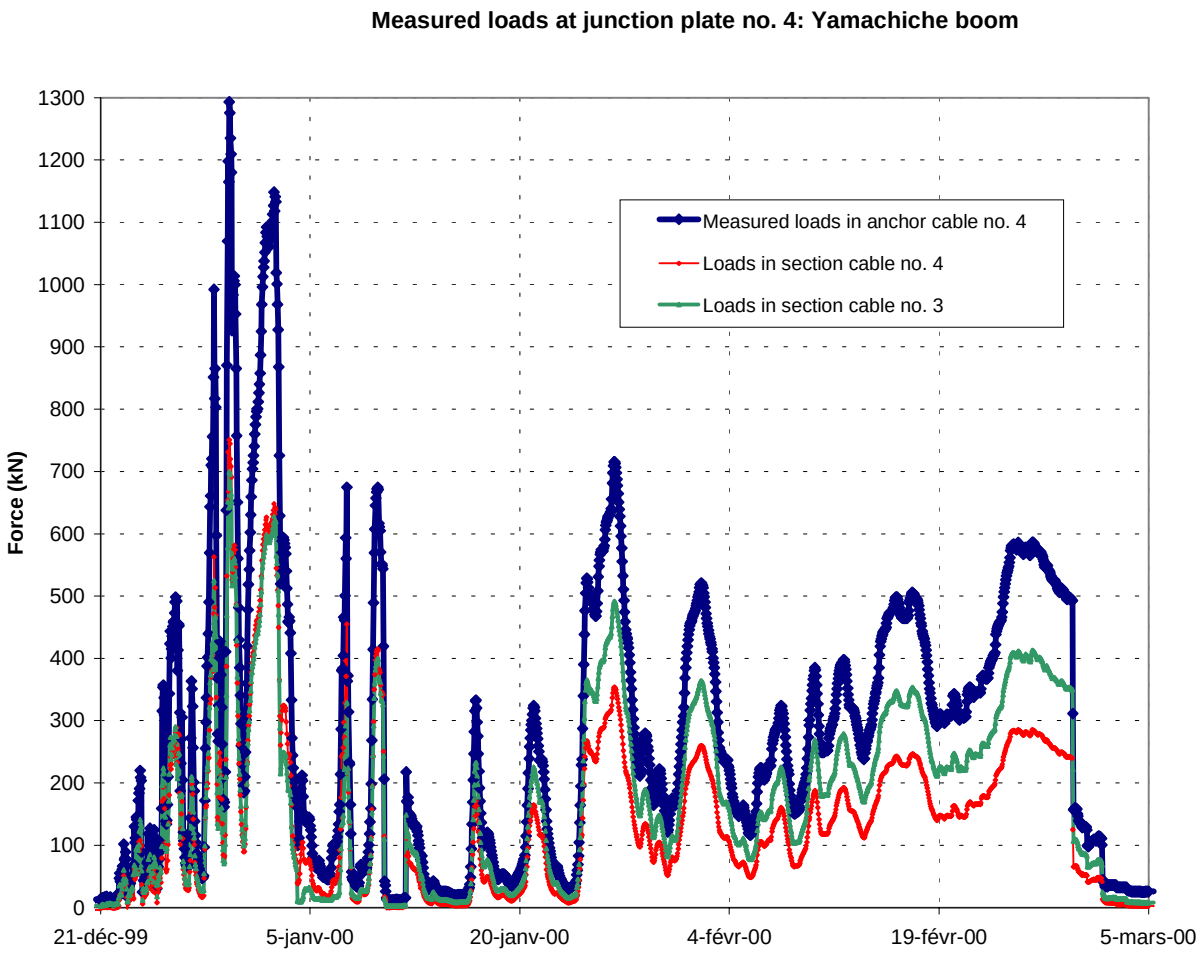


Figure 8.10 Measured loads at junction plate no. 4 of the Yamachiche boom

We note that all the three data sets show the same rises and falls in applied loads. Using the hypothesis that the applied load is uniform over the width, that each section cable is 153 m long and that each section is 122 m wide, the section cables form a parabola and meet the anchor cable at an angle of 36.6 degrees (see development below). Therefore, if there is no acceleration, the sum of the forces in the section cables times cos (36.6) should equal the recorded force in the anchor cable. Figure 8.11 demonstrates that, in general, the load is balanced at the junction plate. During the whole winter, the vector sum of the section cable loads varies between -20 and +10 kN except during the peak load period of December 28$^{th}$ to January 10$^{th}$. Most of the time, the vector sum is about 10kN less than the recorded load on the anchor cable. This offset could come from a number of sources including the non-uniformity of ice loading or the imprecision in the assumed dimensions of the section geometry. It could also depends on the amount added to zero the calibration of the load cells. However, one conclusion is clear: In general, there is a force balance at the junction plate and the assumed parabola cable shape is acceptable.

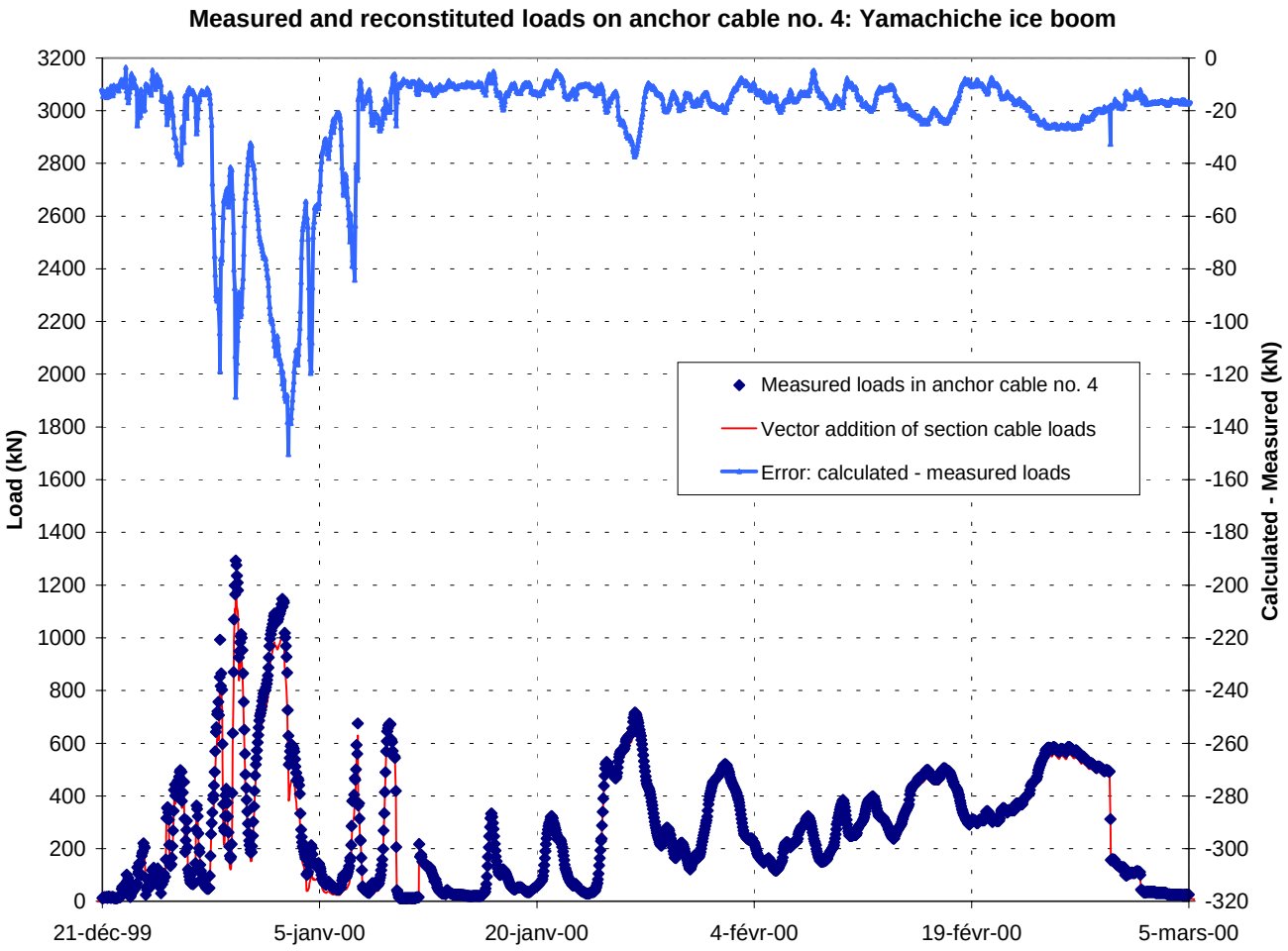


8.11 Measured and reconstituted loads on anchor cable no. 4 at the Yamachiche ice boom

The peak difference of up to 150 kN could come from three sources. First, the calibration of the load cells at these higher loads may be imprecise. This hypothesis, though possible, is unlikely because during the rest of the winter, strong loads were measured but there was no significant difference.

The second reason may be due to the omission of a term (Ma) representing dynamics (mass times acceleration). This would be probable if the difference was positive (i.e. if the calculated vector sum of the forces was greater than the measured values in the anchor cable). However, it is hard to imagine the how this term could account for a negative value.

The third possibility is that in addition to the section cables loads, the anchor cable has an additional burden. This may be the case because attached to the junction plate is a barrel to ensure that the junction plate stays near the surface. Normally, the dimensions of the barrel are some 90 cm in diameter and 1,5 m long. This means that its volume is about 0,38 times the volume of a typical pontoon. However, since this particular junction plate must support three very heavy cages (Figure 8.4) and must float well out of the water to transmit the recorded loads three times a day, the barrel is huge (see Figure 8.5).

It must have a volume at least equivalent to a pontoon. Given that there are normally eleven pontoons per section, we can assume that the anchor cable must carry 1.09 (=(11+1)/11) times more load that the vector sum of the section cables. Given the maximum recorded value of 1133 kN, this extra 9% would represent 100 kN. Although, this does not account for the full difference of 150 kN, it is very close.

The final possibility is that if the load on the boom is somehow concentrated over these two sections, then the boom will contract, the angle between section cables at the junction plate (2 x 36.6°) will contract and more load will be transferred to this anchor cable at the expense of its neighbours.

## 8.4 Load measurement methodology: Summary & Conclusion

This section showed that there are essentially three methods for estimating the ultimate annual load on the structure: (1) by considering broken or intact elements, (2) by mechanical means making use of "ball bearing sandwiches" and (3) by load cell data. Method (1) can be useful if the elements that break are relatively new, if not, it is very difficult to get a reliable estimate. Method (1) also tells us that the loads did not reach a critical value if the elements did not break. Analysis of load cell data (Method no. 3) points to a precision in the order of +/- 20 kN. This conclusion is reached by noting the recorded values during a no-load condition and by comparing the vector sum of the forces. Given this confidence in the load cells, an analysis of mechanical means (method 2) indicates that there is an excellent correspondence between the two methods. The analysis indicates that the factory calibration curve over-estimates the ultimate load by 8%. As such, mechanical values were reduced by 8%.

# 9 Load dynamics

During the previous discussion, we saw that the maximum load during any given two minutes is about 2% to 5% higher than a given load sampled each half second. Furthermore, Figure 8.9 showed that the maximum hourly load is, on average, 3.4% higher than the maximum instantaneous two minute load. These two facts indicate that the boom is not overly subject to high frequency loading.

Previous research (Cornett et al. 1997) also showed that temperature-related forcing can be present especially late in the year when a thick intact cover undergoes thermal

expansion during the day. However, such loading is also shown to be an insignificant design parameter. This is due to the fact that only very rigid structures react to the strains induced by thermal expansion. These two facts demonstrate the beauty of using a flexible structure. They are neither subject to thermal stresses nor to high frequency impact events. Compare this to the results of the CRREL laboratory testing of an rigid structure to arrest ice jams (CRREL, 1999): They found that high frequency dynamic loading was the most important source of forces.

On the other hand, daily fluctuations in loads can be important particularly during the ice cover consolidation period. Data from 1999-2000 at Yamachiche (anchor cable no. 4) show that during the period from December 27th to January 10th, hourly values varied dramatically. In fact the variation in values during any 24 hour period was of the same order of magnitude as the maximum daily value itself. This means that the ice pushing process builds up and is released over period of hours. The boom is really working during this period as the ice cover gradually consolidates and freezes into the bank. So, in a sense, during this period, daily maximum values are somewhat independent. This lends some support to the methodology used in previous studies (Cornett et al. 1997 & 1998) where daily maximum values were fitted to statistical distributions.

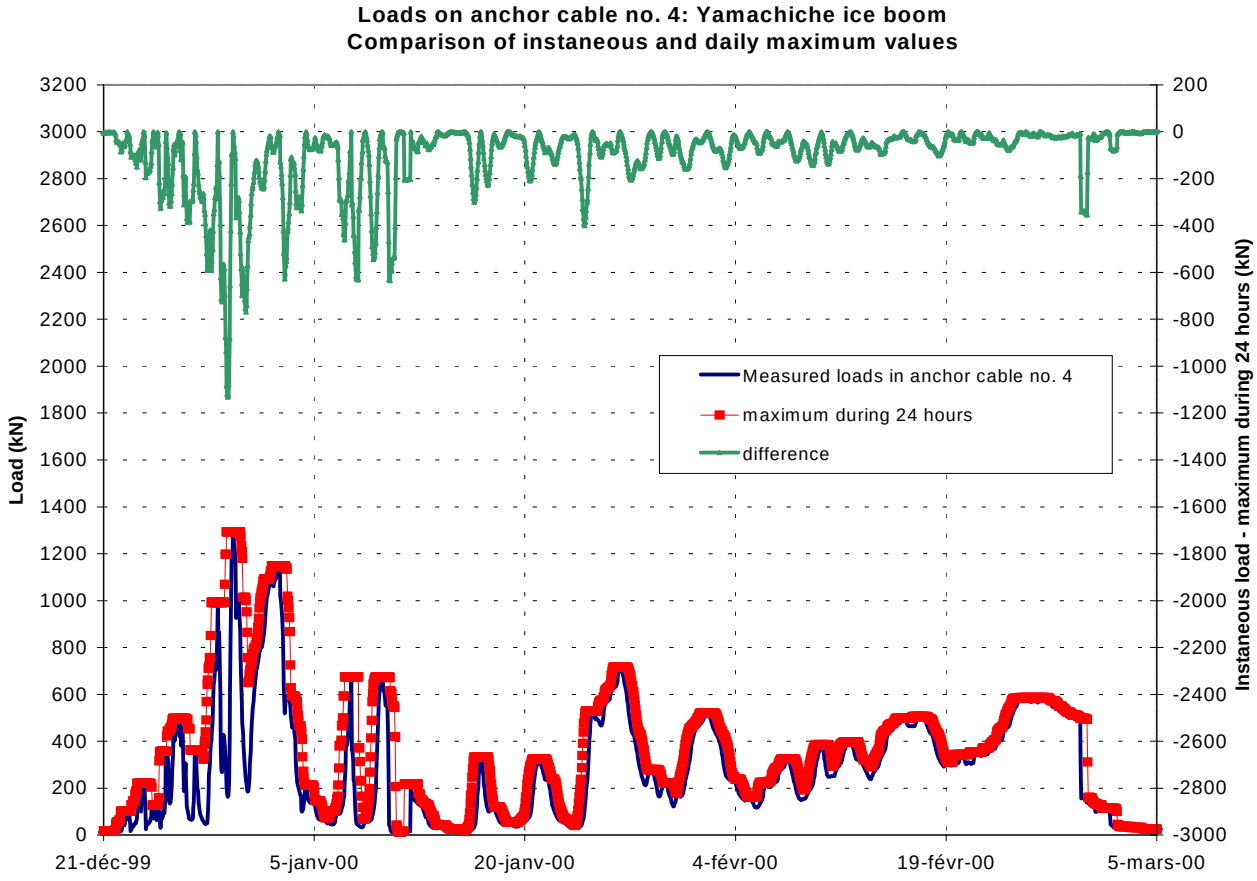


Figure 9.1 Loads on anchor cable no. 4: Yamachiche ice boom, Comparison of instantaneous and daily maximum values section cables

However, there is still important dependence in inter-daily values during this period. All load cell data from all years and all stations show a typical trend. The fluctuation in the hourly and daily loads has a certain amplitude that reaches a peak after some time (say one to two weeks). It is followed by a period where the force fluctuations are gradually smaller until such time as they reach a minimum. In the example presented, the ice cover begins to form on December 21, 1999. Loads reach a maximum of 1293 kN on December 30th. They then fall off to around 200 kN on January 11th.

After the consolidation period, there is often a long period where there are virtually no loads applied to the boom. (However, this is not the case in our example). In the case at hand, the boom is always working, resisting loads up to 700 kN throughout the whole winter. One reason for this fact is that the winter was very mild. (Note on Figure 9.1 that cover cleared out at the 29th of February.) This is a far cry from the winter of 1992-93 when there was a 4 day ice jam from March 17 to March 21, 1993.

In our example, during the winter period, load dynamics are very different than those during the cover consolidation period. Except for a couple of "events", the maximum 24 hour load minus the instantaneous load is usually less than 200 kN and is often less than 100 kN. In other words, dynamics during the winter period are no longer happening on an hourly basis. Rather, we detect about 9 peak loads over a 2 month. This frequency will show up later on in the spectral analysis of the data.

The last period is the break up of the ice cover. Prior to building the booms, forces at break-up were a major concern. Theoretically, the ice cover at this time can be very thick and well consolidated. It was feared that this may generate very high loads that would break the boom. Fortunately, this has not been the experience to date. Perhaps it is because the ice looses its inner strength because of internal melting. Perhaps it is because there are favourable conditions at the ice/boom interface. During the spring, the boom could be an effective source of solar radiation, melting the ice at its interface. Once the cover moves, it just slides over the boom. The only force that generated is that caused by friction.

This year (2000), break-up at Yamachiche occurred on February 29th. The forces associated with the event are only about 600 kN. Most years, the applied load at break-up is not as severe as the loads during the consolidation period. We will discuss these aspects further in our discussion of ultimate loading scenarios.

## 9.1 Section to section loading dynamics

The following is a sketch of the section and anchor cables at the typical junction plate no. 4 of the Yamachiche boom:

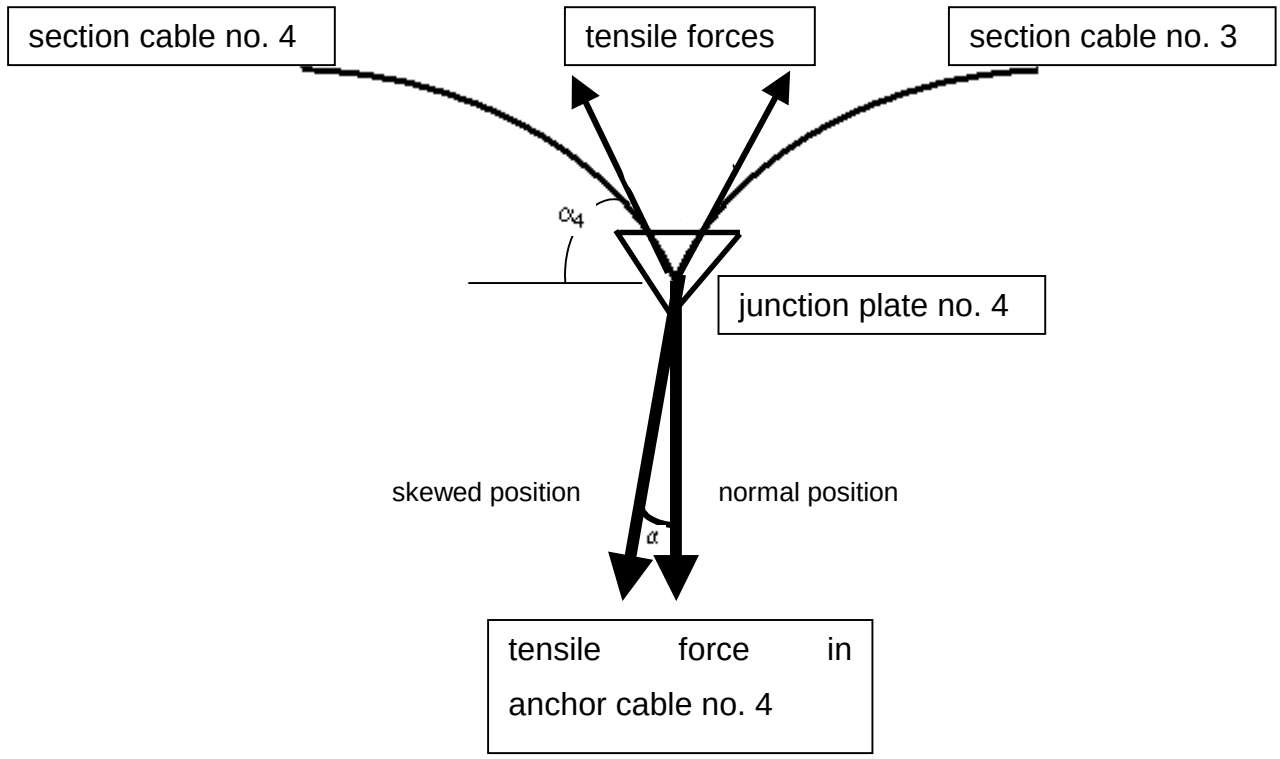


Figure 9.2 Sketch of cables at junction plate under normal and skewed loading

If we assume balanced and uniform loading, then angle no. 3 must equal angle no. 4 because the force in cable no. 3 is equal to the force in cable no. 4 and $\alpha = 0$.

For parabolic cables, the length of the cable is given by:

$$L = 2\int_0^{S/2}\sqrt{1+(\frac{dy}{dx})^2}dx = 2\int_0^{S/2}\sqrt{1+(\frac{wx}{T_o})^2}dx = 2\int_0^{S/2}\sqrt{1+(\frac{8hx}{S^2})^2}dx \qquad (9.1)$$

Traditionally, the Taylor expansion

$$(1+u)^n = 1+nu+\frac{n(n-1)}{2!}u^2+\frac{n(n-1)(n-2)}{3!}u3+... \qquad (9.2)$$

is used to analytically integrate the equation:

$$L = S(1 + 2.6667(\frac{h}{S})^2 - 6.4(\frac{h}{S})^4 + 36.57(\frac{h}{S})^6 - 284.44(\frac{h}{S})^8) \qquad (9.3)$$

Often people use the first three terms to find the sag h since the span width S is known to be 400 ft (122 m) and the length of the cable L is known to be 500 ft (152 m). The calculated value is 150 ft (45.7 m).

However, the Taylor expansion only converges for h/S < 0,25 and therefore in our case, we cannot use expression 9.3. We must solve equation 9.1 directly for h using a numerical method. The resulting value for h is 134,82 ft (41.09 m).

Substituting $dy/dx = 8hx/S^2$ at x = S/2 gives dy/dx = 4h/S at the junction plate. Substituting h = 134.82 ft (41.09 m) and S = 400 ft gives $\tan(\alpha 4)=\tan(\alpha 3)=dy/dx= 1.348$ and $\alpha_4 = \alpha_3 = 53{,}4°$. (Note 53,4° is the complement of the value 36.6° quoted above).

The force in the anchor cable should therefore be $2\sin(\alpha_3) = 1.606$ times the force in each section cable.

This value was confirmed in the preceding section above (Figure 8.11). Except during peak loading during the consolidation period, the vector sum of tensile forces in cables 3 and 4 equalled the measured force in the anchor cable. We explained that the difference was easily attributed to the extra applied force on the barrel is directly connected to the junction plate.

Furthermore, under this assumption, the force in all the section cables must be equal to each other and the force in all the anchor cables must also be equal to each other. In other words, the geometry of the boom cables promotes an equal distribution of loading. This is a very positive design feature.

However, even under ideal conditions, we know that the applied load is not uniform. Under Fleet Technology's depiction of the upstream ice cover, the applied load comes from shear forces acting on a triangular ice cover. Under Caquot's depiction, the forces are more uniform but are still larger in the centre. In fact, Fleet's depiction is valid for a laterally unconstricted booms whereas the silo equation applies to a laterally constricted boom. In our case, depending on the number of boom sections deployed and on the time of the year, the booms at Lanoraie and Lavaltrie are subject to either the triangular or the silo type of loading. At Yamachiche, initially, the loading is triangular. Very quickly, the cover begins to adhere to the north shore and therefore becomes a skewed triangle. Later in the year, the cover becomes well frozen into the artificial islands to the south and hence the loads are more of a silo type.

There are other additional factors that make for non-uniform loading. The first is the fact that the value of the water current pushing the cover from underneath is not laterally uniform. We can easily expect a variation of 30% over the length of the booms. Secondly, we know that the forces are generated by a series of pushes and shoves. Except during a break-up event when the ice is typically flushing simultaneously across the whole boom, we can expect that there are local pushes and shoves which may affect

one or more sections but which do not occur simultaneously across the whole width of the structure.

Figure 9.3 The 2.5 km wide Yamachiche boom viewed from the N-E towards the S-O. At the bottom of the image is the boom. On the viewer's right is the north shore. On the left is the navigation channel. The ice cover is partially retained by artificial islands (too small to see). Further upstream, the cover has a triangular shape because it is unconfined to its right (left side of image).

In our example, under non-uniform time-varying loading, the load in section cable no. 3 must be different than that in section cable no. 4. This is clearly seen in the following figure.

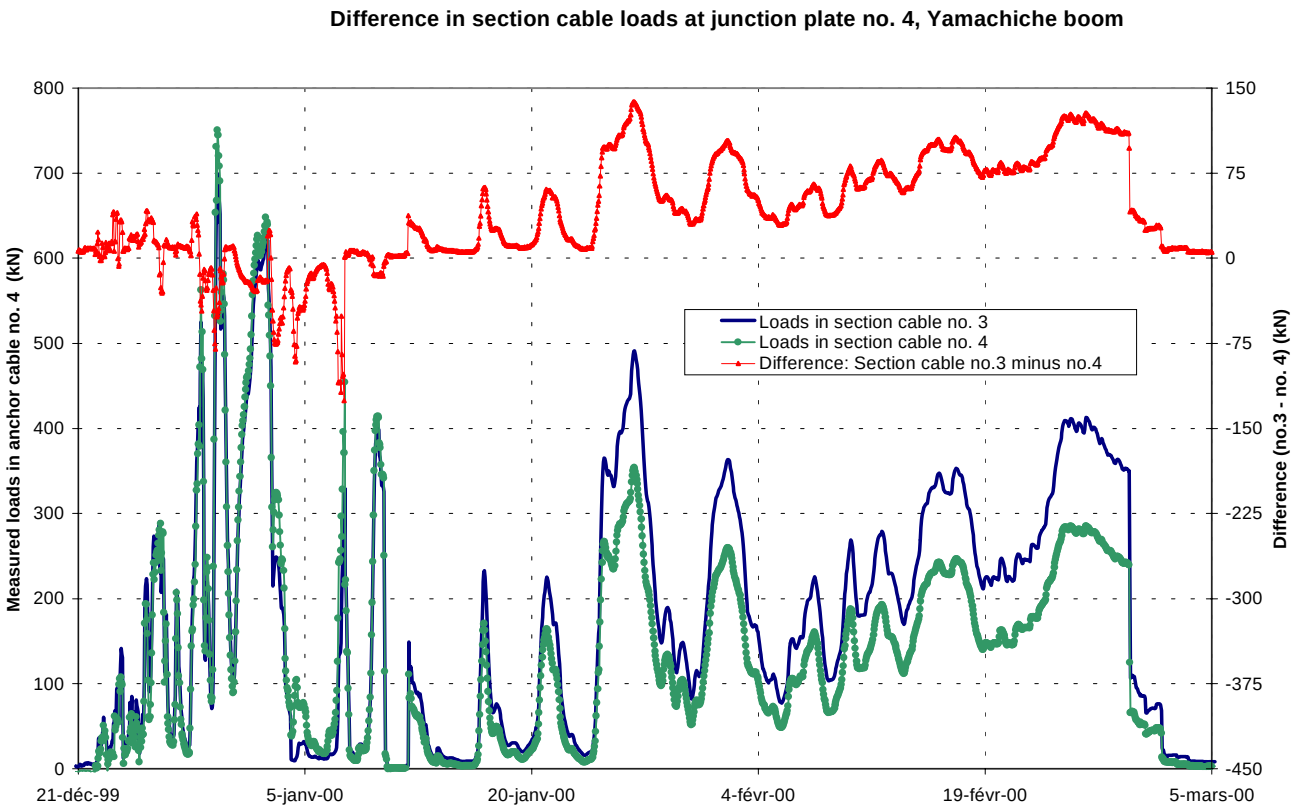


Figure 9.4 Force on anchor cable no. 4: Yamachiche boom section cable

During the ice consolidation period (December 27$^{th}$ to January 10$^{th}$), measured loads in section cable no. 4 were higher than in section cable no. 3. The difference is clearly seen to be directly in phase with the amplitude of the loads. The peak difference is 125 kN. It occurs during one of the peak loading events on January 7$^{th}$. After that period, the load in cable no. 3 is consistently higher than that in no. 4. Again, there are peaks that correspond to events. As the winter progresses, there is a definitive upward trend. The maximum differences were on January 27$^{th}$ (150 kN) and again on Feb 23 (123 kN).

We believe that these differences are explained by the following. During the ice cover formation period, the ice acts as an aggregate and as we explained, the forces in the centre portion of the boom (section 4) are expected to be greater than the forces near the end of the boom (section 3). This is explains the observed differences in first period. After January 10$^{th}$, the ice cover becomes consolidated and the cover becomes frozen in on the north side whereas there are only a few artificial islands to hold the cover on the

south side. Therefore over the winter period, the ice sheet is subject to increasing differential creeping as the consolidation process continues. To understand the second contributing reason for the difference, one must examine the cable set up at anchor plate no. 5. At this location, instead of having just one anchor cable, there is a second one located at an angle of 45° to stabilise the ice boom when it is subject to lateral loading (see Annex 1). As such, forces on the north part of the boom generated in sections 19 through 5 are partially intercepted by the angled anchor cable before they are passed on to section cable no. 4. For the south part of the boom, forces generated in sections 0 through 2 are passed on to section 3. This means that the force in Section no. 3 is a result of all forces applied over sections 0, 1, 2 or 3 whereas the lateral anchor cable at junction no. 5 stops the distribution of forces coming from the north. Therefore, the loads in cable no. 4 are due to local forces only. Therefore, all things being equal, there is more chance of having higher loads in cable no. 4.

## 9.2 Spectral analysis

A spectral analysis was performed on the two-minute force data at Yamachiche anchor cable no.4 for the 1999-2000 season (approximately 65536 data points). Figure 9.5 is a semilog plot of the energy ($kN^2$) against the frequency (cycles per hour). There is a clear decreasing trend from the low frequency down to about 0.15 cycles per hour after which point, there is only noise.

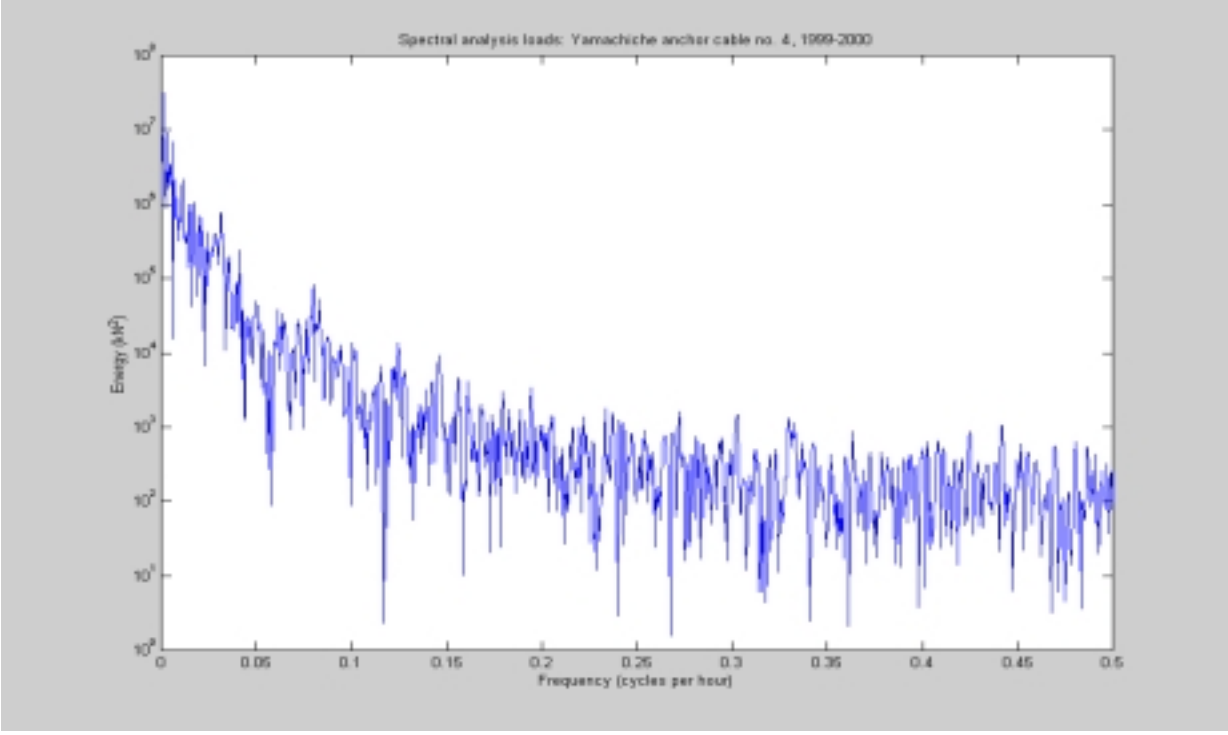


Figure 9.5 Spectral analysis at Yamachiche, winter 1999-2000

It is perhaps easier to visualise the results in the second plot of energy against the period of the dynamics (Figure 9.6). Clearly most of the energy is in the ice cover consolidation period corresponding to about 28 days. Interestingly, there is also energy peaks at 14 and 7 days. One wonders if there is a link with the fortnightly tide (probably not). Despite our previous analysis showing the importance of the daily loading cycle on loading dynamics, the spectral analysis shows that there is comparatively little energy for periods of 1 day compared to the energy in the longer periods.

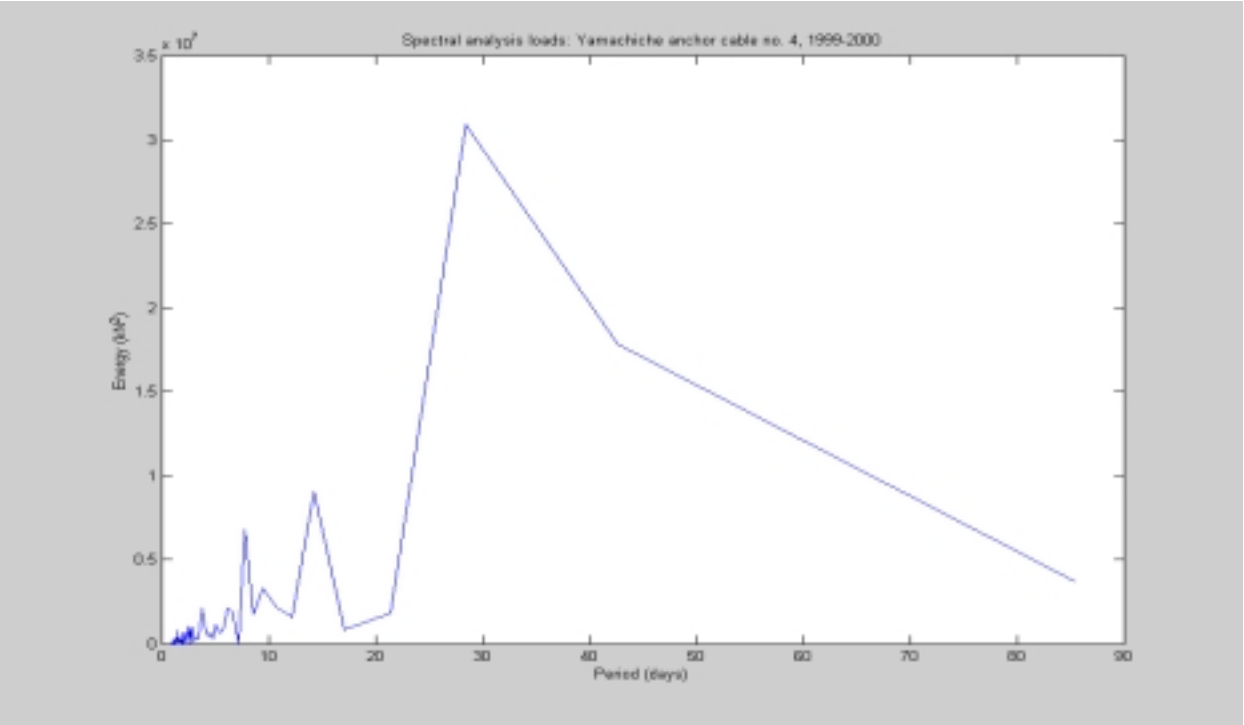


Figure 9.6 Spectral analysis at Yamachiche – alternative view

## 9.3 Seasonal loading

The anchor load data for each year is plotted in Annex 2. Within the data, we detect three loading cycles. The first is at the beginning of winter when the ice cover is building behind the boom in both area and thickness. As the cover builds, the force on the boom increases until some 2 weeks later the maximum force is reached (denoted by the full circle symbol). At the same time, the ice pieces become frozen together to form a full ice sheet and are also freezing into the banks. Over the next couple of weeks, as the cover becomes more frozen into the banks, applied forces on the boom decrease. We call this the consolidation period. The magnitude and the duration of the event vary from one year to the next. For example, at Yamachiche anchor no. 4 during 1998-1999, the consolidation period lasted 10 days and the peak load was very small (333 kN).

Once the cover is well frozen in, there can be a long period during which the forces are very stable and/or close to zero. The most classic example is at the Yamachiche boom, cable no. 4 during the 1998-1999 winter. During this year, the cover froze in quickly during December (consolidation period) and subsequently, all was quiet during January and February (winter period). The exception is a short duration mid-winter event which occurred at the beginning of February. At that time, there was probably a mid-winter thaw, water levels rose, the ice sheet cracked away from the bank and a large load was applied to the boom during a few days. In this particular example, the mid winter load was very high (801 kN) but in some years, the mid-winter event is small and- in other years, non-existent.

Table 9.1 Maximum load cell anchor cable load by season (kN)

| | | Consolidation period | Mid-winter period | Break-up period |
|---|---|---|---|---|
| Lanoraie | 94-95 | 340 | | |
| | 95-96 | 667 | | |
| | 96-97 | | | |
| | 97-98 | 302 | 201 | 637 |
| | 98-99 | | | |
| | 99-00 | 369 | 619 | 611 |
| Lavaltrie | 94-95 | 751 | | |
| | 95-96 | 673 | 258 | 344 |
| | 96-97 | 1023 | 78 | 621 |
| | 97-98 | 661 | 59 | 675 |
| | 98-99 | 404 | 72 | 375 |
| | 99-00 | 850 | | 432 |
| Yam-no.4 | 94-95 | | | |
| | 95-96 | | | |
| | 96-97 | 762 | 237 | 437 |
| | 97-98 | 402 | 426 | 380 |
| | 98-99 | 333 | 801 | 382 |
| | 99-00 | 1297 | 707 | 585 |
| Yam-no. 9 | 94-95 | | | |
| | 95-96 | | | |
| | 96-97 | 1084 | 198 | 765 |
| | 97-98 | 301 | | 447 |
| | 98-99 | 454 | 345 | 276 |
| | 99-00 | 1084 | 461 | 372 |
| Yam-no. 14 | 94-95 | | | |
| | 95-96 | | | |
| | 96-97 | 932 | 117 | 344 |
| | 97-98 | 355 | 10 | 403 |
| | 98-99 | 684 | 507 | 519 |
| | 99-00 | 781 | 250 | 227 |

The winter period is the break-up of the cover which occurs normally during March. Sometimes break-up is violent and short lived (e.g. Lanoraie boom 1999-2000) but most of the time, there is a gradual release of the cover from the banks during which time the loads increase to a peak value before falling off to zero (e.g. Yamachiche boom 1998-1999: peak load = 382 kN).

Table 9.1 and Figure 9.7 are the peak loads recorded by the load cells for each season where and when available. (Obviously, there is some interpretation required in order to determine which value belongs to which period.) Missing values or events are recorded as blanks.

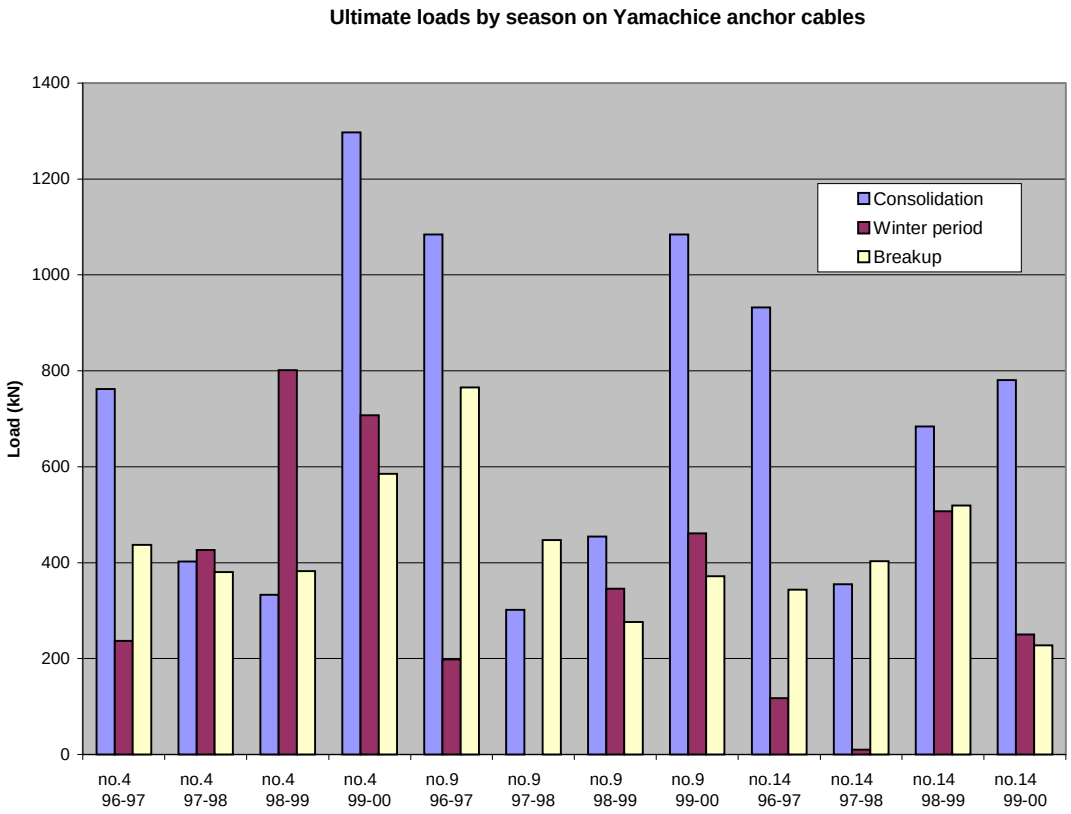


Figure 9.7 Peak load cell seasonal loads on Yamachiche anchor cables

The data show that during any given year at any location, the peak annual load can be attributed to any season. On the other hand, in general, the loads during the consolidation period are the largest. They are followed by loads during the break-up period. They are 60% to 70% of the former. Mid-winter events, though sometimes severe, are, in general, less than 50% of the those generated during the consolidation period.

Of course the largest load is not presented in this table because it was only recorded by mechanical means. The event was during the break-up period but because the event happened in an artificial manner (due to ice breaking of the cover from the banks), it is very similar in nature to a mid-winter event.

## 9.4 Lateral force dynamics

Consider the situation when the force in section cable no. 3 is greater than that in section no. 4. In order for the force balance to be preserved in the cables, the junction plate (no. 4) must move some amount X to the right. This implies that the span of section no. 4 increases by X and that of section no. 3 decreases by X. Using the geometric relationships applicable to parabolas, the new angles 3 and 4 can easily be determined. There will also be a shift in the anchor cable alignment. If the length of the anchor cable is $L_A$ then the angle shift will be very close to the value $\alpha = X/L_A$. Substituting these values into the force balance at the junction plate leads to the following equation 9.4:

$$\frac{T_3}{T_4} = \frac{\cos(\alpha_4) + \sin(\alpha_4)\tan(\alpha)}{\cos(\alpha_3) - \sin(\alpha_3)\tan(\alpha)} \qquad (9.4)$$

Knowing that $L_A$ is normally 38.1 m, by varying the span width by an amount X (ft), we calculate $\alpha_3$, $\alpha_4$and $\alpha$. We then apply this equation to build a functional relationship between the ratio $T_3/T_4$ and X(m). The relationships are shown in the following figure 9.8:

$$X = -2.9277(T_3/T_4)^2 + 15.98(T_3/T_4) - 13.01 \qquad (9.5)$$

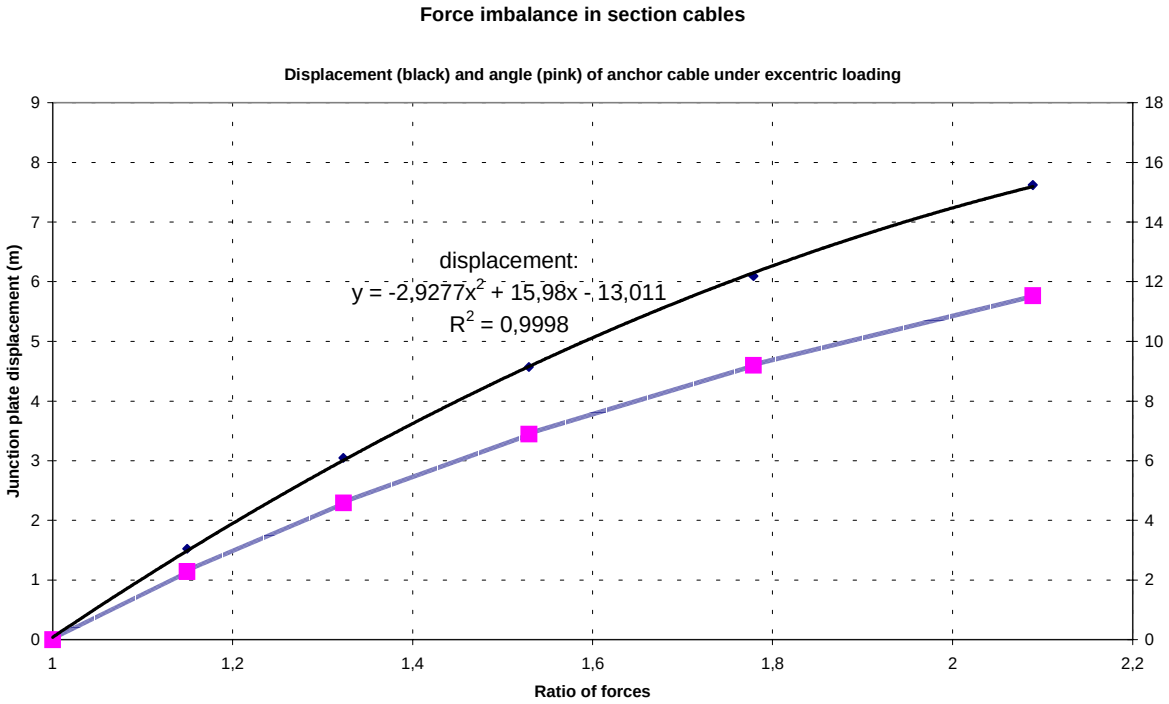


Figure 9.8 Relationship between force imbalance in section cables and displacement of a junction plate

We then applied the resulting relationship 9.5 to measured data for cables 3 and 4 at Yamachiche for the year 1999-2000. The interpreted movement of the junction plate is shown in the following Figure 9.9.

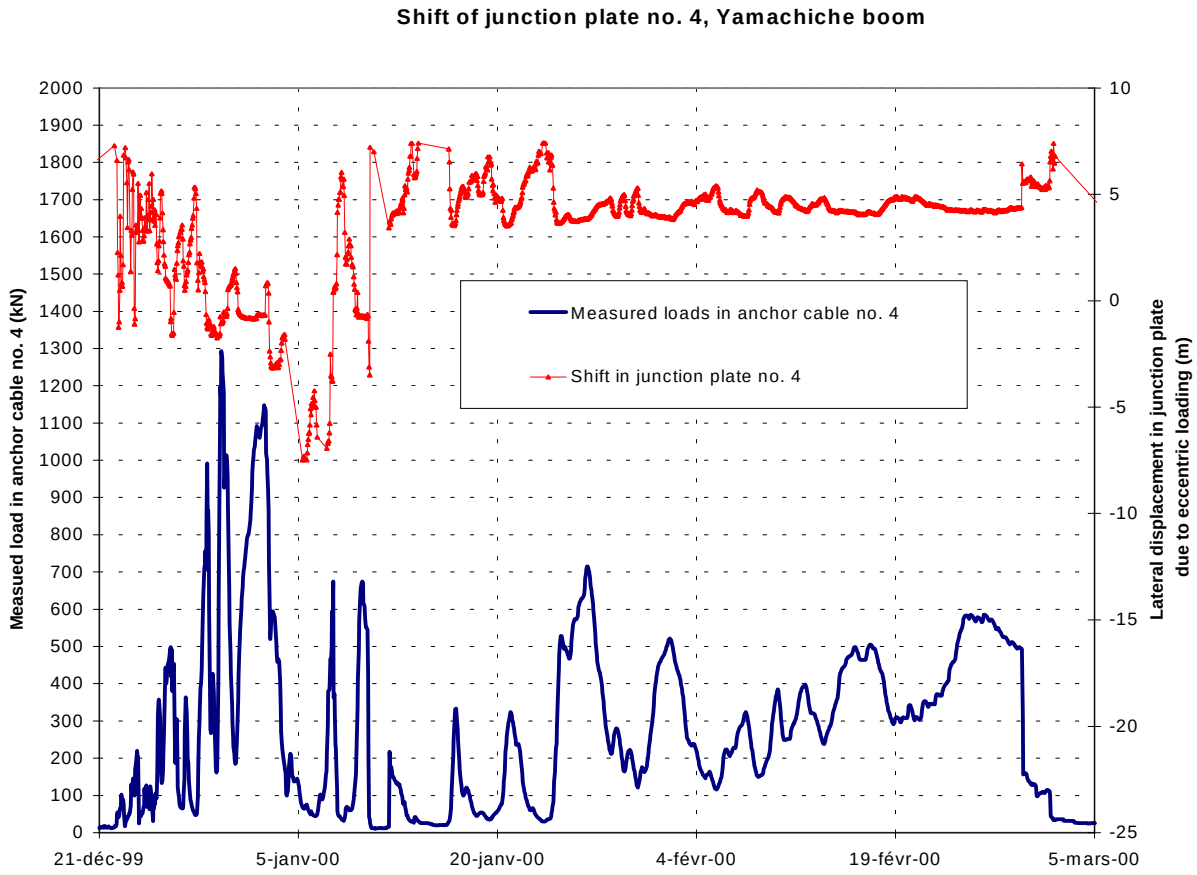


Figure 9.9 Shift in junction plate no. 4 to compensate eccentric loading in section cables

# 10 Analysis of ultimate loads

## 10.1 Spatial-temporal distribution at Yamachiche

The force balance analysis has just shown us that the load in one cable influences the load in all other cables. In fact, in a perfectly symmetrical boom, the force in all cables would be equal. However, we have also seen that there are three additional elements that allow a certain independence between loads in individual cables. At the Yamachiche boom, given that there are lateral anchor cables at junction plates no. 1, 5, 6, 10, 11, 15 and 16, from a force balance point of view, forces in sections 1 to 5, 5 to 10, 10 to 15, 15 to 19 and 0 (all by itself) can act as 5 sub-systems. For example, this means that a peak load event in section no. 17 will be passed in to neighbouring cables 15 to 19 but will normally not be passed to any sections 0 to 14. What this means therefore is measured forces in the 5 different sub-systems can be fairly independent. Given that we have measured the loads on anchor cables no. 3, 4, 7, 9, 13, 14, 17 and 18, we can make the following groups of dependent loads:

(3 & 4)
(7 & 9)
(13 & 14)
(17 & 18)

The second element which brings independence is the fact that the boom moves to absorb non-uniform loading and hence only a certain percentage of the difference is passed on to its neighbour. The further the neighbour is from the peak load, the more independent it is.

The third element of independence is the fact that some of the non-uniform loading is absorbed by the ice cover upstream of the boom. When the ice aggregate is thick and dense or when the cover is consolidated, this may be a very effective filter of load transmission between cables.

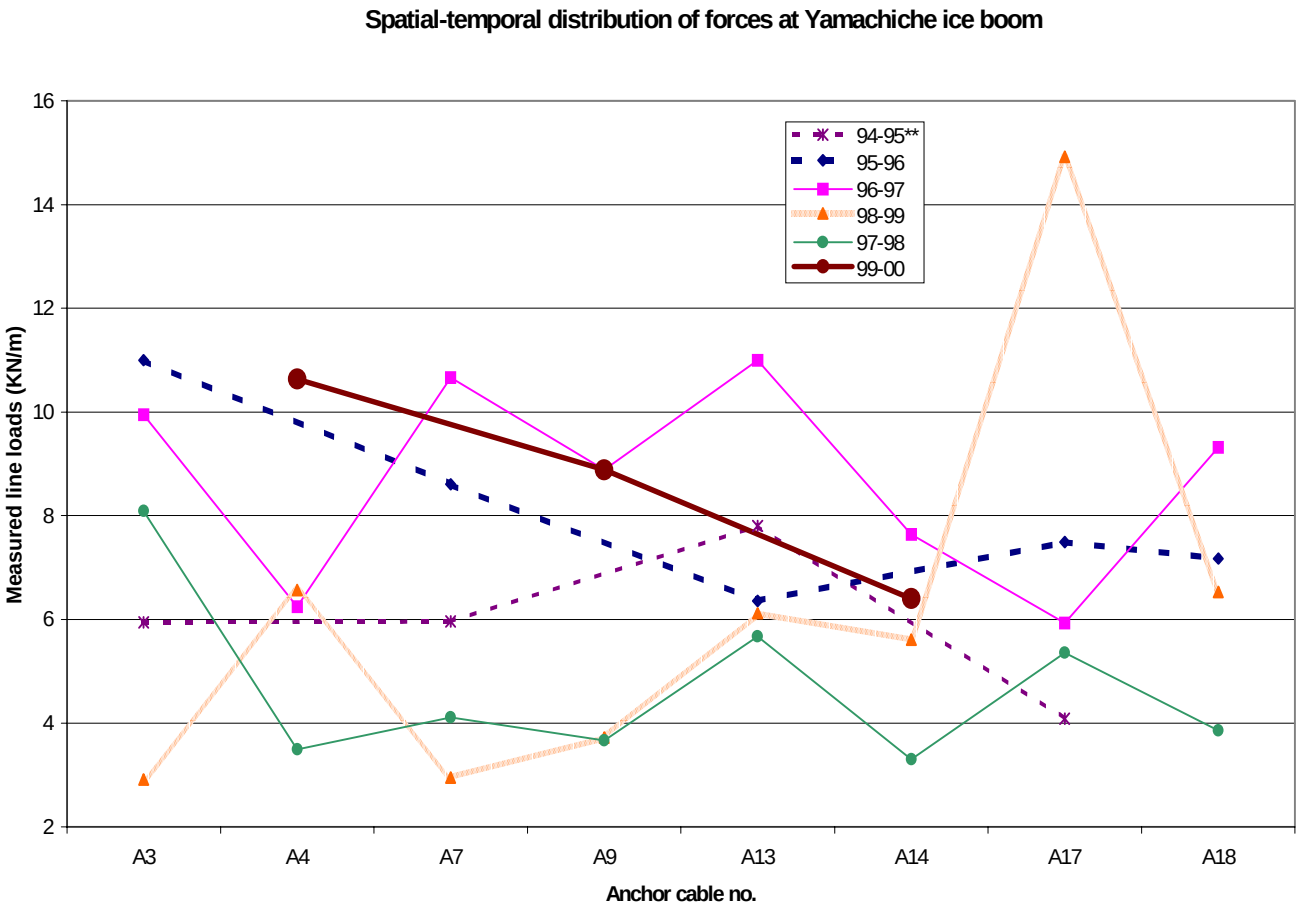


Figure 10.1 Spatial-temporal distribution of maximum anchor cable loads at Yamachiche boom

Figure 10.1 displays the maximum load measured in these anchor cables for each individual year (for convenience, loads are expressed as line loads). The source of the data is the maximum value recorded by the load cells or the ultimate value interpreted from mechanical analysis. In the case of the latter, as explained above, prior to plotting them, they were reduced by 8% to account for the over-estimation in the calibration curve. The values of 1994-95 are known, but due to a mix up at the time of recording, we are not 100% sure of the location of the loads. In addition, the layout of the boom during 94-95 was different than in subsequent years (there were three sections of 76 cm pontoons mixed in with 61 cm pontoons elsewhere) and therefore values should not be directly compared with other years.

How can we interpret the data? First, we see that the load at anchor no. 17 during 1998-99 really stands out. As we explained above, we believe that the mechanism causing this high value was very different from the norm. We believe this event happened near the end of the season when the cover was partially frozen into the boom and the cover was suddenly broken free (on purpose) from the north shore of the lake by CCG ice breaking.

The second striking characteristic of the figure is that there seems to be no discernible pattern to the loads. In other words, we do not find (as we may have expected) higher loads in the centre. Nor do we find higher loads on the south side (A3 & A4) as compared to the north side (A17 & A18).

The ultimate line loads vary by a factor of 5 (between 2.5 kN/m and 11 kN/m). In general, we can see that the winters 95-96, 96-97 and 99-00 are years with higher loads while the winters of 97-98 and (except for the load at A17) 98-99 are lower than normal. We do not necessarily see grouping of forces (A3 & A4, A7 & A9, etc.) predicted by the geometry of the boom.

Also, it seems that there is less variation in loads across the boom than there is between years.

All of the above having been said, there are insufficient data points in space and time to statistically show any significant spatial or temporal dependence or independence. So until we get more years of data, we will treat the values as independent - knowing full well that there are certainly some interdependencies.

## 10.2 Statistical analysis

We performed a statistical analysis on peak annual loads. Table 10.1 summarises the data used. For the most part, it is the same data as those just discussed in the spatial-temporal analysis except that data from Lavaltrie & Lanoraie were also included. Data was retrieved from load cells and mechanical analysis. The adjustment of 8% was applied to the data stemming from the mechanical means prior to analysis.

| | Lavaltrie | Lanoraie | Best estimate of peak annual load at Yamachiche anchor cables | | | | | | | | | | |
|---|---|---|---|---|---|---|---|---|---|---|---|---|---|
| Year | A3 | A4 | mean values | max values | A3 | A4 | A7 | A9 | A13 | A14 | A17 | A18 | A19 |
| 94-95* | 751 | 340 | 762 | 947 | 721 | | 723 | | 947 | | 496 | | 922 |
| 95-96 | 673 | 667 | 986 | 1335 | 1335 | | 1044 | | 771 | | 909 | 870 | |
| 96-97 | 1048 | 627 | 1073 | 1334 | 1207 | 762 | 1294 | 1084 | 1334 | 1051 | 719 | 1131 | |
| 97-98 | 787 | 665 | 572 | 982 | 982 | 426 | 499 | 455 | 688 | 411 | 650 | 468 | |
| 98-99 | 673 | 423 | 749 | 1811 | 353 | 801 | 358 | 454 | 742 | 684 | 1811 | 792 | |
| 99-00 | 850 | 619 | 1054 | 1297 | | 1297 | | 1084 | | 781 | | | |
| Mean: | 797 | 557 | 866 | 1284 | 920 | 822 | 783 | 769 | 896 | 732 | 917 | 815 | 922 |
| Max: | 1048 | 667 | 1073 | 1811 | 1335 | 1297 | 1294 | 1084 | 1334 | 1051 | 1811 | 1131 | 922 |

* Except for Lavaltrie, the location of measured values is uncertain in 1994-1995

Table 10.1 Maximum annual line loads (kN/m) measured on St. Lawrence boom anchor cables (data from load cells and/or mechanical means).

Our choice of data inclusion was based on trying to maximise the number of independent data points while trying to respect data homogeneity. The latter is not perfect because all the booms were slightly modified each year. (A complete history of the changes made to the booms is detailed by Stéphane Dumont in an internal report. The main changes include adding sections at all three locations, changing pontoon sizes and changing the number of pontoons per section.)

Figure 10.2 presents the basic statistics. The number of data points (n) is 44. The maximum (max) and minimum (min) values are 14.84 and 2.89 kN/m. The average value (moy) is 6.79 kN/m. The standard deviation (s) is 2.54 kN/m. The coefficient of variation (CV) is 0.37; the coefficient of skewness (CS) is 0.79 and the coefficient of flatness (CK) is 0.094. Linear statistics are also presented for the standard deviation ($\lambda_2$), coefficient of variation (L-CV), coefficient of asymmetry (L-CS) and flatness (L-CK). They are respectively 1.413, 0.21, 0.13, 0.14.

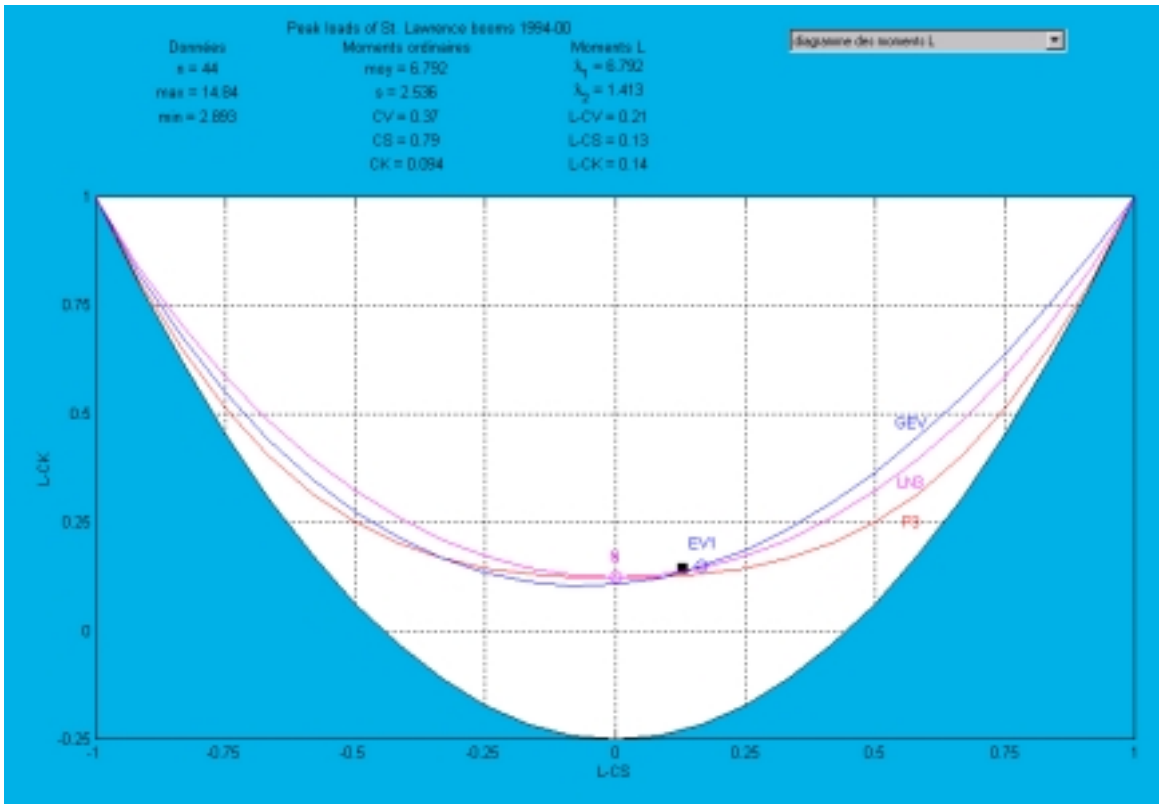


Figure 10.2 Situating Measured line load (kN) peak annual data (black square) within a generic plot of different distributions

Figure 10.2 is a plot of the linear moments L-CK representing the flatness of the distribution against L-CS which represents the asymmetry of the distribution (Vogel and Fennessey, 1993). The normal distribution is represented by an empty square identified by the symbol N (Anctil, 1998). A normal distribution has the co-ordinates (L-CS, L-CK = 0, 0.1226). The Gumbel distribution is represented by the circle next to the symbol "EV1". It's co-ordinates are (0.1699, 0.1504). Other distributions do not have unique L-CS/L-CK co-ordinates. They are represented by lines and include the log-normal-3 (LN3), Pearson-3 (P3) and the Generalised extreme value (GEV) distributions.

Also included in Figure 10.2 are the co-ordinates of the coefficients from the analysed load data (0.13, 0.14). It is represented by the full black square. As we can plainly see, the square falls very close to the co-ordinates of the Gumbel distribution (EV1) and also is next to the lines representing GEV, P3 and LN3. In other words, we can expect that any of these distributions will adequately represent our data. The only distribution that is any distance from our data is the normal distribution.

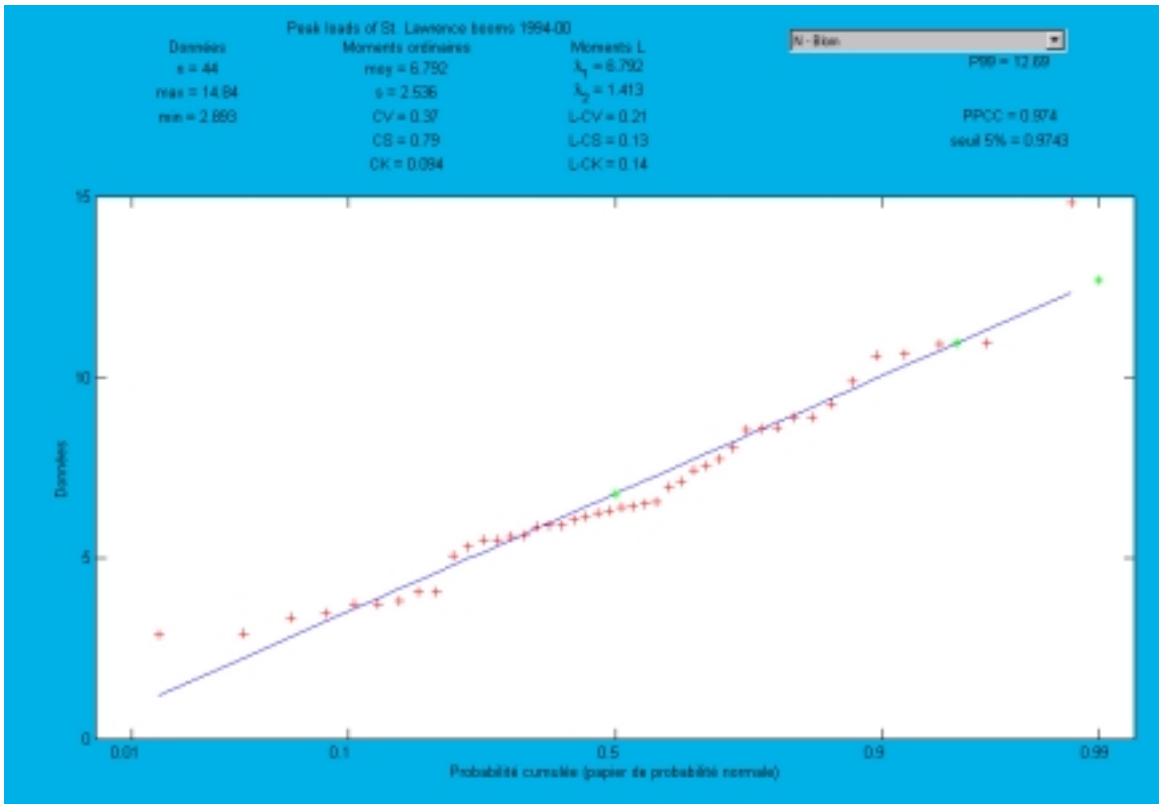


Figure 10.3 Measured line load (kN) peak annual data plotted (red +) against the normal distribution

Figure 10.3 represents the fitted normal distribution. In the centre portion of the data, the distribution is representative but has difficulty representing the tails. The PPCC criterion indicating the goodness of fit is 0.974 whereas the criterion for acceptance at the 5% level is 0.9743. Based on this information, the distribution is only marginally acceptable.

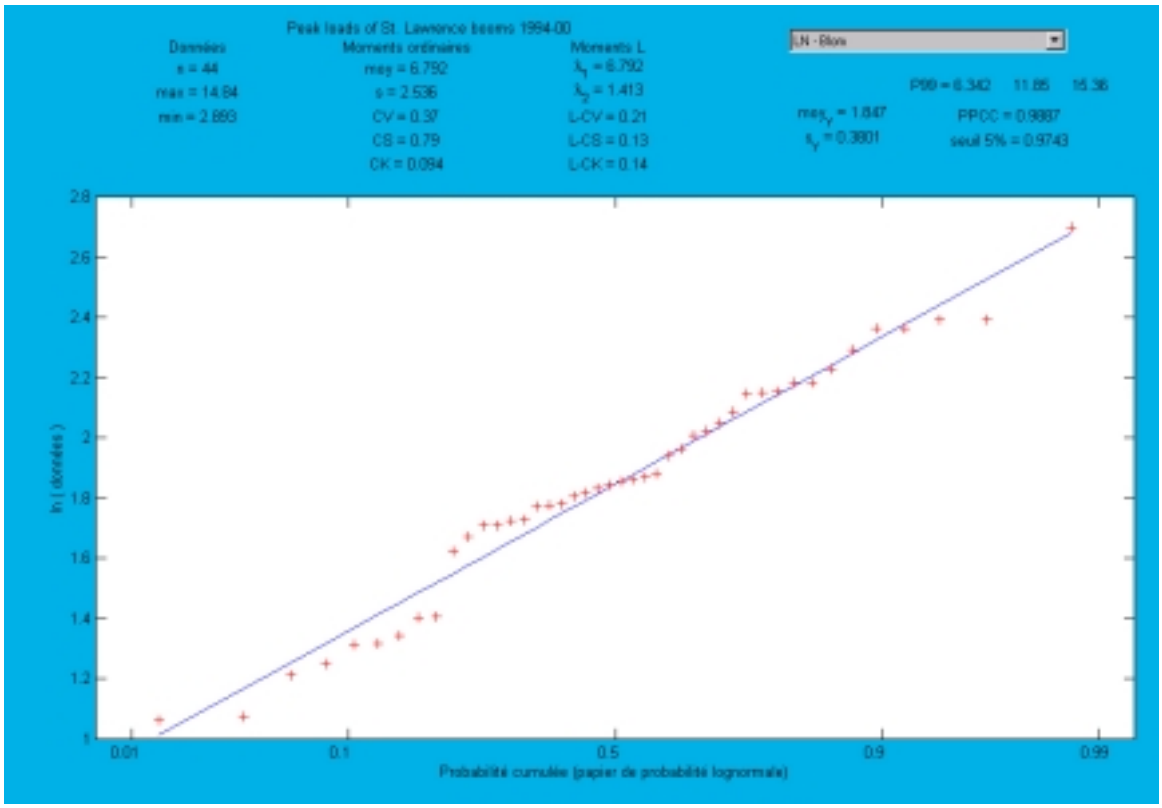


Figure 10.4 Measured line load (kN) peak annual data plotted (red +) against the log-normal distribution

Figure 10.4 shows the log-normal fit. All the data pretty well falls on the line and the goodness of fit 0.989 agrees favourably with the 5% rejection criterion of 0.9743.

(Unfortunately, Figure 10.5 is not available for inclusion)

Figure 10.5 Measured line load (kN) peak annual data plotted (red +) against the Pearson-3 distribution

Figure 10.5 shows the Pearson-3 fit. All the data pretty well falls on the line and the goodness of fit 0.990 agrees favourably with the 5% rejection criterion of 0.968.

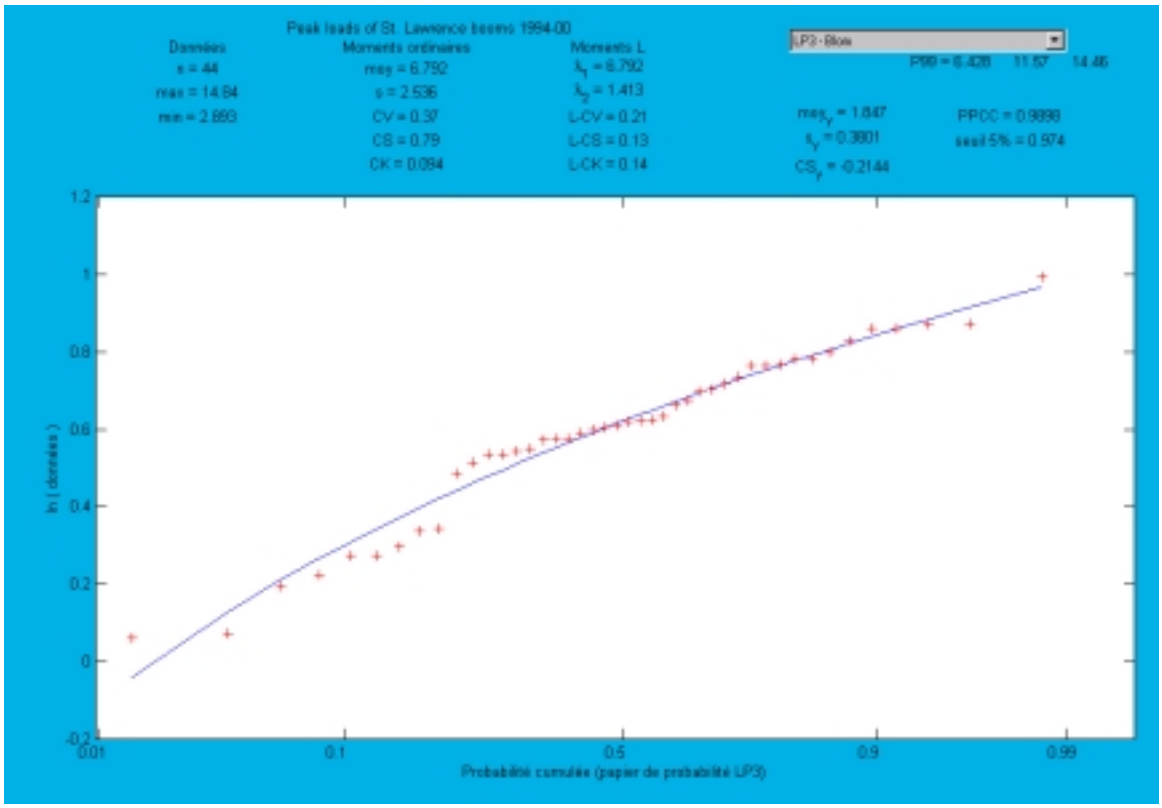


Figure 10.6 Measured line load (kN) peak annual data plotted (red +) against the log-Pearson-3 distribution

Figure 10.6 shows the log-Pearson-3 fit. All the data pretty well falls on the line and the goodness of fit 0.989 agrees favourably with the 5% rejection criterion of 0.974.

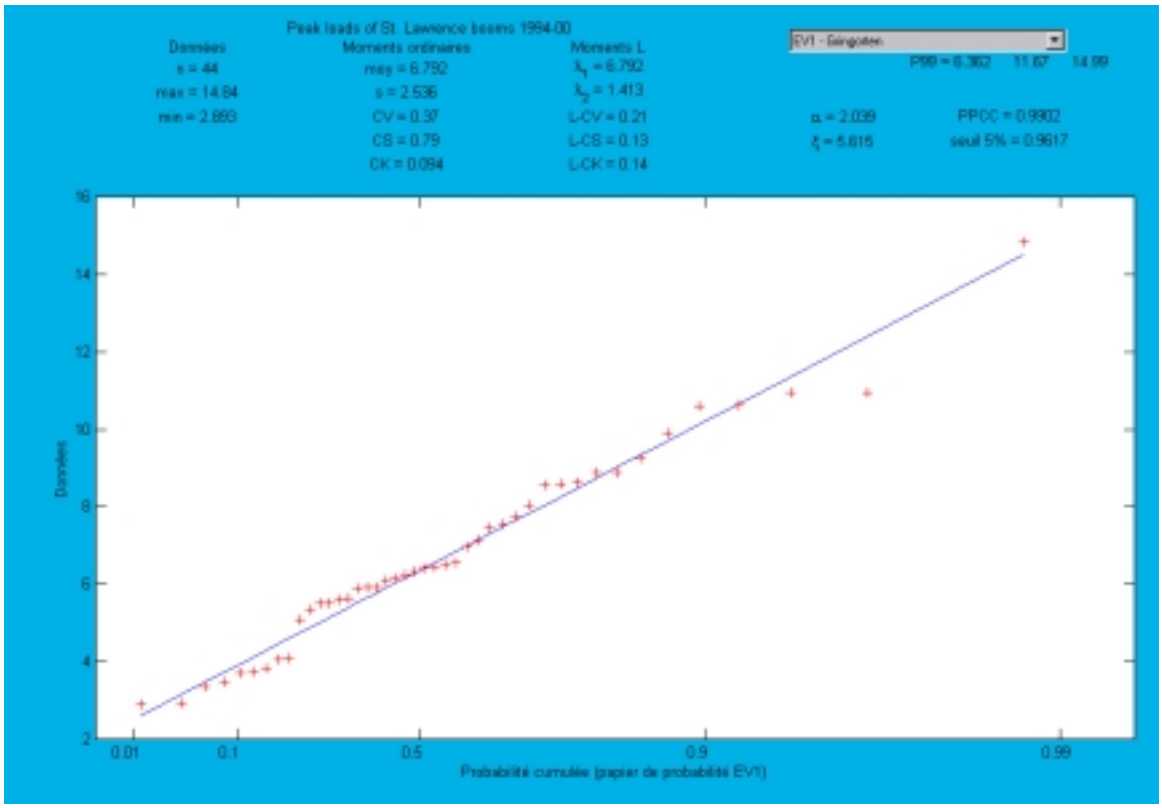


Figure 10.7 Measured line load (kN) peak annual data plotted (red +) against the Gumbel distribution

Figure 10.7 shows the Gumbel distribution fit. All the data pretty well falls on the line and the goodness of fit 0.990 agrees favourably with the 5% rejection criterion of 0.9617.

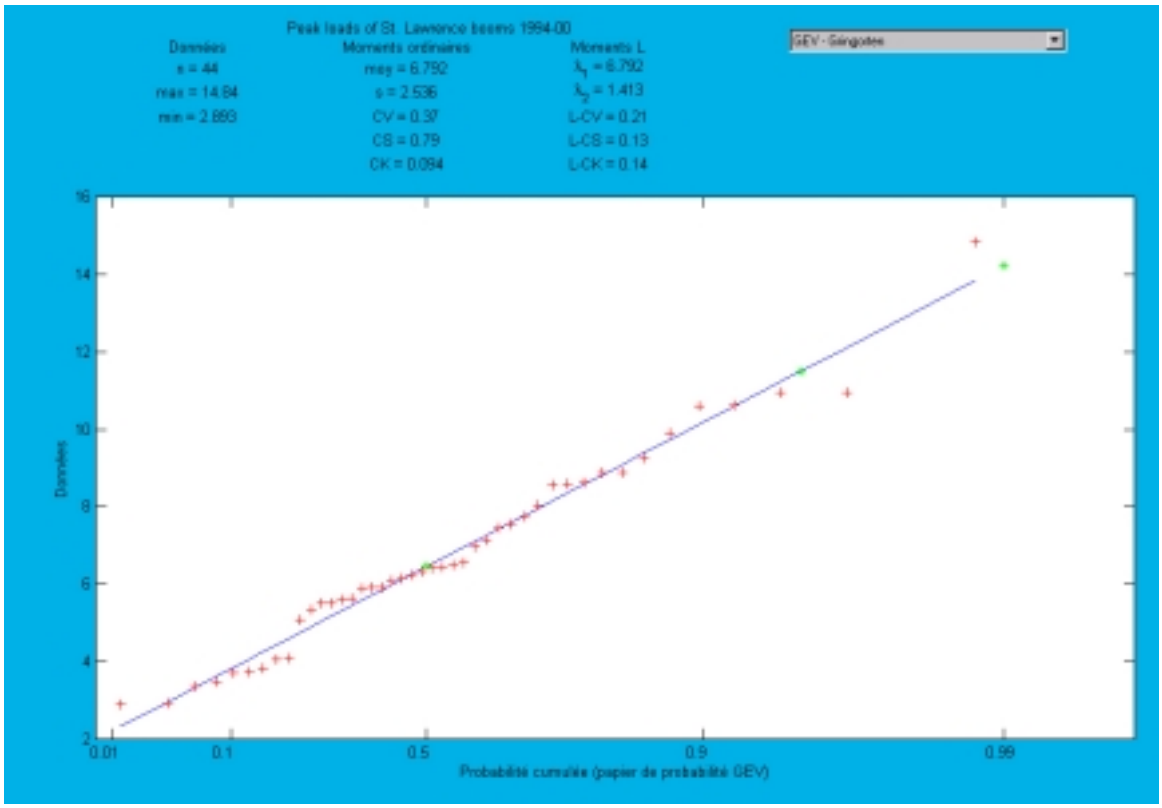


Figure 10.8 Measured line load (kN) peak annual data plotted (red +) against the log-normal distribution

Figure 10.8 shows the Generalised extreme value fit. All the data pretty well falls on the line.

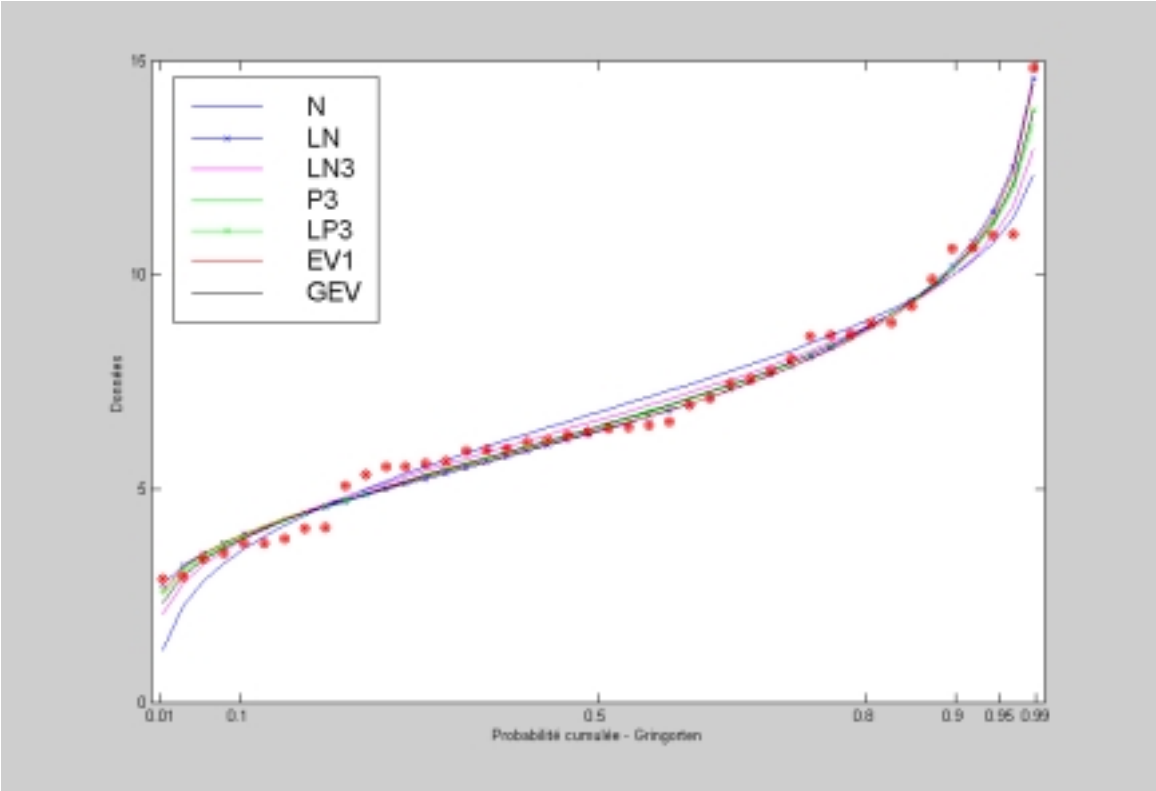


Figure 10.9 Measured line load (kN) peak annual data (red +) plotted against all distributions

The resulting fitted distributions and the probabilities calculated from the measured data according to Gringoten's formula are plotted in Figure 10.9. Except for the normal distribution, all the others are pretty well equivalent. Figure 10.10 provides a zoom in at the high end of the curves.

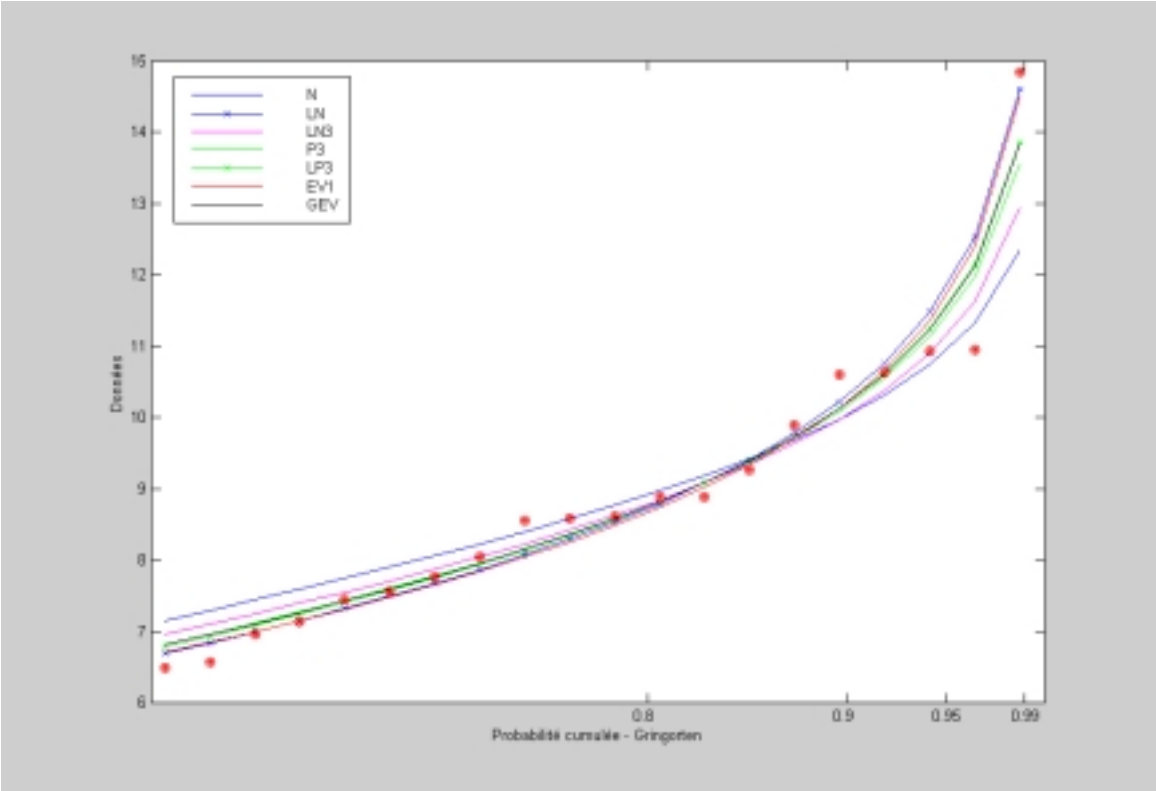


Figure 10.10 Measured line load (kN) peak annual data (red +) plotted against all distributions (zoom in).

Having fitted the distribution, the following are the calculated line loads (kN/m) according to a given level of probability:

| | Estimated line load (kN/m) As a function of cumulative probability | | |
|---|---|---|---|
| Distribution | 50% | 95% | 99% |
| Normal | 6.79 | 10.96 | 12.69 |
| Log-Normal | 6.34 | 11.85 | 15.35 |
| Log-Normal-3 | 6.60 | 11.16 | 13.40 |
| Pearson-3 | 6.46 | 11.44 | 14.11 |
| Log-Pearson-3 | 6.43 | 11.57 | 14.46 |
| Gumbel | 6.36 | 11.67 | 14.99 |
| Generalised extreme value | 6.46 | 11.50 | 14.24 |
| Average (not including the normal distribution) | 6.4 | 11.5 | 14.4 |

### 10.2.1 Statistical distribution

Putting the results of the normal distribution aside, all distributions predict very similar values. On average, the 50% probability ultimate annual line load on the booms is 6.4 kN/m, the 95% probability is 11.5 kN/m and the 99% probability is 14.5 kN/m. We note that the 50% value is slightly lower than the calculated mean (6.8 kN/m). The 99% value is also slightly lower than maximum measured value (14.9 kN/m). Given the goodness of fit of the distributions and the consistency of the results, we are led to accept the average values as representative of the measured loads. Outside of the normal distribution, one could choose among any distribution.

How should one interpret the results? If we accept that the data really represent independent events equivalent to 44 winters then we can say that there is a 1% chance of having a line load in excess of 14.5 kN in any given year. However, we feel that there must be some interdependence between measured values and the data is not representative of 44 years. How then should we interpret it?

One way to interpret the data is to assume that the observed measurements correspond to the risk of an event to occur over a 6 year period (we call this method 1). Since on average, we have m = 7.3 events (= 44/6) per year, we could say that the actual risk R corresponding to the 44 year analysis is given by

$$R = 1 - P^m \qquad (10.1)$$

where P is the calculated probability and m is the number of independent locations that ice loads can be applied on a boom.

*In our case, a 99% value of P yields an actual risk of 7% per year rather than 1% as assumed above. A 95% value of P yields an actual risk of 30% and a 50% probability is actually a 99% risk.*

Alternatively, (method 2) we could use our knowledge that the log-normal distribution is representative of the process and analyse only the maximum peak loads for each year (6 data points), we get line loads of 10.3, 15.2, 17.9 kN/m corresponding to the 50%, 95% and 99% levels respectively. These values are 1.6, 1.3 and 1.2 higher than the previous assumption. These values are representative of the maximum peak load likely at any spot on any of the St. Lawrence river booms.

Note that the 95% value of method 2 (15.2 kN/m) corresponds very well with the 7% risk value calculated above from method 1 (14.5 kN/m). This shows that using the 44 measurements and the concept of risk (method 1) is more or less equivalent to method 2 using 6 measurements and the calculated probabilities.

### 10.2.2 Summary

For the St. Lawrence booms, there is a 50%, 95% and 99% likelihood that the peak annual loads on all the booms for all measured locations will not exceed 10.3, 15.2 or 17.9 kN/m respectively.

For booms similar to those on the St. Lawrence, we can use the statistics calculated from method 1 to calculate the risk of a load based on the length of the boom. To do this, one could assume that every fourth anchor cable is independent and calculate the annual risk based on m' (= no. of anchor cables in the boom ÷ 4) and use equation 10.1 to calculate the risk of having a load of 6.4, 11.5 or 14.4 kN corresponding to the values of P = 0.5, 0.95 and 0.99. For example, for the Lavaltrie boom, there are 10 anchor cables giving m' = 2.5. The annual risk corresponding to the values of 6.4, 11.5 or 14.4 are then estimated to be 82%, 12% and 2.5% respectively.

# 11 Findings

## 11.1 Peak loads

- According to two different approaches, the maximum environmental push exerted by the ice on the boom is presented in Table 6.6 When there is lateral confinement, the estimated line loads under very severe conditions are 20 to 21 kN/m for all three booms. When there is no lateral confinement, the estimated loads are 5, 10 and 15 kN/m for Yamachiche, Lanoraie and Lavaltrie respectively. These values need to be updated as better field data becomes available. Observations show that the confinement is partial and therefore the maximum environmental push is closer to the 20kN/m value.

- According to the CRREL report EM 1110-2-1612, page 3-4, measured loads on traditional timber booms vary between 6 and 20 kN/m.

- According to laboratory studies at CHC (Timco and Cornett, 1996), in the flexural failure mode, the maximum peak load for 61 cm booms was 1.76 kN. Dividing by the width of the boom used in the laboratory test (1.5 m) gives a line load of 1.17 kN/m. Assuming that the force is proportional to the ice thickness, this would correspond to prototype loads of 16 kN/m (= 65 cm / 4.7 cm ice thickness used).

- The laboratory tests also suggested that in buckling, the line load would be 2.9 instead of 1.76 which would translate into a prototype value of 26 kN/m.

- Figures 7.6 and 7.7 show the resistance of the ice sheet as a function of its internal strength and it's thickness. For a consolidated cover greater than 15 cm, its resistance in flexure is greater than the boom's ability to support the load. For example, for 400 MPa ice, a 50 cm sheet can deliver a 16 kN/m push. However, for thin ice sheets, (less than 10 cm) the ice will fail before the boom will sink.

- Figure 7.7 shows that ice is always weaker in flexure than under buckling. It also shows that the boom will fail before the ice will buckle.

- A new method was developed to estimate the load retention capacity of the boom as a function of pontoon size, pontoon submergence, boom geometry, water levels, ice/structure friction coefficient and ice thickness. The analysis showed that the geometry of the ice at the interface, ice thickness and friction coefficient all play a key role. Estimated retention capacities correspond very well with observed values.

- Measured loads on anchor cables, 44 quasi-independent annual peak loads were statistically analyses for the Yamachiche and Lavaltrie booms. The average peak load was 6.8 kN/m with a standard deviation of 2.5 kN/m. The maximum recorded value was 14.8 kN/m.

- Peak loads annual loads at Lavaltrie were, on average, 8% lower than the average of the peak annual loads at Yamachiche. However, they were 38% lower than the peak maximum annual loads at Yamachiche.
- Peak loads at the Lanoraie rectangular timber boom were correspondingly 20% and 48% lower.
- Whereas there is no statistical difference in the Lavaltrie/Yamachiche data, clearly forces on the timber boom at Lanoraie are significantly lower and were therefore excluded from the statistical analysis.
- With the exception of the Normal distribution, virtually all the statistical distributions fit the data extremely well. Based on the results and a risk analysis, for the St. Lawrence river booms, in any given year, there is a 7% chance of exceeding a 14.5 kN/m load, a 30% chance of exceeding a 11.5 kN/m load and a 99% chance of exceeding a 6.4 kN/m load.
- Based on an alternative statistical analysis of 6 events, data was extrapolated well beyond the scope of observations to yield the estimated values of 10.3, 15.2 and 17.9 kN/m corresponding to an annual probability of 50%, 5% and 1%.
- A method was also devised to calculate the risk for any given boom structure in similar environmental conditions. An example is detailed in the report at the end of Chapter 10.
- Given that there are chains that break every year, the estimated peak ***local*** load can well exceed 40 kN/m.

In general, there is a good correspondence between theoretically computed environmental loads, those estimated from laboratory studies and the field data.

## 11.2 Spatial-temporal analysis

- Flexible booms tend to spread local loads over their entire structure. The one exception are those sections close to the banks. At times, they can be subject to very high local forces generated by booms being frozen into the ice cover.
- There are no systematic trends in the variation of line loads over the width of the structure.
- Loads seem to vary from one year to the next (for example, some year's loads are higher than other years). However, there is no statistically significant way to show this.
- Section cable analysis shows that the force in one cable can be up to two times the force in the neighbouring section cable. The boom adjusts to the non-uniform loading by modifying its span lengths. A new formula (6.2) developed for this

purpose indicates that junction plate movement can be in the order of 7 m for the Yamachiche boom corresponding to a shift in the anchor cable of about 10°.

- Field data and theoretical analysis tend to show that maximum loads at one anchor cable are more or less interdependent of their neighbours. We prefer using the concept that the nearest neighbours are dependent while those cable further away are independent.

## 11.3 Loading dynamics

- Maximum two-minute loads are about 3% greater than loads sampled at 2 Hz.
- Maximum hourly loads are about 3% greater than maximum two-minute values.
- During the consolidation period, loads may substantially vary during the course of any given day.
- Spectral analysis shows a logarithmic decline of energy with increasing frequency.
- Frequencies smaller than 1 per day have virtually no energy in them.
- Spectral analysis shows that there seems to be peaks load every week and/or every other week.
- The overwhelming energy content corresponds to the length of the consolidation period. This normally last between 1 and 5 weeks.
- A seasonal analysis of the loading at many locations over the 6-year period shows that the peak annual load can happen during any given season. However, normally, it happens during the consolidation period.
- On average, peak loads during the consolidation period are normally 40% higher than at break-up and 50% higher than for mid-winter events.

The data clearly shows that the fact that the boom is flexible, the ice/structure interaction is very favourable. Peak local loads are distributed and high-frequency impact loading is negligible.

# 12 Conclusions

Our analysis shows that the 61-cm pontoon cylindrical ice boom is a very efficient structure. Due to its three-dimensional nature, it effectively filters out high frequency and eccentric loading.

Applied forces depend primarily on environmental factors, ice strength properties, ice thickness, the ice/structure friction coefficient and the size and buoyancy of the

pontoons. Methods to determine these effects are presented. Calculated and measured values are in good agreement.

Although deterministic analyses are useful to provide insights into processes and to design members, observed values are clearly stochastic in nature. Equations are presented to calculate the probability of load exceeds a given value as a function of the boom length and the number of years considered. The mean and maximum recorded peak loads for the St. Lawrence River booms were 6.8 kN/m and 14.8 kN/m. Some 3 to 8 chains connecting the pontoons to the cables break every year. This implies that local loads (over a 10 m width) exceed 40 kN/m.

# 13 References


Abdelnour, R., Comfort, G., and Gong, Y. 1995. Phase III: Field observation program, Canadian Coast Guard's Yamachiche, Lanoraie and Lavaltrie ice booms. Draft Report prepared for New York power Authority by Fleet technology Limited, May 1995.

Abdelnour, R., Comfort, G., and Gong, Y. 1994. Phase I: Assessment of ice boom technology for application to upper Niagara river. A Report #3987C.FR Submitted by Fleet Technology Limited to New York Power Authority, June.

Abdelnour, R., Cowper, B., and Gong, Y. 1995. The development of a field observation and monitoring for the Yamachiche ice boom (lac St. Pierre). A Report Submitted to the Transportation Development Centre and the Canadian Coast Guard, Fleet Technology Limited report 4267-5C, December.

Abdelnour, R., Crissman, R. D., and Comfort, G. 1994. Assessment of ice boom technology for application to the Upper Niagara River. In Proceedings of the IAHR Symposium on Ice, 23-26, August 1994, Trondheim, Norway, Vol 2, pp.734-743.

Abdelnour, R., and Croasdale, K. 1986. Ice forces associated with ridge-building: Model tests and results compared with theoretical models. IAHR Symposium, Iowa.

Abdelnour, R., Gong, Y., Comfort, G., and McGoey, L. 1993. Lavaltrie ice boom : preliminary design for new boom pontoons. Fleet Technology Report FTL-4319, Kanata, Ont.

Abdelnour, R., Murray, A., and Eryuzlu, E. N., 1990. Etude en Modèle Réduit du Comportement d'un Couvert de Glace Autour du Pilier d'un Pont Avec Ilot protecteurs, Proceedings of CSCE, Burlinton, Ont.

Anctil, F. 1998. Introduction à l'hydrologie physique. Notes de cours. Université Laval. Québec.

Ashton, G. D., 1986. River and lake ice engineering. Water Ressources Publications, Post Office Box 2841, Littleton, Colorado 80161, USA.

Beauchemin, R., and Pellegrin, C., 1969. Lavaltrie – 1969 Survey. Ministry of transport Internal Memorandum.

Beltaos, S. 1995. River ice jams. Water Ressources Publications, LLC, P. O. Box 260026, Highlands Ranch, Colorado, 80163-0026, USA.

Beltaos, S. 1995. Monograph on river ice jams. River Modelling Project, River Research Branch, National Water Research Institute, Canada Centre for Inland Waters, Burlington, Ontario.

Berdennikov, V. P. 1964. Dynamic conditions of formation of ice jams on rivers. Soviet Hydrology, Selected papers, Washinton, Am. Geoph. Union, pp. 101-108.

Bolsenga, S. J. 1968. River ice jams – a literature review. U. S. Army Corps of Engineers Lake Survey District, Detroit, Michigan, Research Report 5-5.

Bryce, J. B., and Berry, G. T. 1967. Lake Erie-Niagara Ice Boom.

Calkins, D. J., Deck, D. S., and Martinson, C. R. 1982. Resistance coefficients from velocity profiles in ice-covered shallow streams. Canadian Journal of Civil Engineering, Vol. 9, No. 2, June 1982.

Campbell, W. 1965. The wind-driven circulation of ice and water in polar ocean. Journal of Geophys. Research, 70, 3279-3300.

Caquot, A., and Kérisel, J. 1956. Traité de Mécanique des Sols, Gauthier-Villars.

Carter, D. 1995. Ice Management in Lac Saint-Pierre, TP 12439E. Report prepared for Transportation Development centre, Policy and Co-ordination, Transport Canada, Montreal.

Carter, D. 1994. Forces sur les estacades. Report prepared for Transport Canada, Québec, Qué.

Charlebois, J. F. R., Gélinas, R., and LeBlanc, L. G. 1977. Relève des Mesures de Glace, Hiver 1976-1977, CCG Ministry of Transport Internal Report.

Comfort, G., Abdelnour, R., and El-Tahan, H. 1987. Lateral ice pressure on vessels in ice covered waters. Fleet Technology Report, Transportation Development Centre.

Comfort, G., and Ritch, R. 1992. Pack ice stress measurements. proceedings of OMAE, Calgary.

Comfort, G., and Ritch, R. 1990. Field measurements of pack ice stresses. Proceedings of OMAE, Houston.

Cornett, A. M. 1997. Analysis of Ice Boom Loads: 1996-97. Controlled Technical Report HYD-CTR-038, Canadian Hydraulic Centre, national Research Council of Canada, Ottawa, Canada.

Cornett, A. M., and Frederking, R. 1996. Analysis of Ice Boom Loads from 1994-95 and 1995-96. Technical Report HYD-CTR-013, National Research Council and Canadian Hydraulics Centre.

Cornett, A. M., Frederking, R., Morse, B., and Dumont, S. 1997. Ice boom loads in the ST. Lawrence river, 1994-95 & 1995-96. Proceedings of 7th International Offshore and Polar Engineering Conference, ISOPE'97, Vol. II, pp. 442-448, Honolulu, USA.

Cornett, A. M., and Timco, G. W. 1995. Model tests of three ice-control Booms. Proceedings of Canadian Society for Civil Engineering Annual Conference, Ottawa, Canada, Vol. 1, pp. 87-96.

Cowper, B., Abdelnour, R., and Gong, Y. 1994. Phase II: Ice boom load measurement program. A Report Submitted to the New York power Authority, Fleet Technology Limited Report 4316C, August.

Croasdale, K., Comfort, G., graham, B., Frederking, R., and Lewis 1987. A pilot experiment to measure arctic pack ice driving forces. Proceedings of POAC, Fairbanks.

Croasdale, K. R., and others 1994. Overview of load transmission through grounded ice rubble. report prepared for the National Research Council of Canada, Ottawa, Ont., Canada.

Charlebois, J. F. R., Gelinas, R., and Leblanc, L.G. 1977. Relève des Mesures de Glace, Hiver 1976-1977. CCG Ministry of Transport Internal Report.

Cornett, A. M., and Timco, G. W. 1995. Model tests of three ice control booms. Proceedings of the 12th Hydrotechnical Conference, Ottawa, Ont., Vol. 1, pp. 87-96.

Danys, J. V. 1979. Artificial islands in lac St. Pierre to control ice movement. proceedings of 1st Canadian Conference on Marine Geotechnical Engineering, NRC and CGS.

Danys, J. V. 1978. Ice management of Lac St. Pierre, Québec. Canadian Journal of Civil Engineering, Vol. 5, no. 3.

Deck, D., and Perham, R. 1981. Evaluating the effects of installing a floating ice control structure in the Allegheny River at Oil City, Pa. Draft Report for U. S. Army Engineers District, Detroit Pittsburgh, U. S. A. Cold Regions Research and Engineering Laboratory.

Demuth, M.N., and Prouse T.D. 199X. A physical model of ice overthrust during the break-up of intact river-ice covers. Northern hydrology. Selected perspectives.

Enoki, k., Kunimatsu, S., Ohira, M., Muraki, Y., and Saeki, H. 1991. Control of the ice flow movement by using ice boom. Proceedings of the 7th Cold Region Technology Conference, pp. 638-643 (in Japanese).

Ettema, R., and Aquirre, G. 1990. Friction and Cohesion in Ice Rubble Fields Reviewed. 6th International Specialty Conference on Cold Regions Engineering, Sponsored by the ASCE, CSCE, CGS, and the SWG, Hanover, NH.

Evgin, E. & Sun, L. 1989. Review of analytical modelling of ice cover evolution. Final report for CHC. Dept. of Civil Eng. University of Ottawa.
Foltyn, E. P., and Tuthill, A. M. 1996. Design of Ice Booms. Cold Regions Technical Digest No. 96-1, April 1996.

Foulds, D. M. 1983. lake Eric Ice: Research's dream – Designers nightmare. Ice Consultat, RR#4 Uxbridge, Ontario.

Gold, L.W. and Williams, G.P. 1968. Ice pressures against structures. Proc. of a conference held at Laval University. Quebec, 10-11 Novembre, 1966.

Graham, B. W., Potter, R. E., Wood, K. N., and Comfort, G. 1984. Rubble protected drilling system development. IAHR Ice Symposium, Hamburg.

Hopkins, M.A., Hibler III, W.D. & Flato, G.M. 1991. On the Numerical Simulation of the Sea Ice Ridging Process. J. of Geophysical Research. Vol. 96. No. C3, pages 4809-4820.

Hunkins, K. 1972. Water stress and ocean current measurements at camp 200. AIDJEX Bulletin No. 12, Division of Marine resources, University of Washington, Seattle, Washington, 98105, Feb. 1972.

Hunkins, K. 1966. Ekman drift currents in the arctic ocean. Deep-Sea Research, 13, 607-620.

Jansen, 1895. Versuche Üeber Getreiderdruck in Silozellen. Zeitschr. Der Vereins Deutsche Jng. No. 35.

Johannessen, O. 1970. note on some vertical profiles below ice floes in the Gulf of St. Lawrence and near the North »Pole. Journ. Geophys. Res., 75.

Joint Board of Engineers, 1927. Report on the St. Lawrence Waterway Project. Printed by F.A. Ackland, Ottawa, Canada.

Karelin, I. D. and Timokhov, L. A. 1972. Experimental determination of the wind drag on an ice sheet. AIDJEX Bulletin No. 17, Division of Marine Resources, Univ. of Washington, Seattle, Washington, 98105.

Kennedy, R. J. 1958. Forces involved in pulpwood holding grounds. The Engineering Journal, Engineering Institute of Canada, Vol. 41, 58-68.

Kry, P. R. 1977. ice rubble fields in the vicinity of artificial islands. proceedings of POAC, St. John's.

Langleben, M. P., and Pounder, E. R. 1971. Remote sensing, ice mechanics and morphology, an outline of the problem. AIDJEX Bulletin No. 5, Division of Marine Resources, University of Washington, Seattle, Washington, 98105.

Latyshenkov, A. M. 1946. Investigations of Ice Booms, Hydraulic Structures, No.15: 4, USSR.

Lawrie, C. J. R. 1972. Ice control measures on the St. Lawrence Seaway. Proceedings of the 29th Eastern Snow Conference, Oswego, N.Y., pp. 123-146.

Leonard, J.W. 1988. tension Structures: Behavior and Analysis. New York: McGraw-Hill.

Ling, Chi Hai and Untersteiner, N. 1974. On the calculation of the roughness parameter of sea ice. AIDJEX Bulletin No. 23, (Arctic Ice Dynamics Joint Experiment), Division of Marine resources, University of Washington, Seattle, Washington, 98105, Jan. 1974.

Loset, S., and Timco, G. W. 1992. Laboratory testing of a flexible boom. Proceedings of OMAE.

McPhee, M. G. 1975. Measurements of the turbulent boundary layer under pack ice. AIDJEX Bulletin No. 29, Division of Marine Resources, University of Washington, Seattle, Washington, 98105, July 1975.

Michel, B. 1978. Ice Mechanics, Laval University Press.

Michel, B. 1971. Winter regime of rivers and lakes. U. S. Army Cold Regions Research and Engineering Laboratory, Hanover, N. H., CREEL Monograph III-Bla.

Michel, B. 1966. Thrust exerted by an unconsolidated ice cover on a boom. Proceedings of a Conference Ice Pressures against Structures held at Laval University, Québec 10-11 November 1966, National Research Council, Ottawa, Canada.

Michel, B., and Ramseir, R. 1971. Classification of river and lake ice. Canadian Geotechnical Journal, 8(1): 38-45.

Morton, F.i. 1963. Criteria for the stability of ice covers on rivers. Proceedings of the 1963 Annual Meeting, Eastern Snow Conference, Québec city, Canada.

Nishizawa, s. and Tanaka, S. 1988. Structural design of new type three legged ice barrier. IAHR Ice Symposium, Sapporo, Japan, August 1988.

Nezhikhovsky, R. A. 1964. Coefficient of roughness of bottom surfaces of slush ice cover. Soviet Hydrology: Selected Papers, No. 2, pp. 127-150.

Olofsson, T. , Fransson, L. & Sandkvist, J. 1991. Ice Crushing. Coldtech91-1. www.luth.se/depts/lib/coldtch/ct91-1.html.

Pariset, E., and Hausser, R. 1961. Formation and evolution of ice covers on rivers. Transactions of the Engineering Institute of Canada, 5(1): 41-49.

Pariset, E., Hausser, R., and Gagnon, A. 1966. Formation of Ice Covers and Ice Jams in Rivers. Journal of the Hydraulics Division, Proceedings of the American Society of Civil Engineers, ASCE, Vol. 92, No. HY6, Proc. Paper 4965, November 1966.

Perham, R. E. 1988. Inventory of ice problem sites and remedial ice control structures. CRREL Special Report 88-7.

Perham, R. E. 1983. Ice Sheet Retention Structures. CRREL Report 83-30.

Perham, R. E. 1978. Performance of the St. Marys river ice booms, 1976-1977. U. S. Army CRREL Report 78-24, Hanover, N. H.

Perham, R. E. 1978. Righting moment in a rectangular ice boom timber or pontoon. Proceedings of the IAHR Symposium on Ice Problems, Lulea, Sweden, 7-9 August, pp. 273-286.

Perham, R. E. 1977. St.Mary's river ice booms. CRREL Report 77-4.

Perham, R. E. 1974. Forces generated in ice boom structures. Special Report 200, U. S. Army CRREL, Hanover, N. H.

Perham, R. E., and Racicot, L. 1975. Forces on an ice boom in the Beauharnois canal. Third International Symposium on Ice Problems.

Rothrock, D. A. 1973. The steady drift of an incompressible arctic ice cover. AIDJEX Bulletin No.21, Division of Marine Resources, University of Washington, Seattle, Washington, 98105.

Potter, R. E., et al 1982. Development and field testing of a Beaufort sea ice boom. Offshore Technology Conference.

Pratte, B. D., and Timco, G. W. 1981. Anew model basin for the testing of ice-structure interaction. Proceedings of POAC'81, Vol II, pp. 857-866, Québec City, Canada.

Saeki, H. 1992. Ice control in northern harbors. IAHR Ice Symposium, Banff, Alberta.

Sarpkaya, T. and Isaacson, M. 1981. Mechanics of Wave Forces on Offshore Structures. Van Nostrand Reinhold Publishers, Toronto, Canada.

Siefert, W. J., and Langleben, M. P. 1972. Air drag coefficient and roughness length of a cover of sea ice. Journal of Geophsical Research, Vol. 77, No. 15, 20 May, pp.2708-2713.

Simard, L. 1976. Relève des Mesures de Glace, 1975-76. Ministère des Transports Internal Report.

Simard, L. 1975. Relève des Mesures de Glace, 1974-75. Ministère des Transports Internal Report.

Simard, L. 1974. Relève des Mesures de Glace, 1973-74. Ministère des Transports Internal Report.

Sodhi, D. S., and Adley, M. D. 1984. Experimental determination of buckling loads of cracked ice sheets. Proceedings of the 3rd International Offshore Mechanics and Arctic Engineering Symposium (OMAE'84), New Orleans, La., USA, Vol. 3, pp. 183-186.

Timco, G. W. 1986. EG/AD/S: A new type of model ice for refrigerated towing tanks. Cold Regions Science and Technology, Vol.12, pp.175-195.

Timco, G. W. 1984. Ice forces on structures: physical modelling techniques. Proceedings of IAHR State-of-the-art Report on Ice Forces on Structures, in Proc. IAHR Ice Symposium, Vol IV, pp. 117-150, Hamburg, Germany.

Timco, G. W. 1981. Invited Commentary: on the test methods for model ice. Cold Regions Science and Technology, Vol. 4, pp. 269-274.

Timco, G. W., and Cornett, A. M. 1994. Laboratory tests of ice interaction with the booms in Lac St. Pierre. National Research Council of Canada, Ottawa, Ont., Report IECE-CEP-TR-003.

Timco, G. W., and Cornett, A. M. 1996. Laboratory tests of ice interaction with steel booms. Canadian Journal of Civil Engineering 23: 560-566.

Timco, G. W., and O'Brien, S. 1994. Flexural strength equation for sea ice. Cold Regions Science and Technology 22: 285-298.

Tsang, G. 1982. Resistance of the Beauharnois canal in winter. Journal of the Hydraulics division, ASCE, 108(HY2).

Tuthill, A. 1995. structural ice control: Review of existing methods. USA Cold Regions Research and Engineering Laboratory, Special Report 95-18.

Untersteiner, N., and Badgley, F. 1965. Roughness parameters of sea ice. Journ. Geophys. Research, 70, 4573-4577.

Uzuner, M. S. and Kennedy, J. F. 1972. Stability of floating ice blocks. Journal of the Hydraulics Division, ASCE, 98(HY12):2117-2133.

Vivatrat, V., and Kreider, J. R. (1981). Ice force predication using a limited driving force approach. Proceedings of the 13th Annual Offshore Technology Conference, Houston, Texas.

White, K. D. 1992. Salmon River experimental ice boom 1989-90 and 1990-91 winter seasons. USA Cold Regions Research and Engineering Laboratory, Special Report 92-20.

Yamaguchi, T., Yoshida, H., and Ando, M. 1981. Field test study of pack ice barrier. POAC 81, Québec City, Québec, Canada.

Zabilansky, L.J. 1996. Ice force and scour instrumentation for the White River, Vermont. CRREEL special report no. 96-6.

# 14 Annex 1. Section and anchor cables of the St. Lawrence river booms

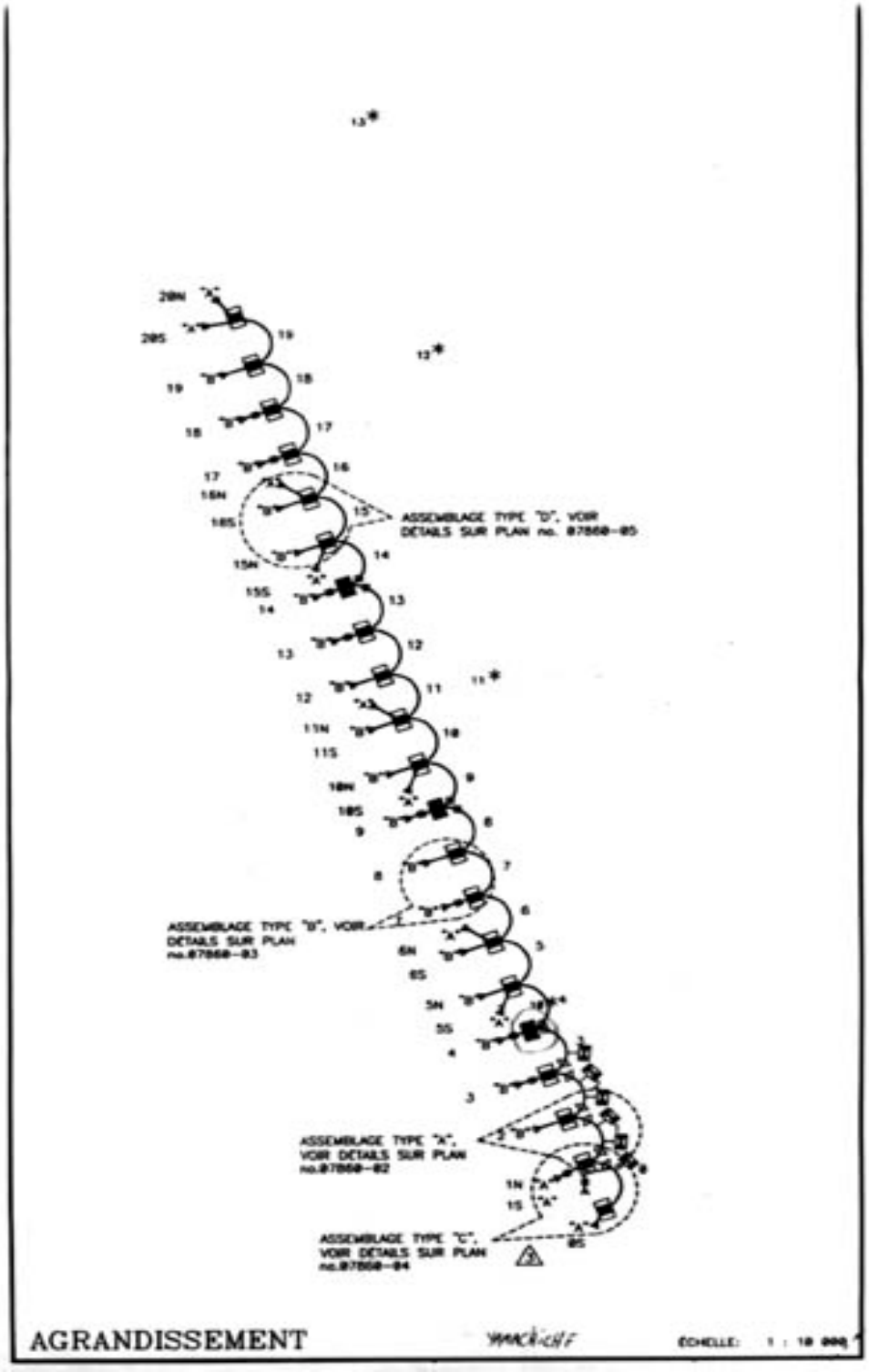


Figure 14.1 Yamachiche boom

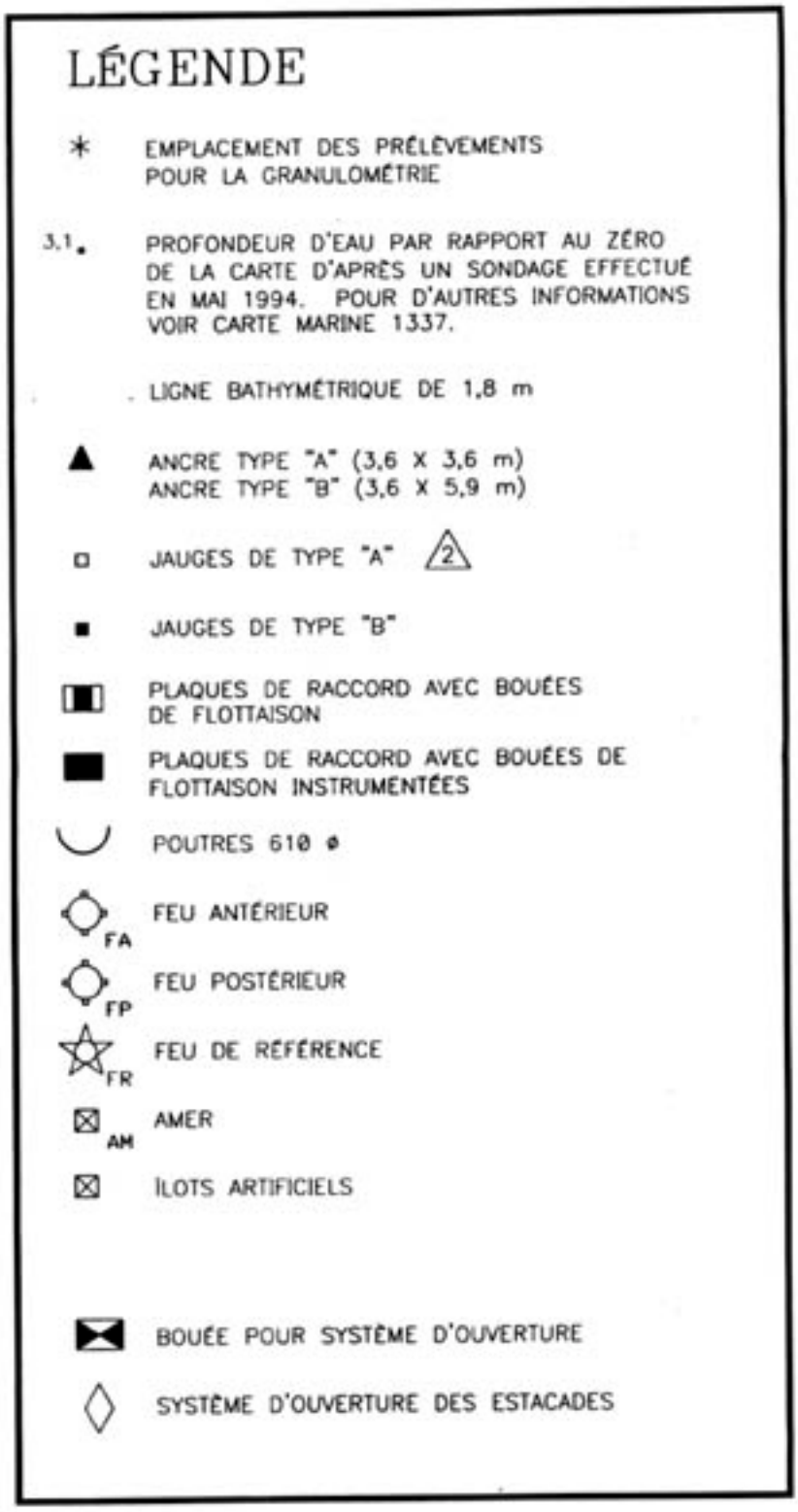


Figure 14.2 Legend for Yamachiche boom

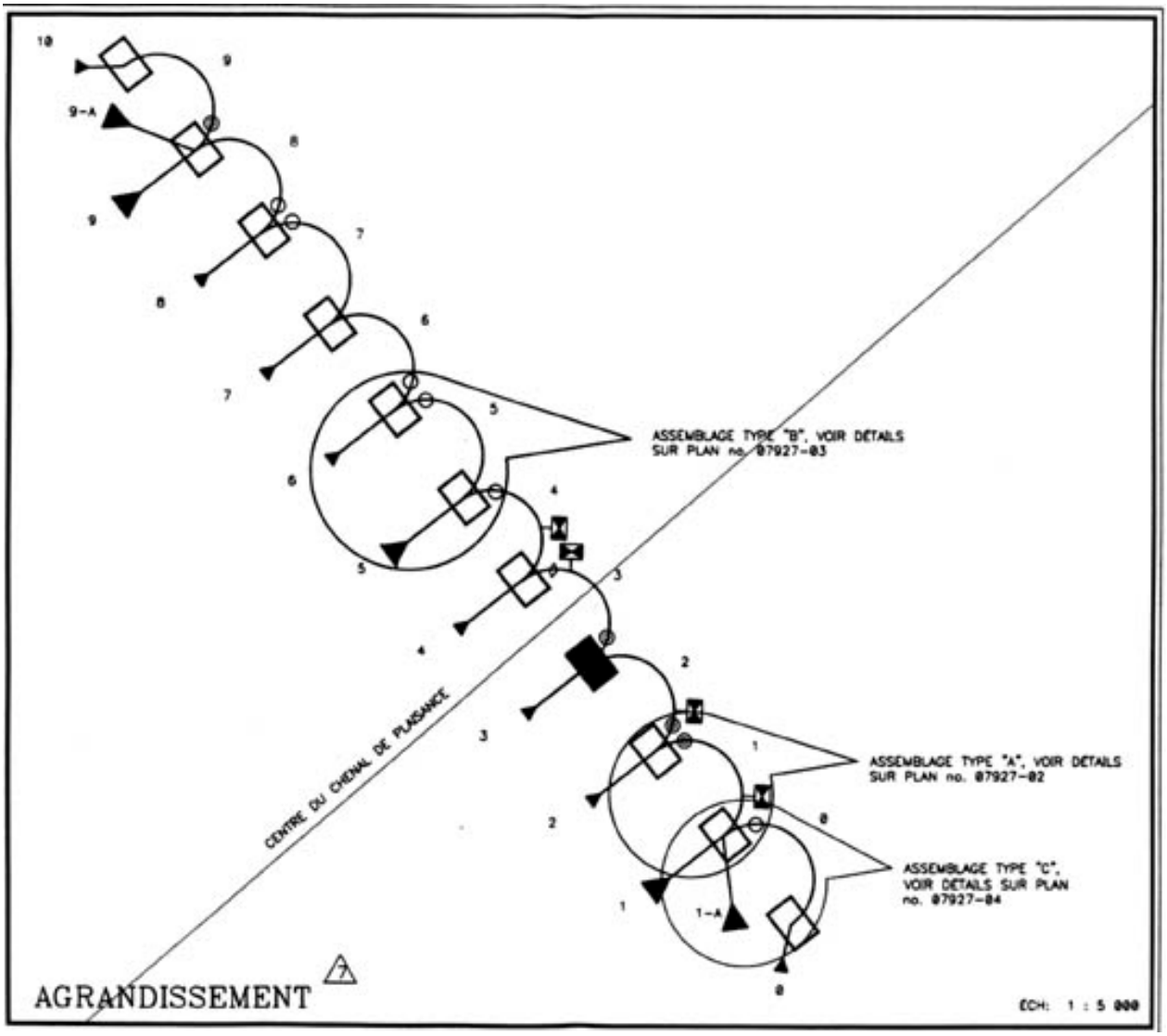


Figure 14.3 Lavaltrie boom: (Not to scale)

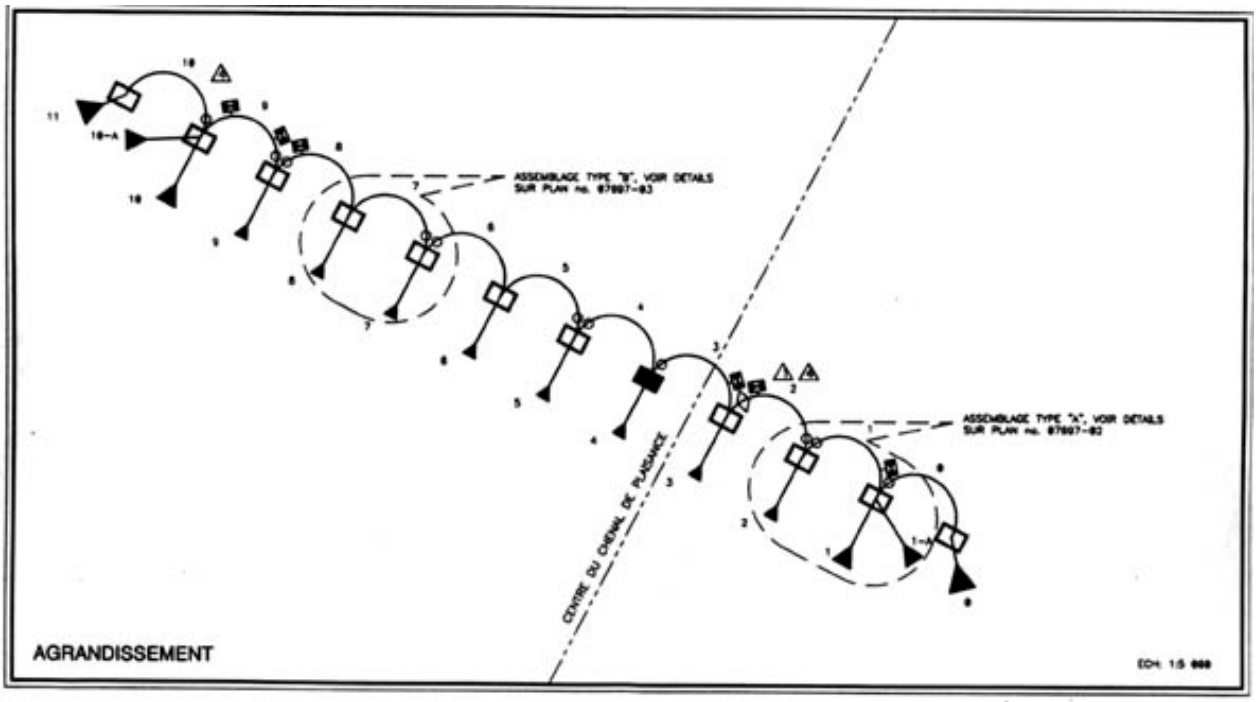


Figure 14.4 Lanoraie boom (not to scale)

# 15 Annex 2. Measured Anchor Loads on St. Lawrence River Ice booms at Yamachiche, Lavaltrie and Lanoraie 1994-2000

## Measured Loads on Anchor Cables

St. Lawrence River Ice booms

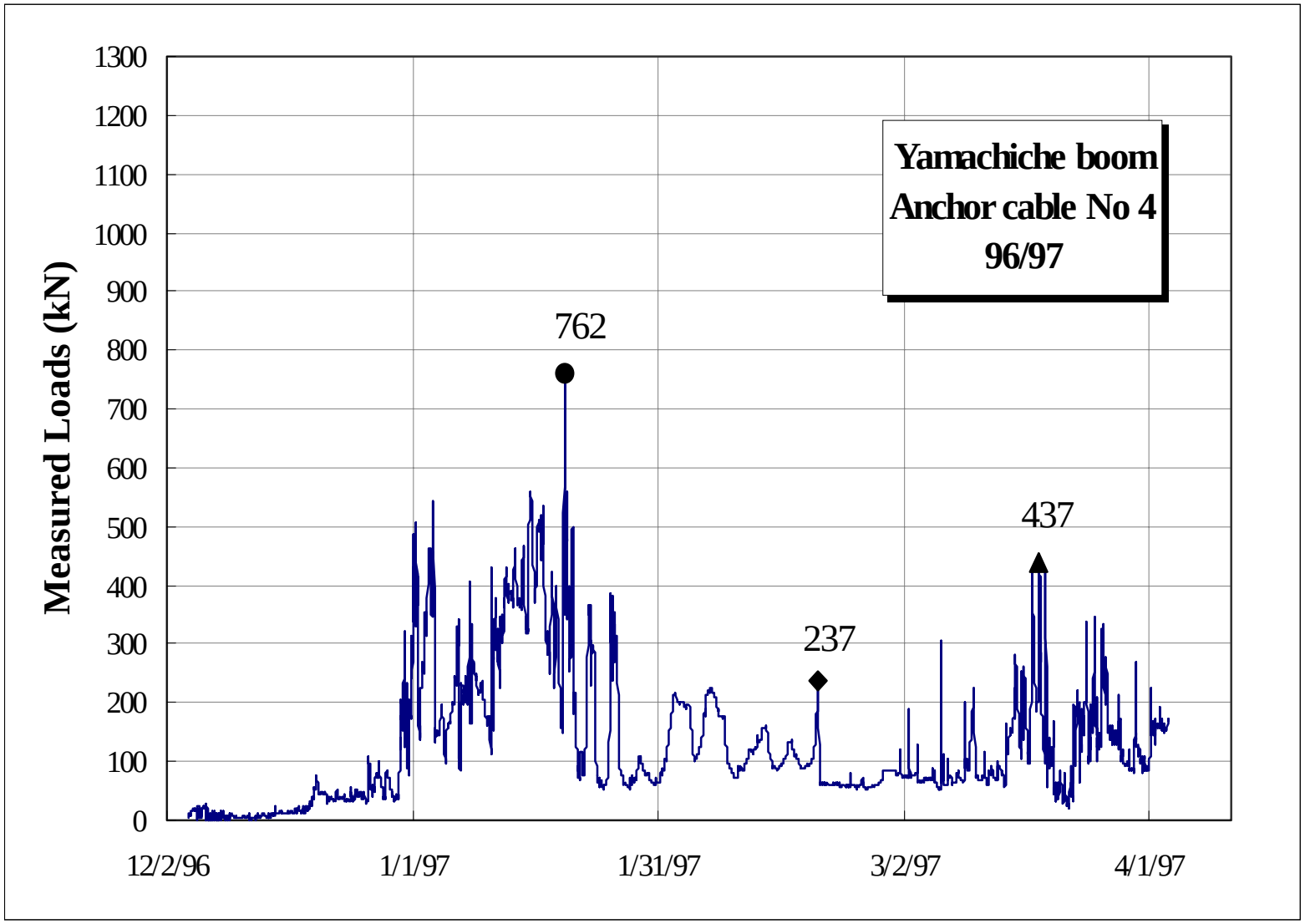


Forces on wide structures, B. Morse, PERD/CHC Report 10-56, page .99

## Measured Loads on Anchor Cables

St. Lawrence River Ice booms

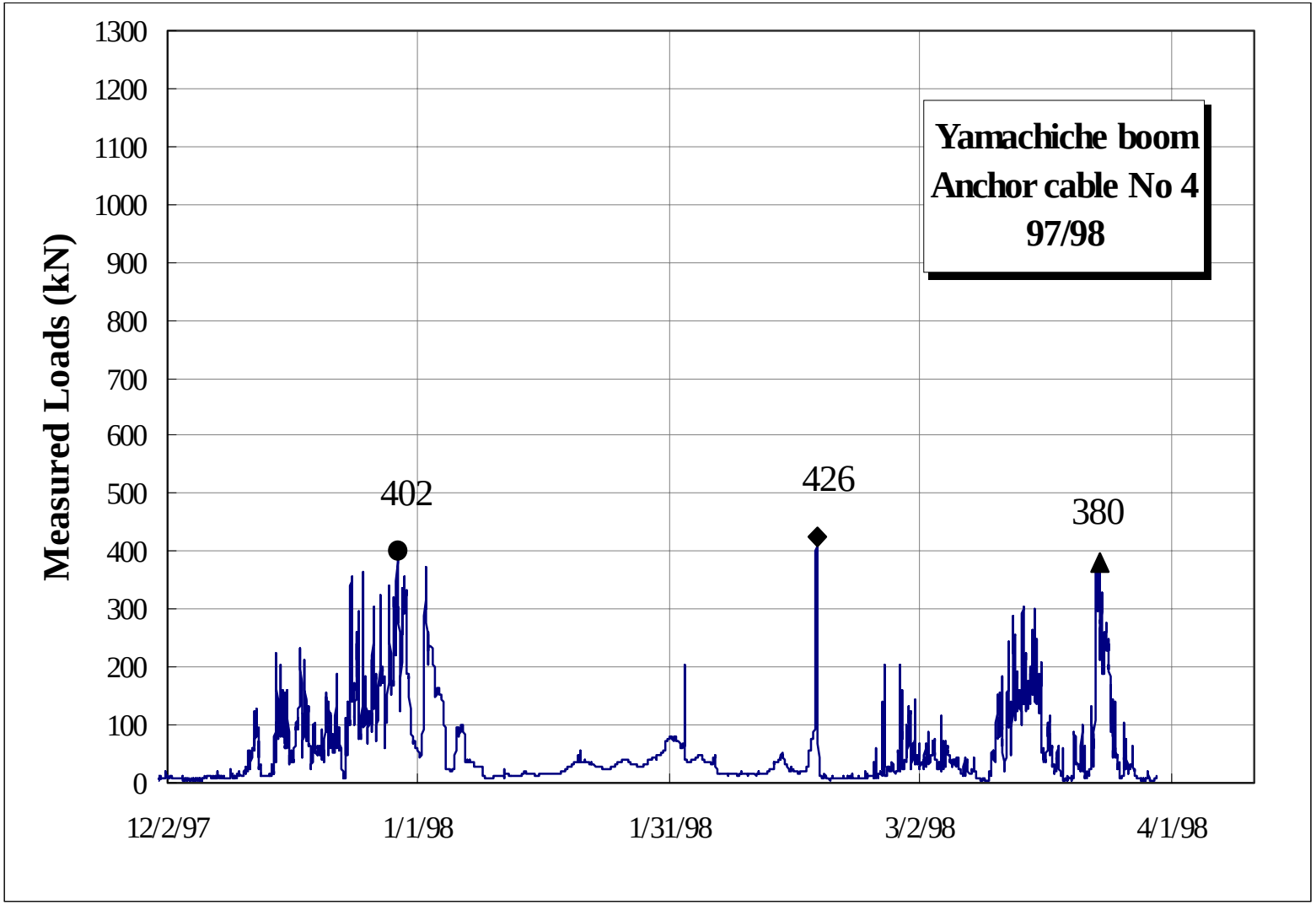

## Measured Loads on Anchor Cables

St. Lawrence River Ice booms

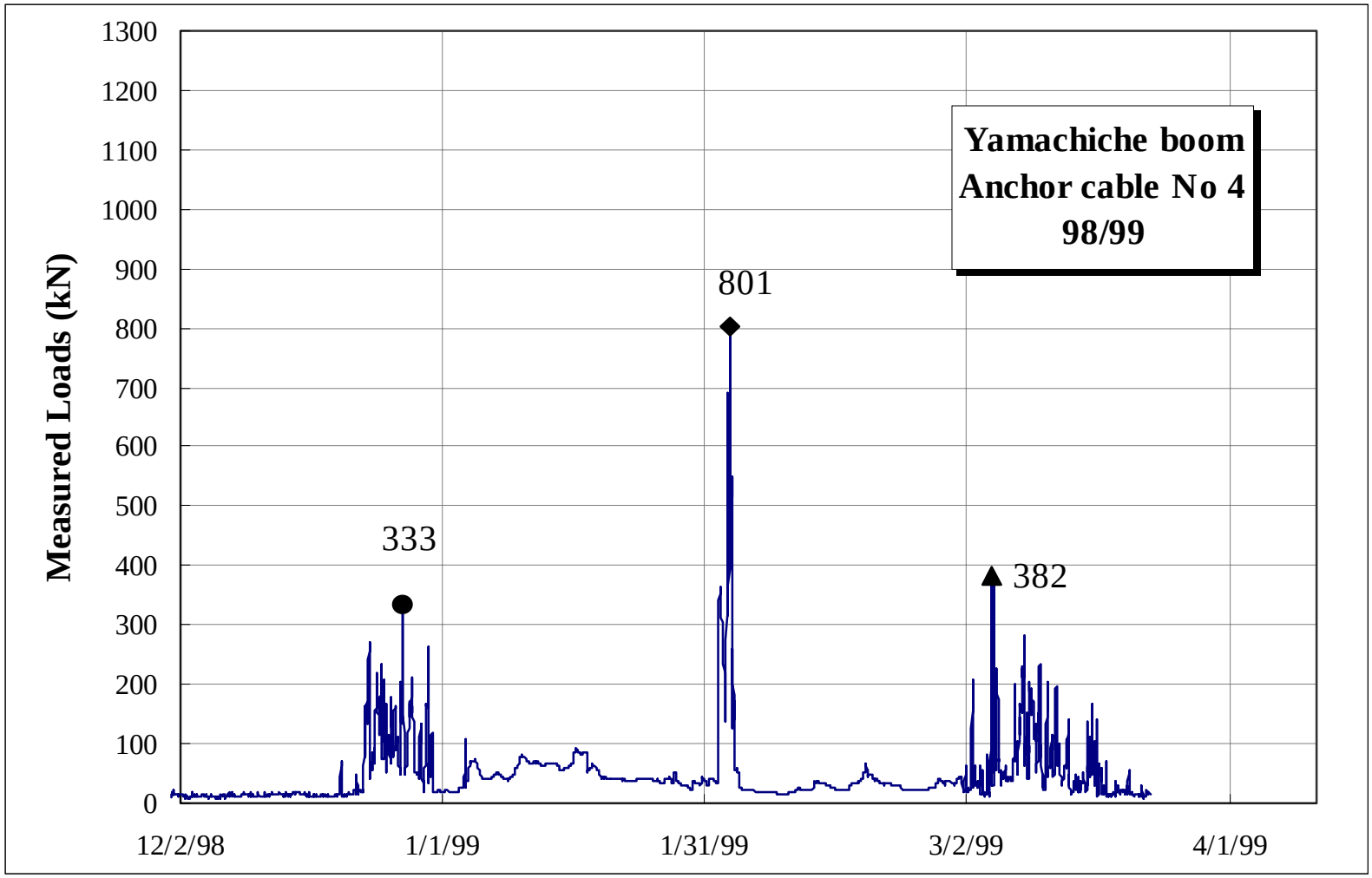

## Measured Loads on Anchor Cables

St. Lawrence River Ice booms

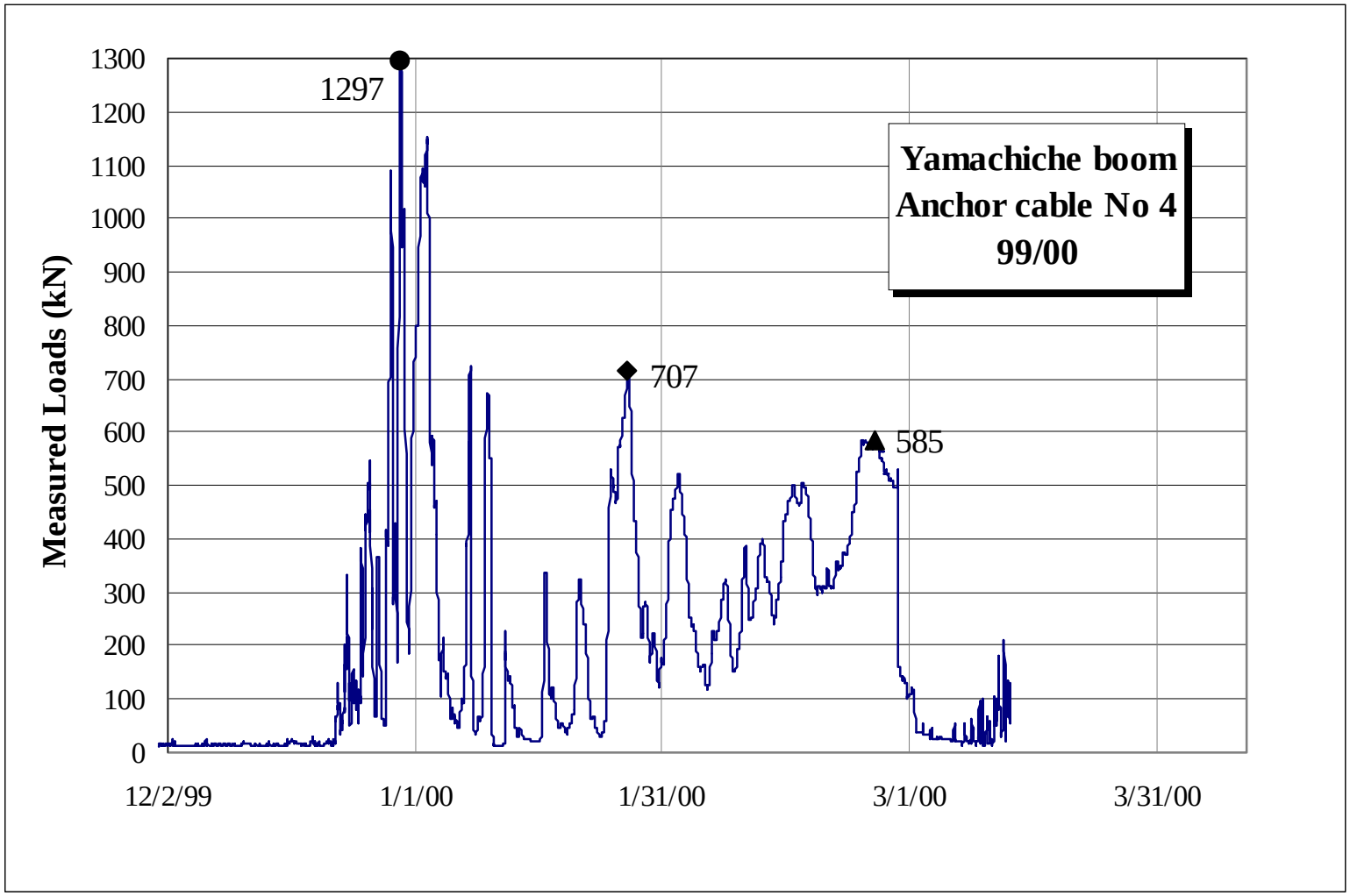

## Measured Loads on Anchor Cables

St. Lawrence River Ice booms

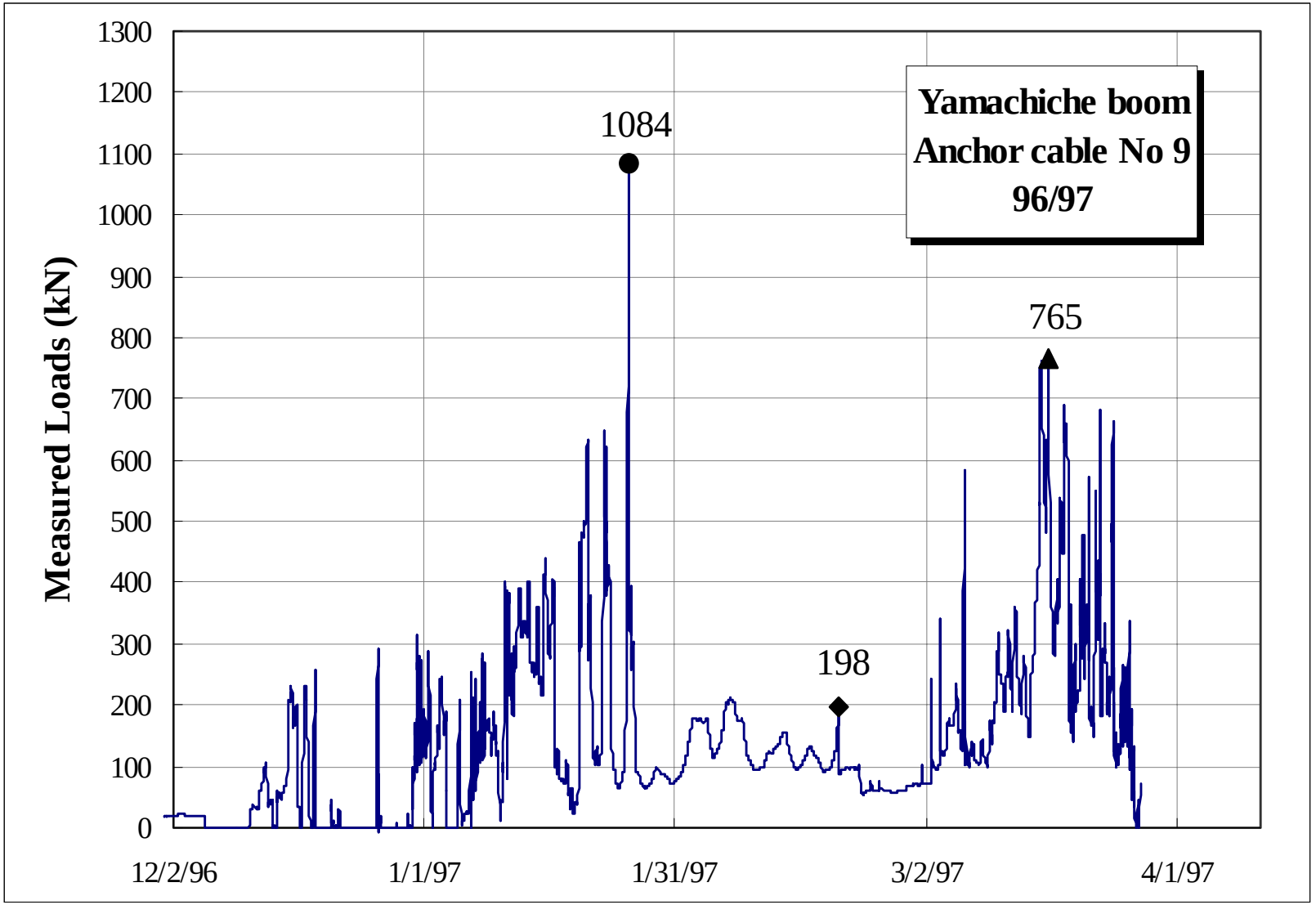


Forces on wide structures, B. Morse, PERD/CHC Report 10-56, page .103

## Measured Loads on Anchor Cables

St. Lawrence River Ice booms

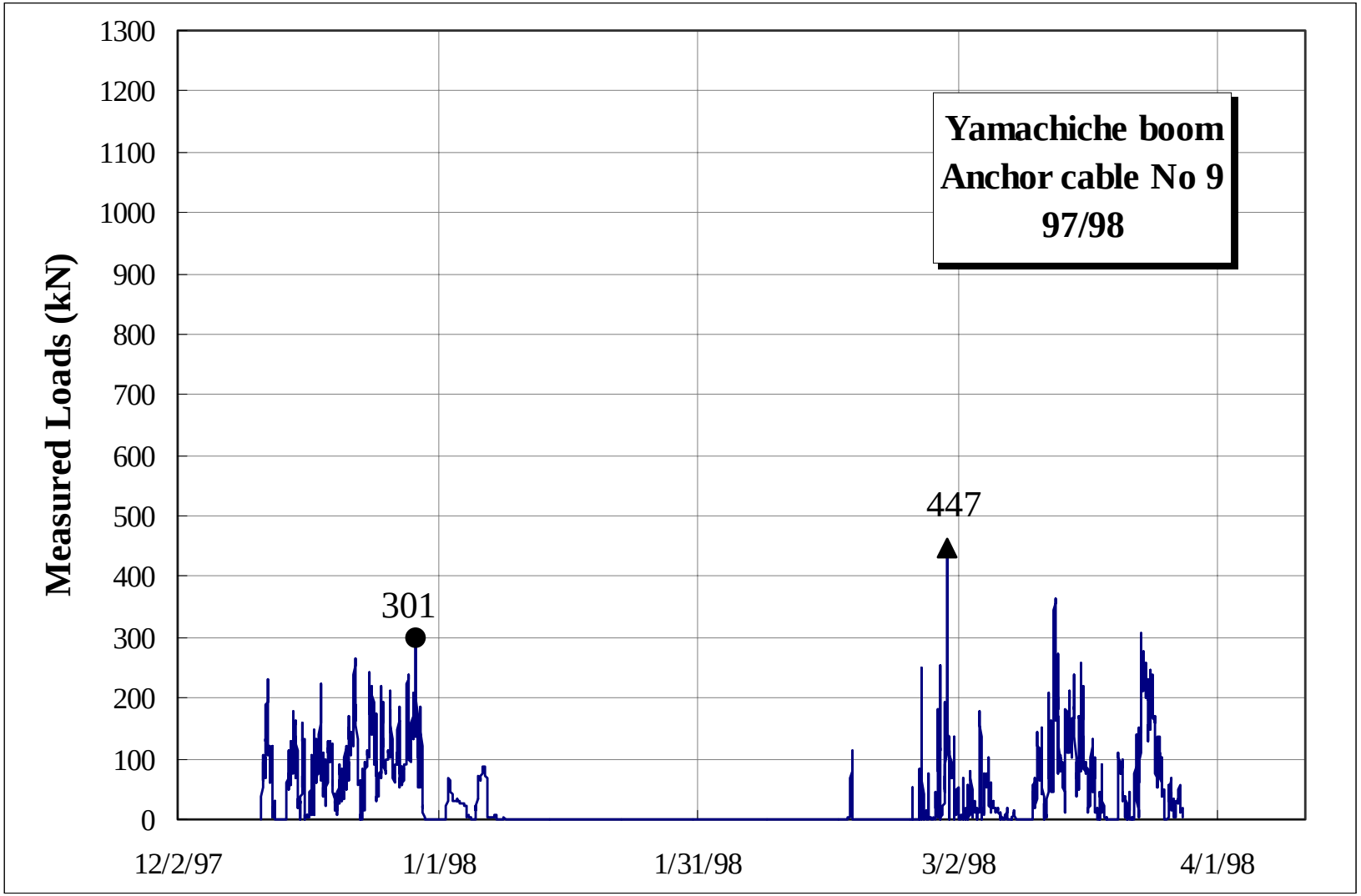


Forces on wide structures, B. Morse, PERD/CHC Report 10-56, page .104

## Measured Loads on Anchor Cables

St. Lawrence River Ice booms

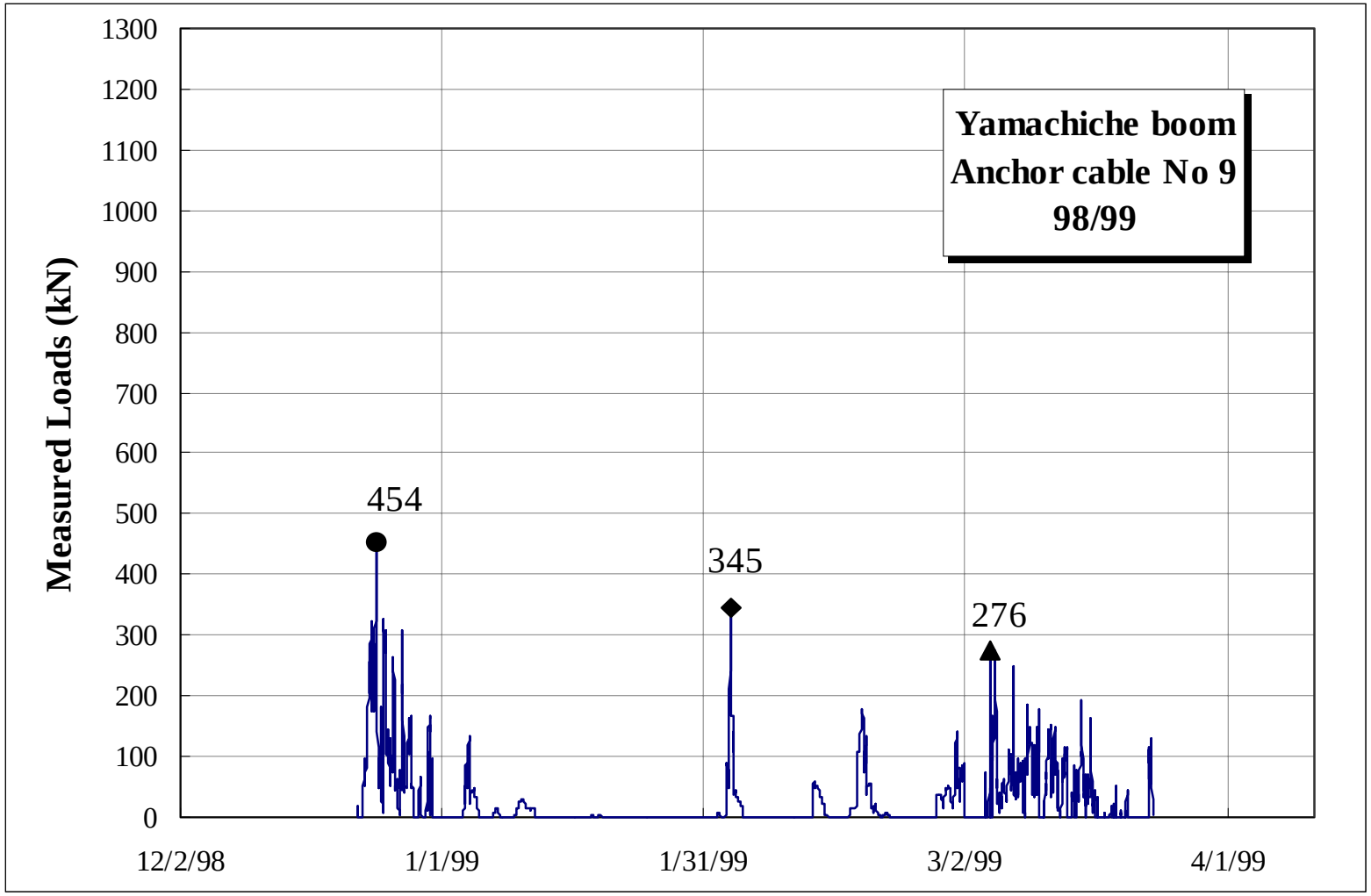

## Measured Loads on Anchor Cables

St. Lawrence River Ice booms

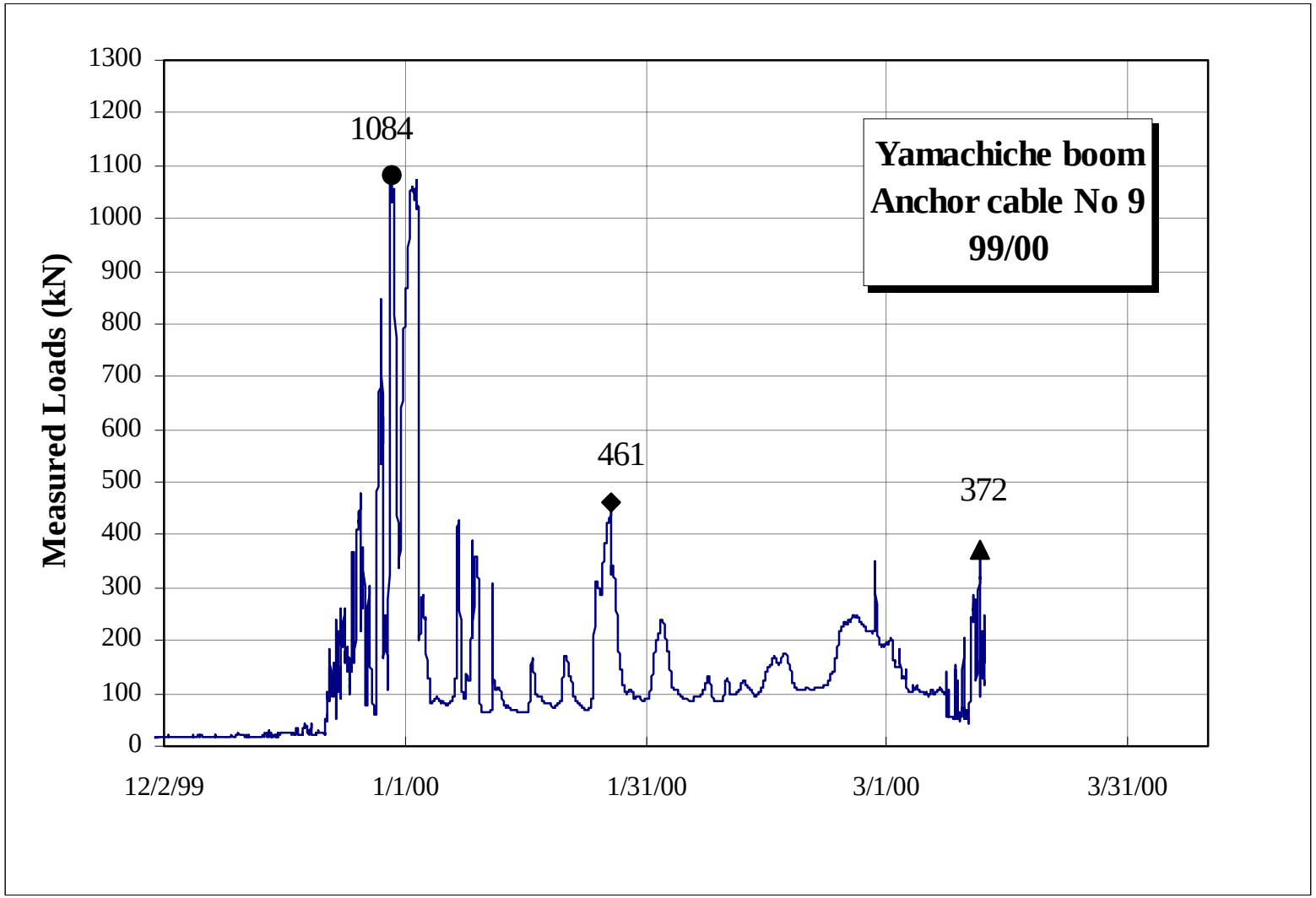

## Measured Loads on Anchor Cables

St. Lawrence River Ice booms

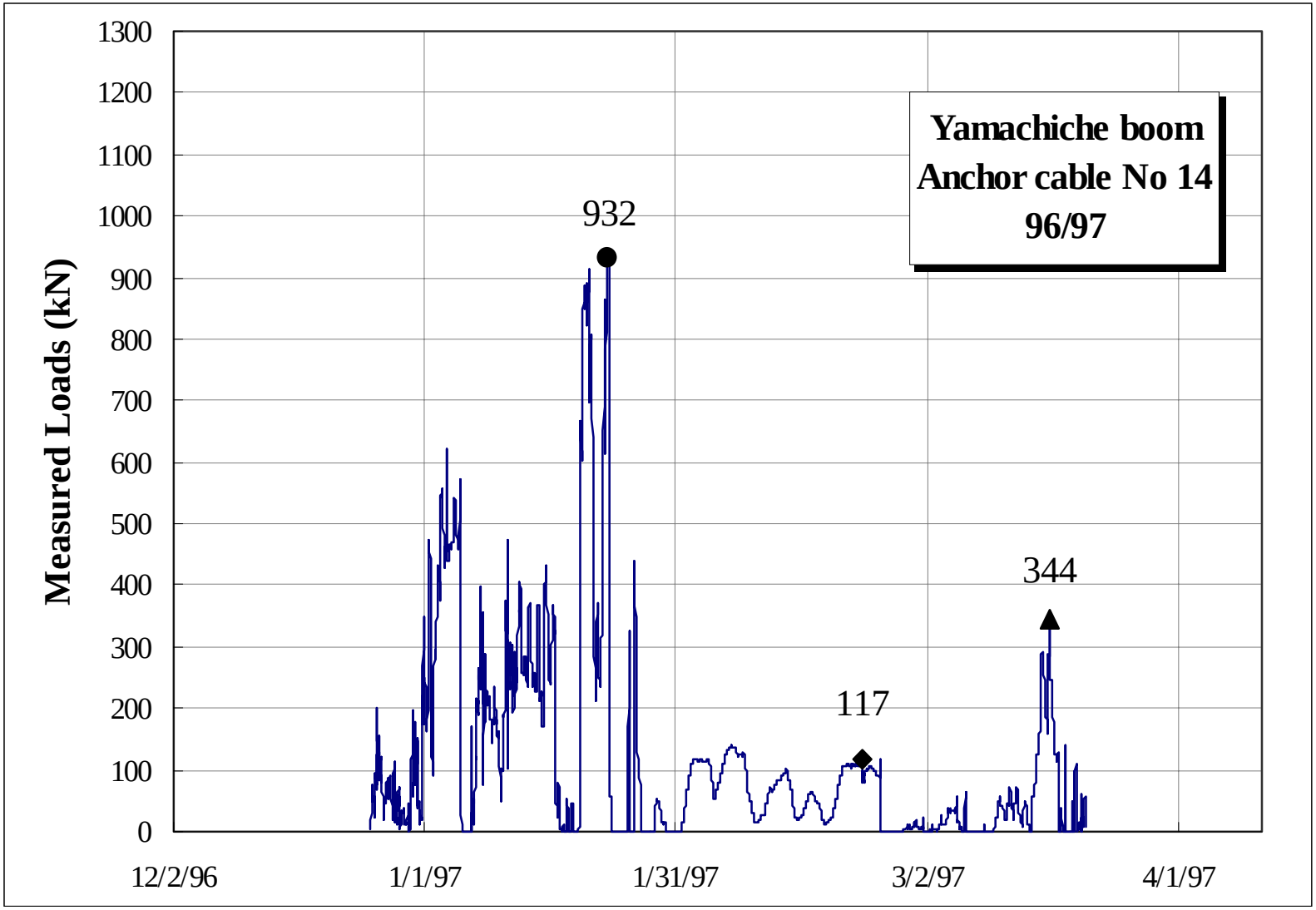


Forces on wide structures, B. Morse, PERD/CHC Report 10-56, page .107

## Measured Loads on Anchor Cables

St. Lawrence River Ice booms

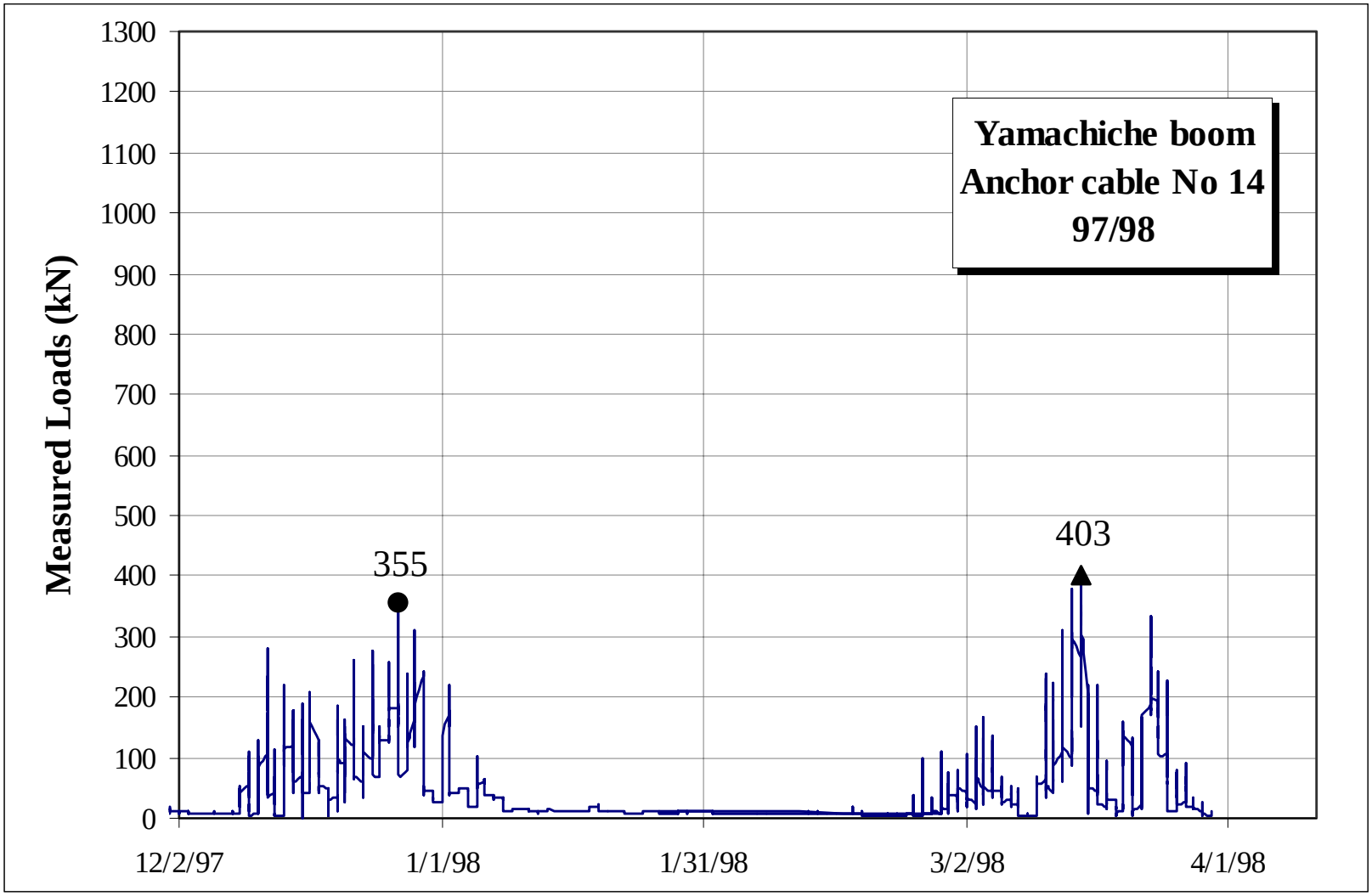

## Measured Loads on Anchor Cables

St. Lawrence River Ice booms

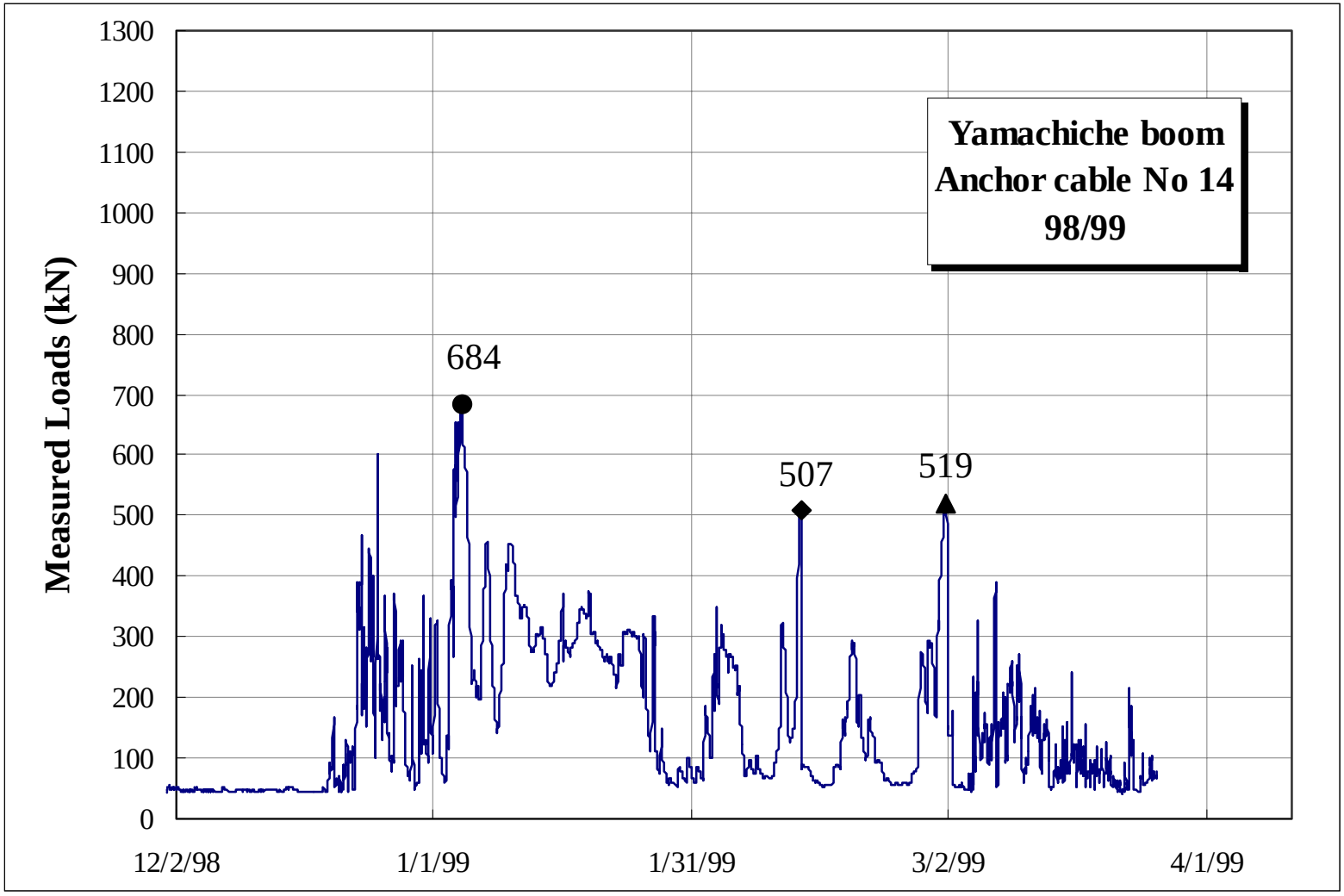


Forces on wide structures, B. Morse, PERD/CHC Report 10-56, page .109

## Measured Loads on Anchor Cables

St. Lawrence River Ice booms

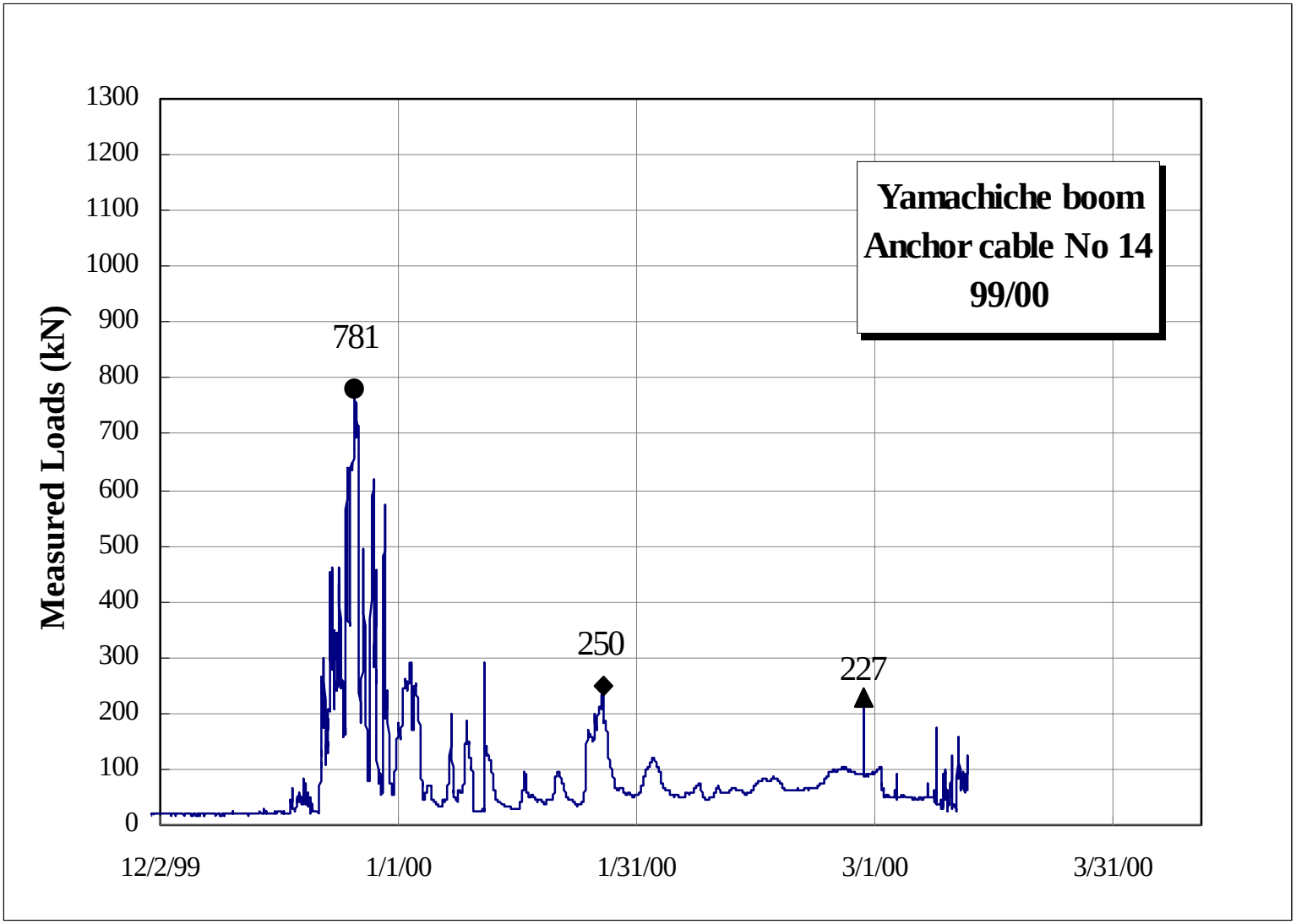

## Measured Loads on Anchor Cables

St. Lawrence River Ice booms

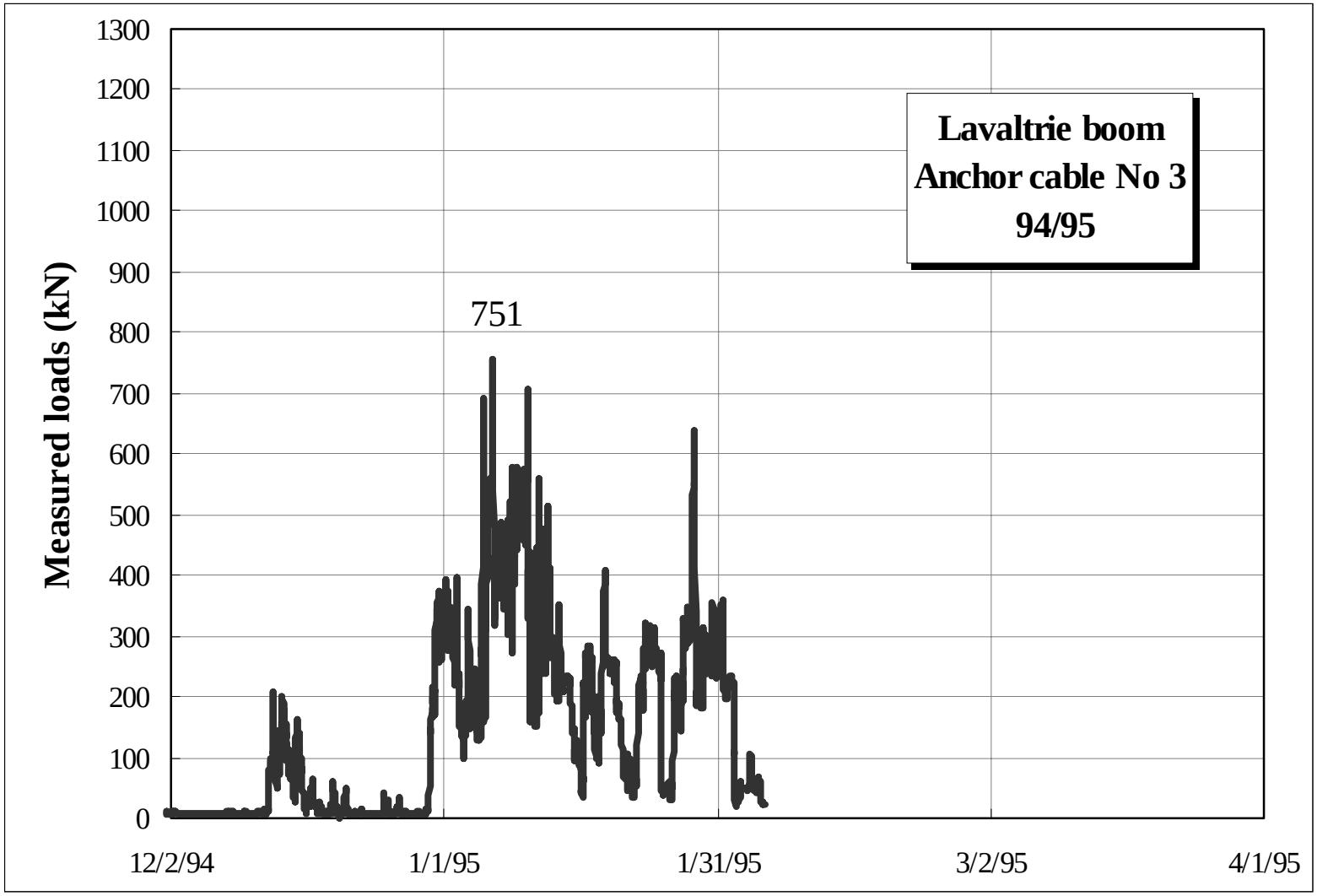

## Measured Loads on Anchor Cables

St. Lawrence River Ice booms

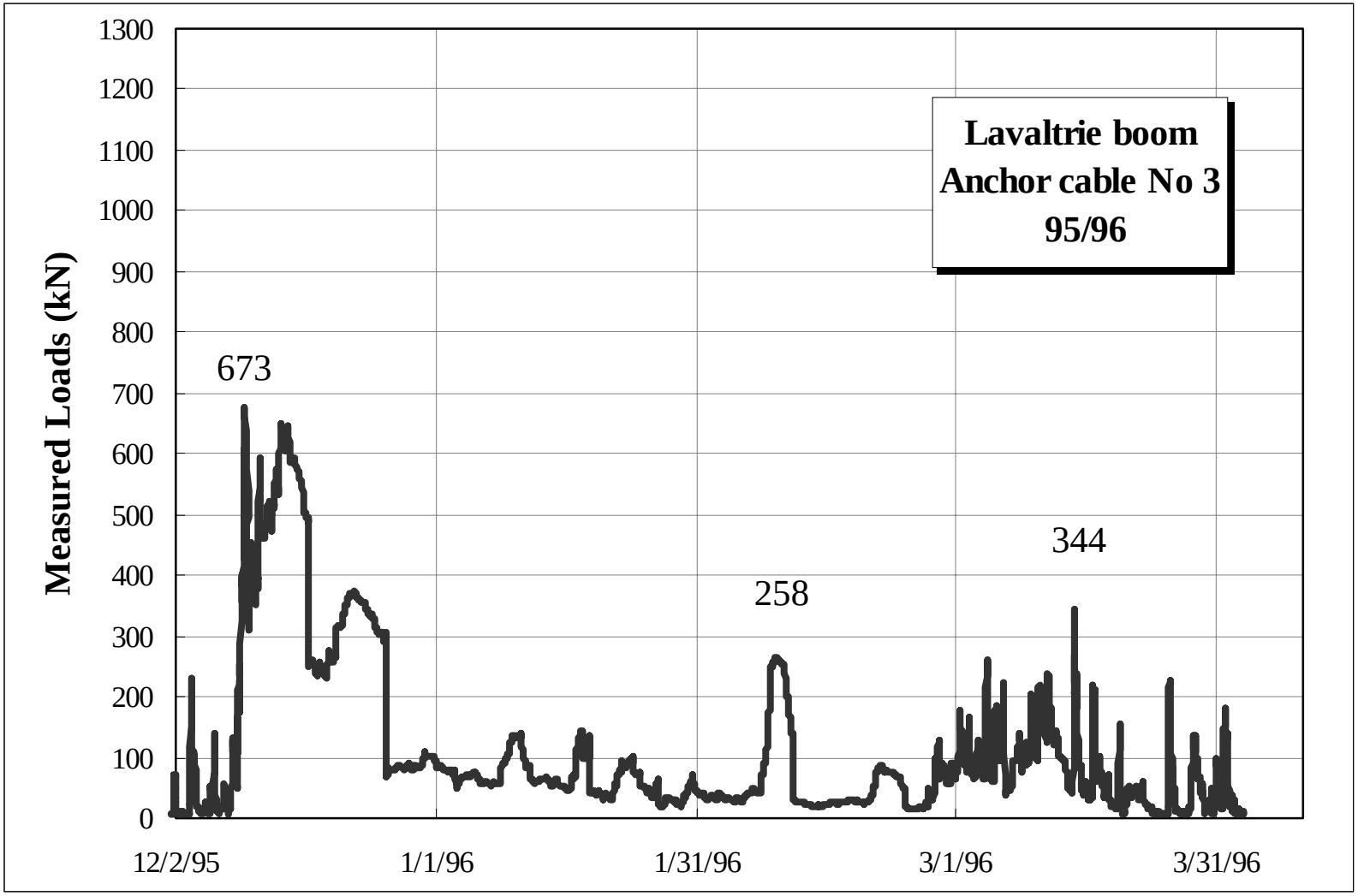

## Measured Loads on Anchor Cables

St. Lawrence River Ice booms

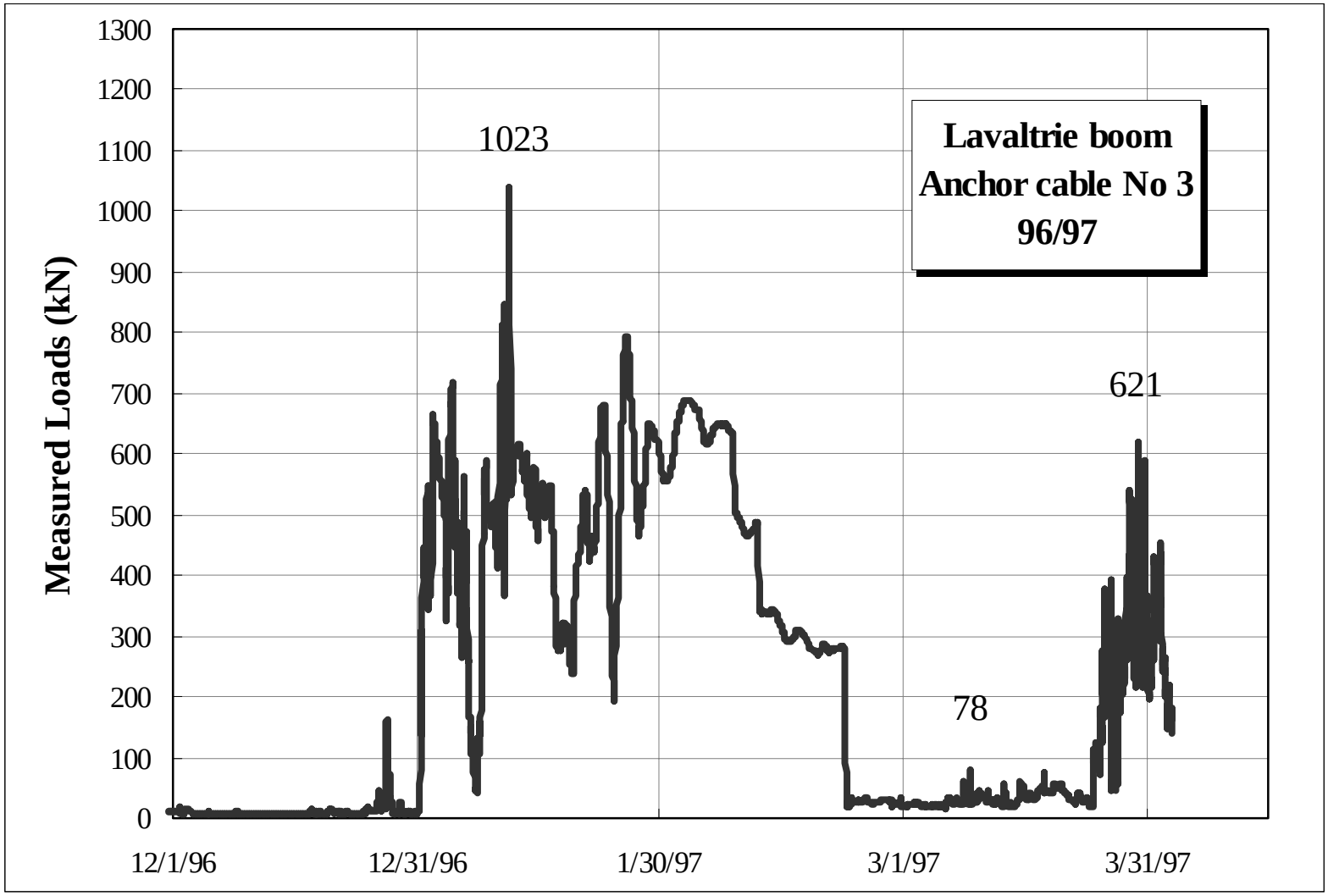

## Measured Loads on Anchor Cables

St. Lawrence River Ice booms

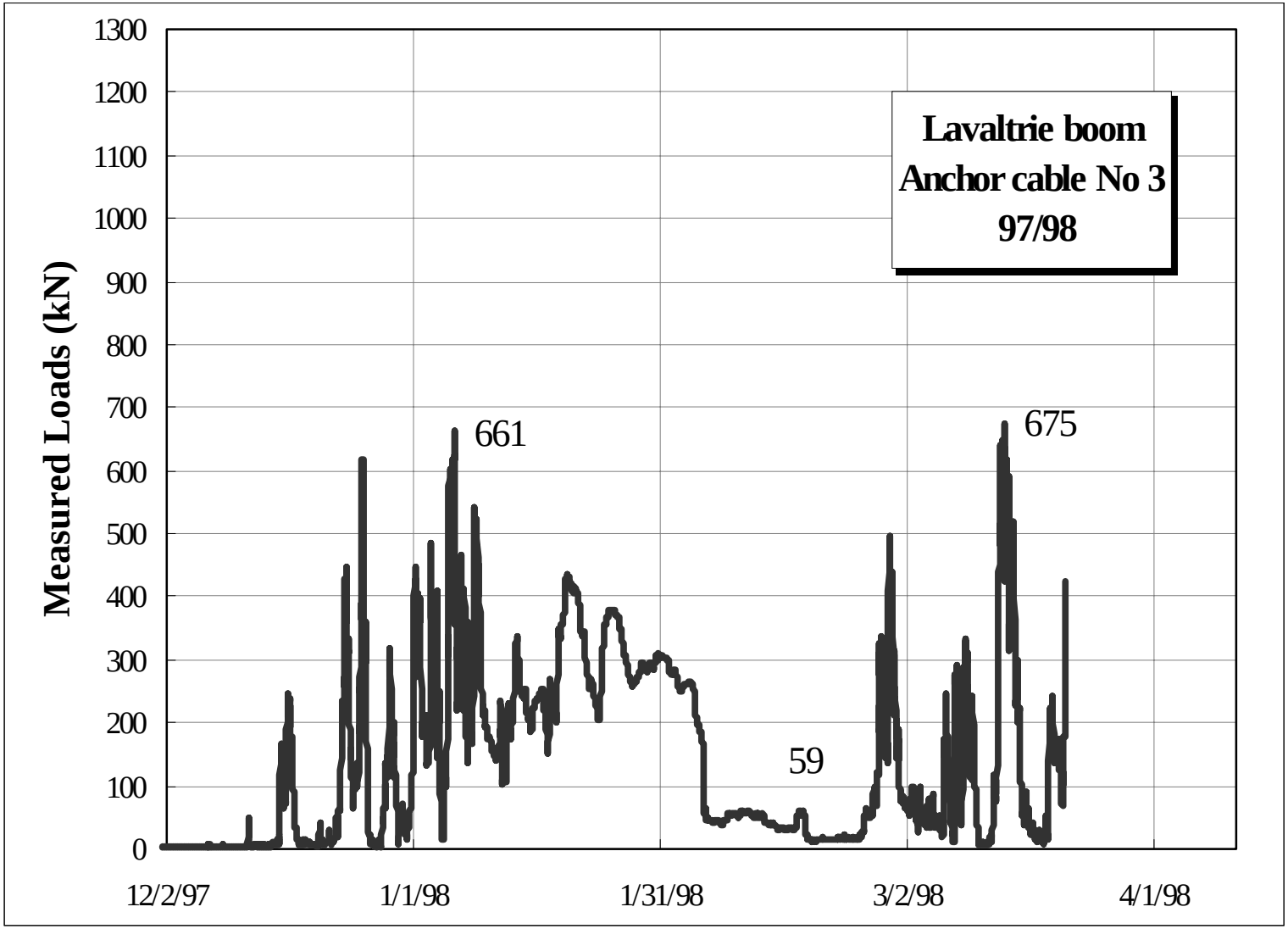

## Measured Loads on Anchor Cables

St. Lawrence River Ice booms

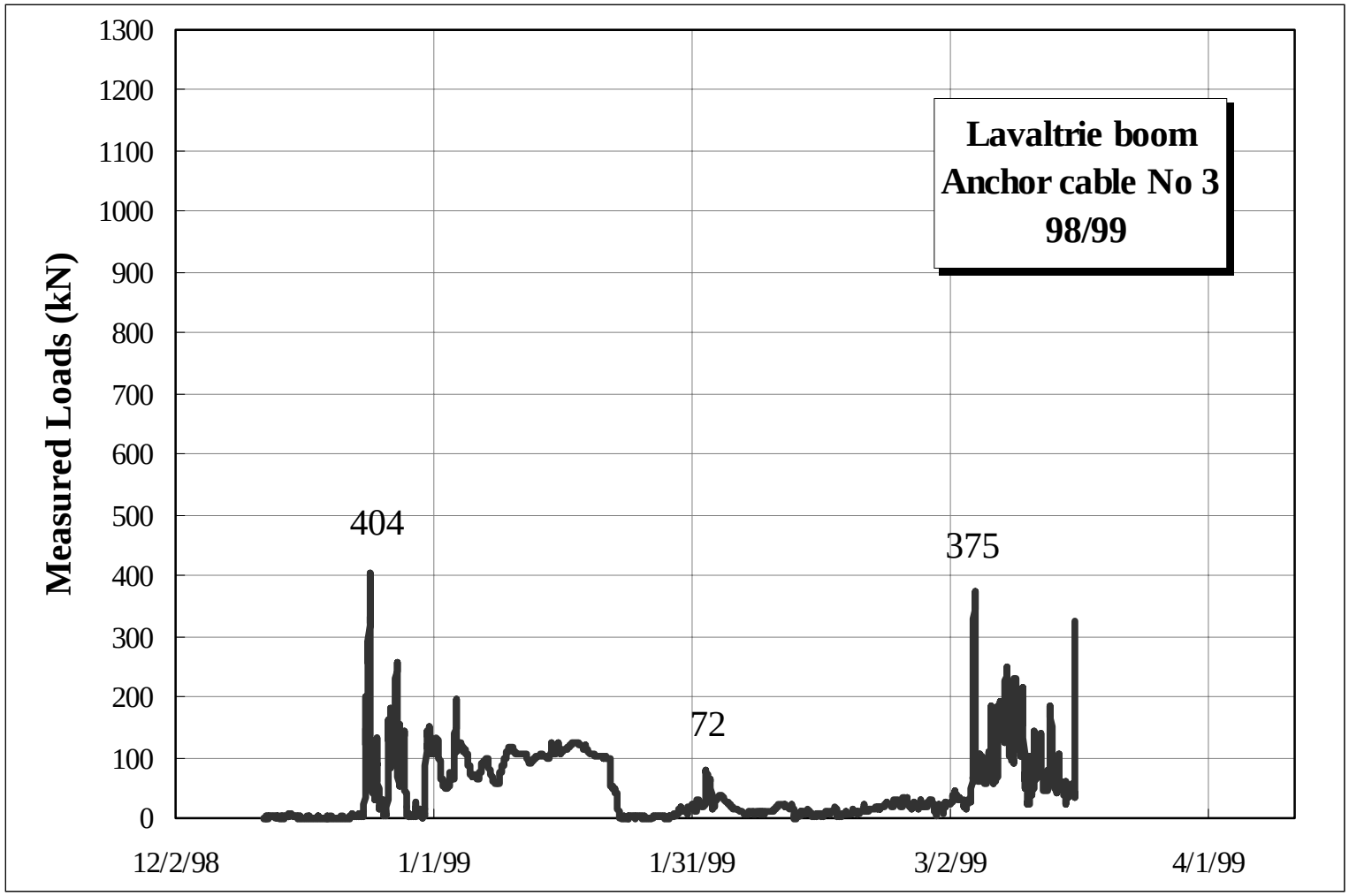

## Measured Loads on Anchor Cables

St. Lawrence River Ice booms

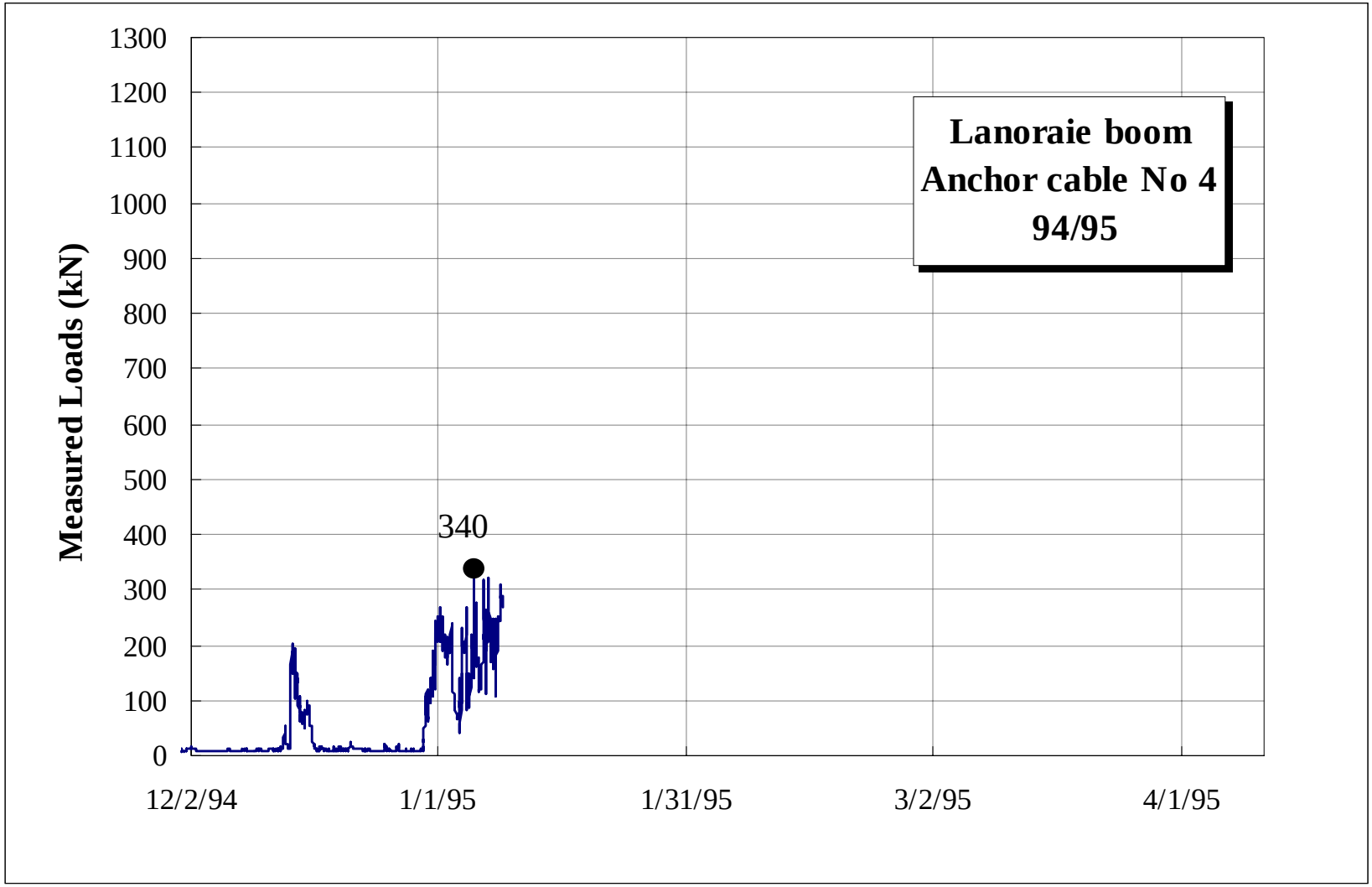

## Measured Loads on Anchor Cables

St. Lawrence River Ice booms

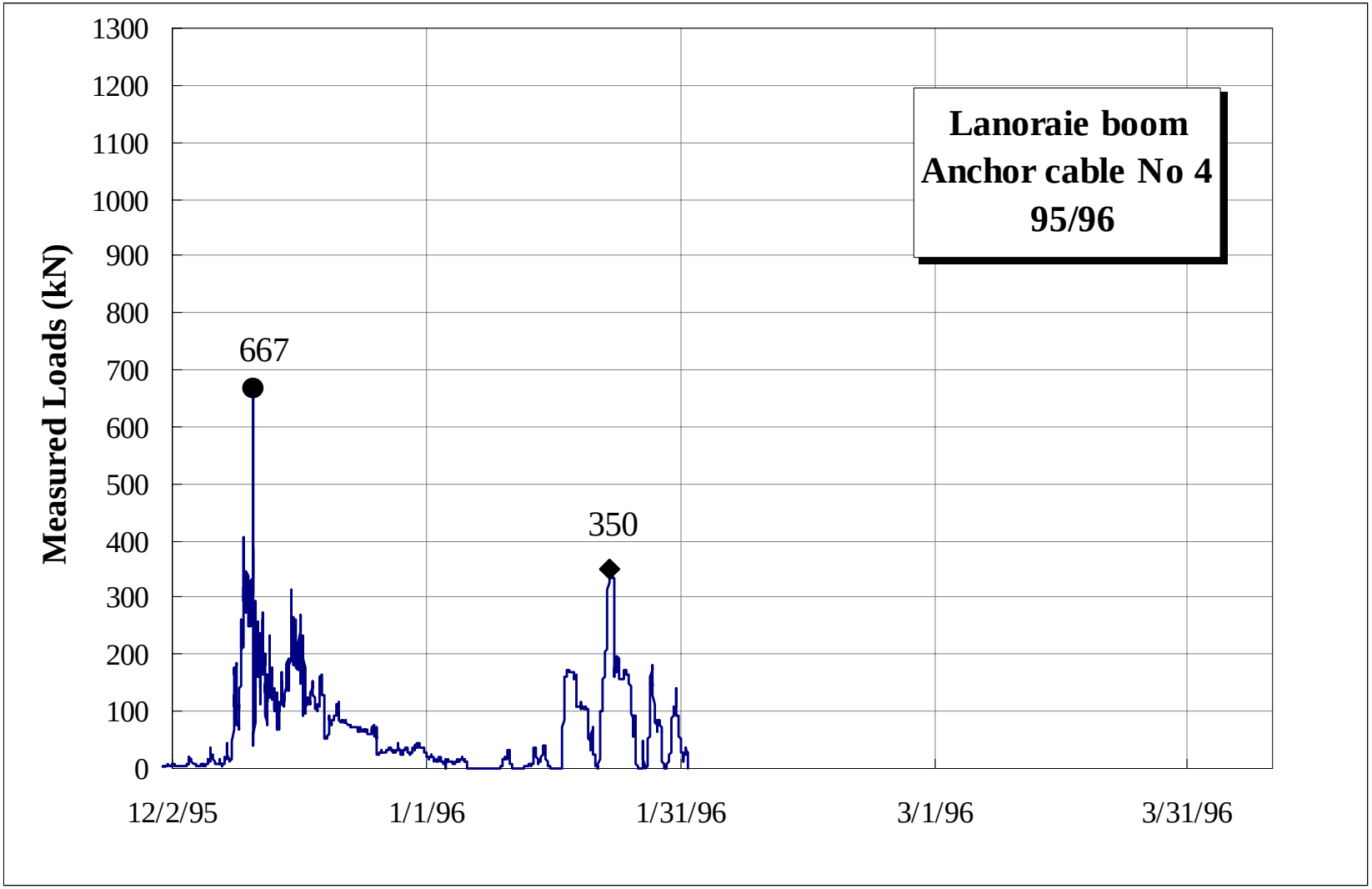

## Measured Loads on Anchor Cables

St. Lawrence River Ice booms

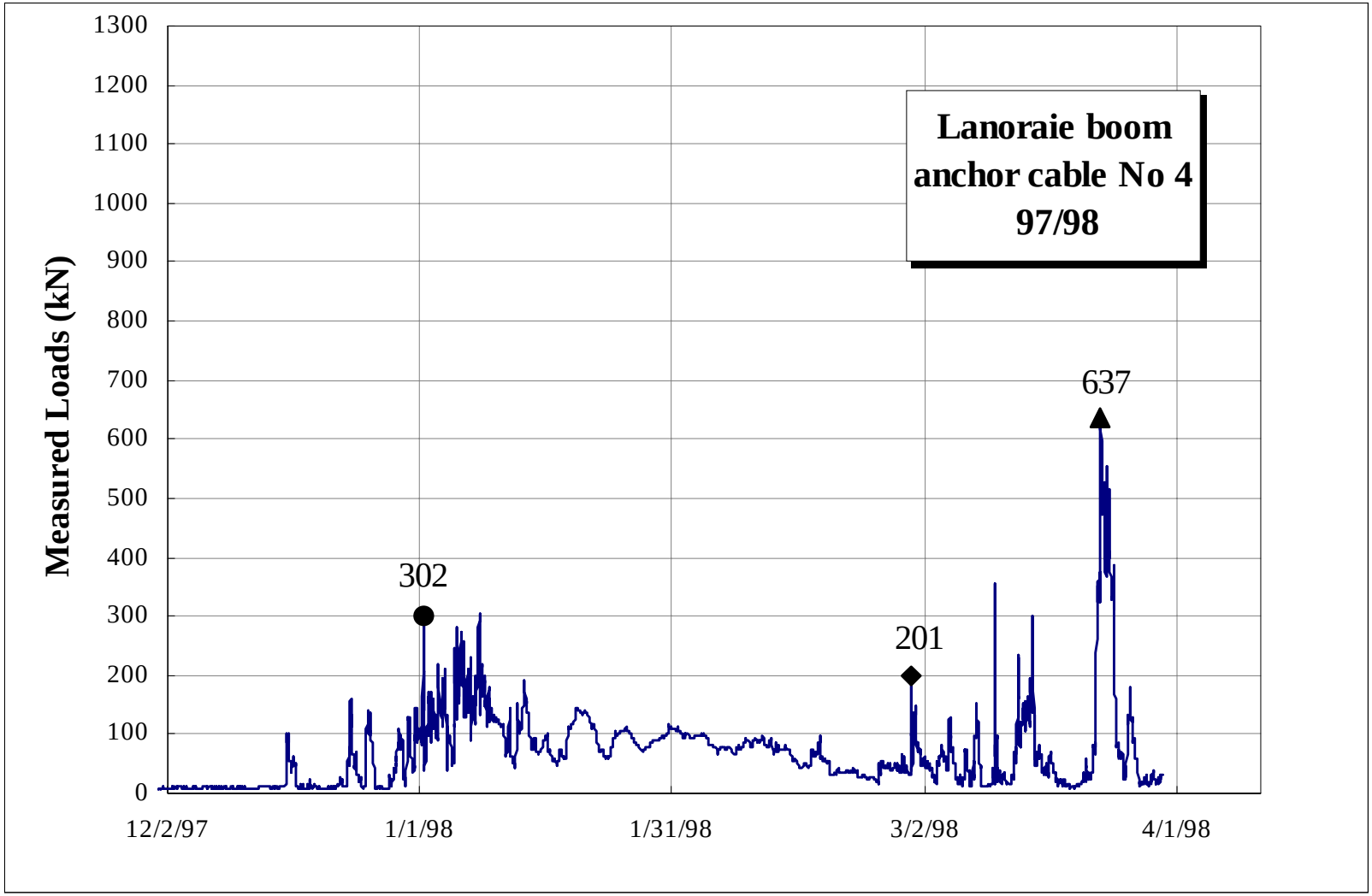

## Measured Loads on Anchor Cables

St. Lawrence River Ice booms

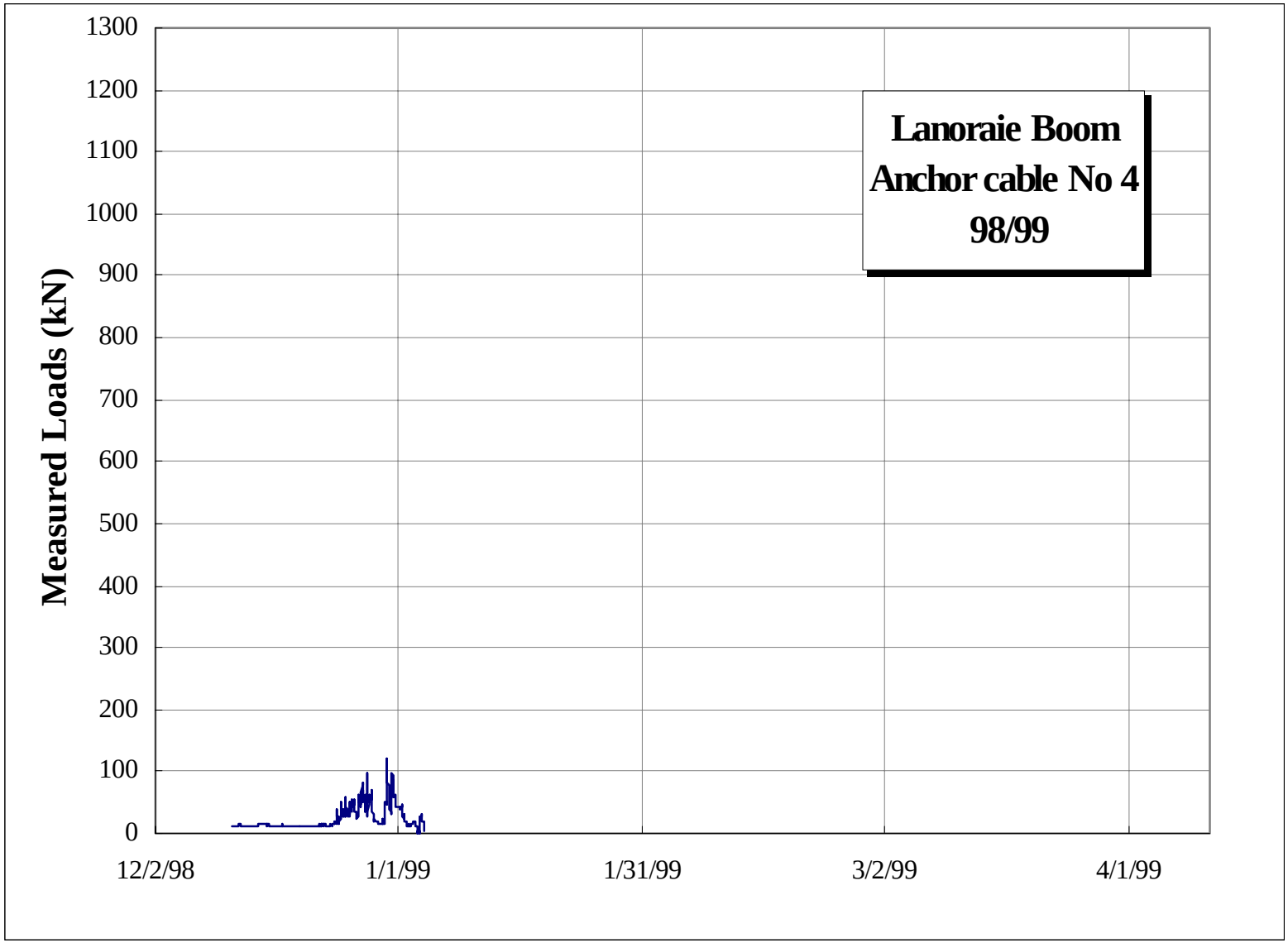


Forces on wide structures, B. Morse, PERD/CHC Report 10-56, page .119

## Measured Loads on Anchor Cables

St. Lawrence River Ice booms

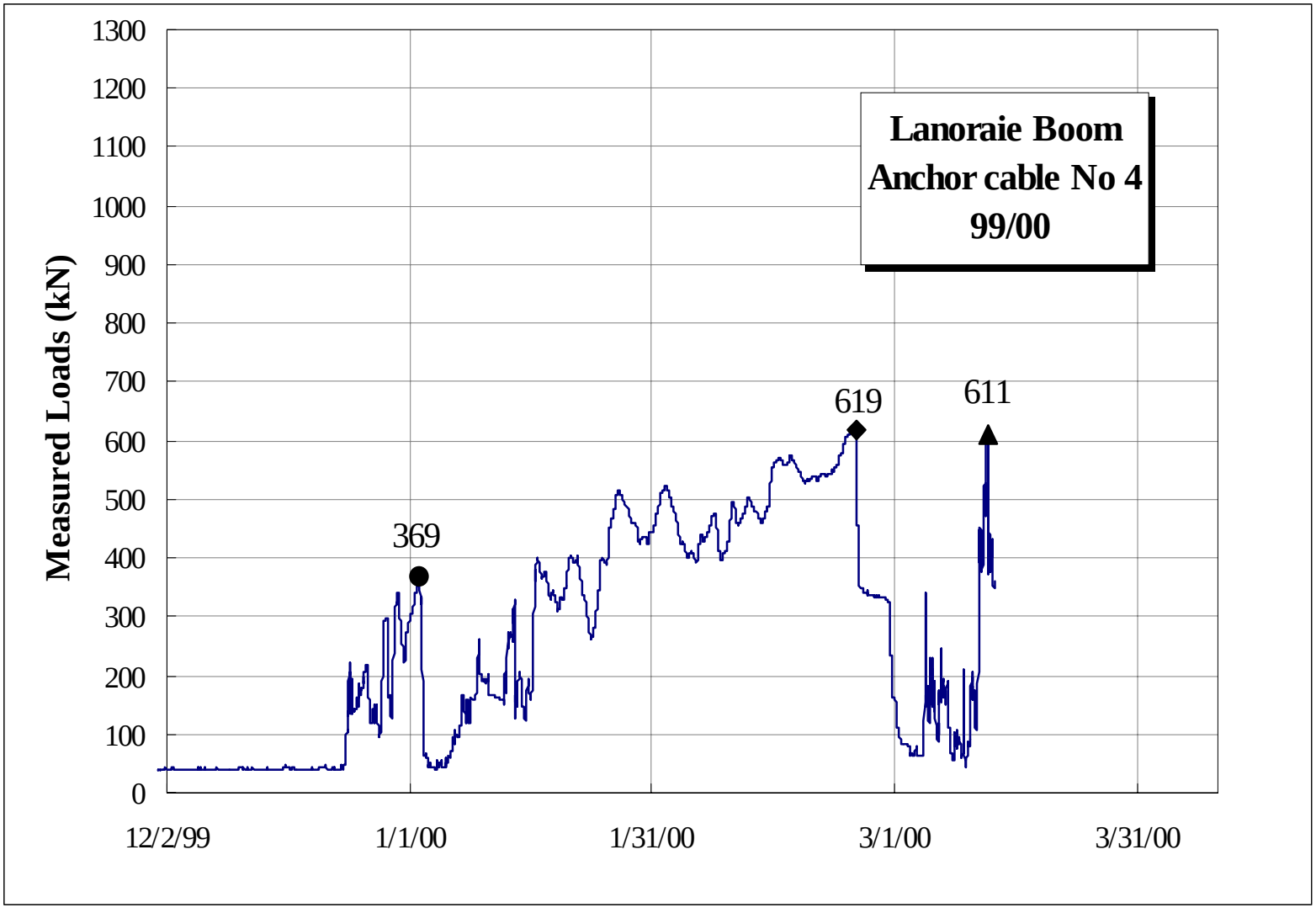


Forces on wide structures, B. Morse, PERD/CHC Report 10-56, page .120

# Measured Loads on Anchor Cables

St. Lawrence River Ice booms